Integrated hydrological modeling of surface and groundwater interactions in Heuningnes catchment (South Africa)

IRENE K KINOTI
Feb, 2018

SUPERVISORS:
Dr. M.W Lubczynski
Dr. Ir. CM Mannaerts

Integrated hydrological modelling of surface and groundwater interactions in Heuningnes catchment (South Africa)

IRENE K KINOTI

Enschede, The Netherlands, February, 2018

Thesis submitted to the Faculty of Geo-Information Science and Earth Observation of the University of Twente in partial fulfilment of the requirements for the degree of Master of Science in Geo-information Science and Earth Observation.
Specialization: Water Resources and Environmental Management

SUPERVISORS:
Dr. M.W. Lubczynski
Dr. Ir. C.M. Mannaerts

THESIS ASSESSMENT BOARD:
Dr. Ir. C. van der Tol (Chair)
Dr. P. Gurwin University (External Examiner, University of Wraclow)

ABSTRACT

Heuningnes catchment is characterised by numerous surface water bodies, including rivers, wetlands and seasonal pans. Both primary and secondary porosity aquifers exist. The water table is relatively shallow and rises above the surface during rainy seasons. The catchment is also characterised by low topographic relief with elevation ranging between -14 to 833 m a.s.l. The hydrological cycle is governed by interactions between surface water and the directly connected shallow aquifer. The extent and spatial distribution of the interaction between surface water and groundwater are influenced mainly by topography and rainfall patterns. This research aimed to quantify and analyse the nature of surface-groundwater interactions and their impacts on water balance dynamics, and focused on Upper Nuwejaar River Catchment covering an area of ~500 km^2.

An integrated hydrological modelling approach, realised by coupling MODFLOW-NWT, SFR2, UZF1 and Reservoir Packages, that describes the spatial and temporal water balance dynamics was applied. Groundwater flow system was conceptualised into two aquifer layers, the upper unconsolidated and the bottom consolidated based on the available borehole logs and hydrological cross-sections obtained from UWC. An IHM model was then built in ModelMuse environment and calibrated in both steady-state and transient state for a period of 16 months, for which data was available. This was followed by water balance analysis and sensitivity analysis of different model parameters carried out on the calibrated model.

Based on this analysis, the following observations were made: 1) groundwater was responsive to rainfall events as observed from the simulated heads and groundwater fluxes; 2) direct recharge from precipitation was the main inflow into the groundwater system accounting for 87.4% of total precipitation (P = 398.6 $mm.y^{-1}$; 3) base flow was negligible as stream leakages into and from groundwater were almost equal; 4) the wetland simulated using the Reservoir Package was gaining groundwater throughout the simulation period; 5) despite low rainfall rates and large groundwater fluxes, a net recharge of 0.3 $mm.mth^{-1}$ was observed 6) Surface water and groundwater fluxes had a simultaneous impact on water balance dynamics; 7) large spatial variability of groundwater fluxes due to varying depth to water table and variation in land cover classes

The results of the steady-state model were similar to those of the transient model, and thus both could be used for prediction of fluxes in the catchment.

Keywords: Integrated hydrological modelling, surface-groundwater interactions, water balance, recharge, Heuningnes Catchment

ACKNOWLEDGEMENTS

First and foremost, I thank Almighty God for his favour, protection and good health throughout this study.

I am grateful to ITC for granting me the opportunity to study in the faculty and to the Government of the Kingdom of the Netherlands through the Ministry of Foreign affairs for the fellowship grant to support my study.

I would like to express my heartfelt gratitude to my first supervisor, Dr M.W. Lubczynski, for his patience, guidance and valuable support starting from proposal phase, field work to the final phase of thesis writing. I am also grateful to my second supervisor for his guidance especially with processing of climatic data.

This study would not have been possible without the support of the Institute of Water Studies, University of Western Cape and the Water Research Commission of South Africa. To Prof. Dominic Mazvimavi, thank you for granting me an opportunity to carry out this study and providing the necessary data. My heartfelt felt gratitude to Dr Jaco Nel and family for his support, guidance and ensuring I had a comfortable stay in South Africa during fieldwork and for his generous guidance during field visits. I enjoyed working with you and learned a lot. To my fellow researchers at UWC - Yonela Mkunyana, Eugene Maswanganye, Vincent Banda and Daniel Mehl – thank you for your endless support and cooperation in sharing the data required for this study.

Thank you to the administration and teaching staff of ITC-WRS department for building our theoretical background which was very helpful during research. To my friends and fellow classmates, I am grateful to have met you and you became my family away from home.

Last but not least I am grateful to my family for their prayers and moral support while away from home.

TABLE OF CONTENTS

LIST OF FIGURES

LIST OF TABLES

1. INTRODUCTION

1.1. Background

Two-thirds of South Africa is covered by arid and semi-arid lands (van Wyk et al. 2012) with an average of 500 mm per year of precipitation and 21% of the country receiving less than 200mm (Tadross and Johnston 2012). The country has limited water resources and is ranked globally amongst the twenty most water-scarce countries (Woodford et al. 2005). Optimising water yield from catchments within the country has thus become a crucial element of catchment management to reduce pressure on water resources caused by population growth, inadequate management and land use and climate change (Bugan et al. 2012).

Unlike surface water, of which 98% has been developed, groundwater in the country is under-developed (Levy and Xu 2012) and constitutes only 15% of total consumption although 65% of the population depends on it (Woodford et al. 2005). According to (DWA 2010) the utilisable groundwater exploitation potential is 10 343 million m^3 per annum (or 7 500 million m^3 per annum under drought conditions) while the amount that is in use is between 2000 and 4000 million m^3 per annum. Over 80% of the country is underlain by relatively low yielding, shallow, weathered and/or fractured rock aquifer system (Woodford et al. 2005) with fractured sedimentary rock as the most dominant covering 55% of the land area (Levy and Xu 2012).

Historically, surface water and groundwater in the country, have been considered separate entities and the focus has been on either groundwater or surface water monitoring and evaluation. Surface-groundwater interaction has, however, received a lot of focus in the recent past (Levy and Xu 2012) due to its importance to the functioning of ecological systems, sustainability of water resources (Unland et al. 2013) and also due to the fact that development or contamination of one usually affects the other. However, accurate quantification or even conceptualization of these interactions has proved challenging due to: hydrological complexity of such interactions (Seward et al. 2006) enhanced by heterogeneity and anisotropy (Hassan et al. 2014); difficulty in parameterization; scale problem; typical lack of data required to quantify interaction processes including unavailability of structural geological information (Tanner and Hughes 2015), which would be useful in understanding the likely system dynamics.

Understanding the nature of surface-groundwater interaction processes requires integrated hydrological models also known as fully coupled models as opposed to traditional standalone models realised with either surface or groundwater codes. For instance, integration of MODFLOW-2005 (Harbaugh 2005) and MODFLOW-NWT (Hunt and Feinstein 2012) with packages such as Unsaturated Zone Flow (Niswonger et al. 2006), Stream Flow Routing (Niswonger and Prudic 2010), Lake (Merritt and Konikow 2000) and Reservoir (Fenske et al. 1996) extends the capability of the standard MODFLOW to represent and simulate surface water-groundwater interactions.

In this study interaction between surface water and groundwater were simulated by both steady state and transient models built using MODFLOW-NWT code coupled with SFR, UZF and Reservoir Packages under ModelMuse (Winston 2009) environment.

1.2. Problem statement

Heuningnes Catchment (Figure 1) is one of the 3rd order catchments of South Africa (Clark et al. 2009). It is characterised by numerous surface water bodies which include rivers and wetlands (riparian and non-riparian floodplains, pans, freshwater springs) with Nuwejaars and Kars as the main rivers. The wetlands in the catchment are interlinked with streams. The most distinguished of these are the Soetandalsvlei and Voelvlei which are inundated all year round and are directly connected to the Nuwejaars River while the smaller pans are ephemeral. Soetendalsvlei is moderately saline whereas several of the smaller pans are hypersaline. River waters are brackish and alkaline as a result of passage through limestone-bearing sands (RHP 2011). The riparian areas have been encroached by invasive plant species (*Acacia longifolia*) which are believed to have an impact on both water quantity and quality in the catchment.

Groundwater is characterised by both primary (intergranular) and secondary (fractured) porosity aquifer types and freshwater springs. Fractured aquifers occur mainly in the upper part of the catchment while the lower catchment is characterised by intergranular aquifers, primarily shale, with low yield. Groundwater is used for domestic and livestock watering purposes (DWS 2017). According to Mazvimavi (2017), the current knowledge on the availability of water resources in the catchment is based on Pitman model (Pitman 1973) as part of national water resources assessment.

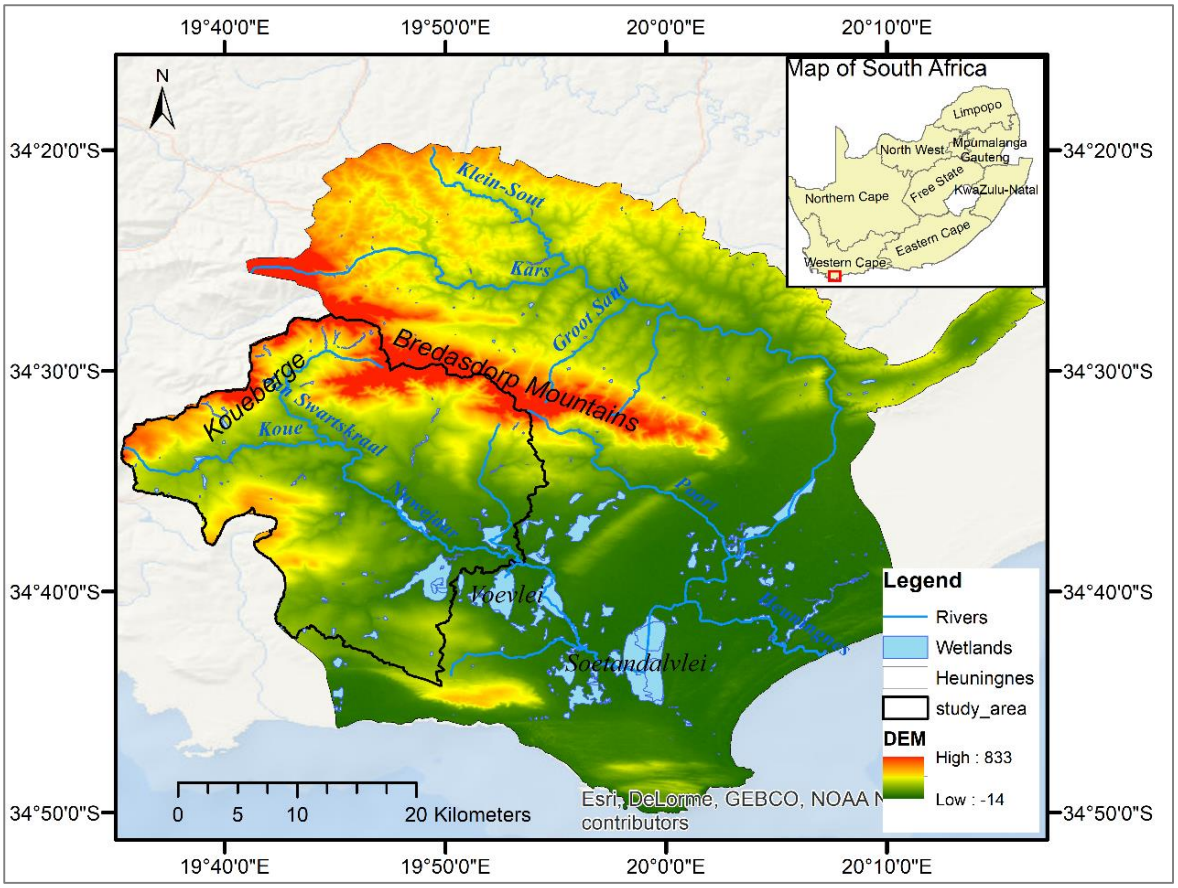

Figure 1: Heuningnes Catchment

1.3. Research setting

1.3.1. Research objectives

Main objective

To investigate, quantify and analyse the nature of surface water-groundwater interactions and their effect on water balance dynamics within Heuningnes Catchment.

Specific objectives

i. To develop a conceptual model of the Heuningnes Catchment;
ii. To develop and calibrate a distributed numerical hydrological model of the Heuningnes Catchment;
iii. To quantify water balance components in the Heuningnes Catchment;
iv. To quantify spatial-temporal dynamics of SW-GW interactions in the Heuningnes Catchment.
v. To analyse and quantify the effects of SW-GW interactions on water balance dynamics in Heuningnes Catchment

Research questions

Main research question

What is the effect of surface water-groundwater interactions on the water balance dynamics of Heuningnes Catchment?

Specific research questions

i. How is the spatiotemporal distribution of the water balance components in Heuningnes Catchment
ii. How do surface-groundwater interactions vary in space and time within Heuningnes Catchment?
iii. What are the effects of SW-GW interactions on the water balance dynamics

1.4. Hypothesis

It is hypothesised that surface water and groundwater in Heuningnes Catchment are inter-connected

1.5. Research novelty

Previous studies in the catchment were done separately for both surface water and groundwater as part of national water resources assessment. While evaluation and quantification of surface water resources started as early as 1952, assessment of groundwater resources in the catchment was initiated in 1995 through a national-wide joint programme by the Department of Water Affairs (DWAF) and Water Research Commission (WRC) (Braune et al. 2014). The results were a series of national groundwater maps built mainly on the work of Vegter (1995) as cited by Braune et al. (2014). This was followed by Groundwater Resource Assessment II (GRA11), carried out between 2003 and 2005, and involved assessment and quantification of groundwater resources at fourth order catchment level (DWS 2015). These studies were based on (Pitman 1973) conceptual models. No integrated numerical model has been developed for the catchment before.

This research, therefore, aims to develop and apply a numerical integrated hydrological model (IHM) to quantify surface-groundwater interactions as well as the water balance of Heuningnes Catchment. The results of this study will improve the understanding of the hydrological regime within H.C as well as give an estimate of the water resources in the catchment. This will ensure informed decision making in water

resources management. Moreover, it will lead to better water allocation plans and thus increased social, economic and ecological benefits.

1.6. Assumptions

- Both surface water and groundwater abstraction rates are negligible
- Groundwater flow system is not influenced by salinity downstream, i.e. water has equal density throughout the study area and simulation period.
- Effects of invasive, *Acacia Longifolia*, species were assumed to be similar to indigenous shrubs due to lack of data on their spatial coverage.

2. STUDY AREA

2.1. Location

Heuningnes Catchment (Figure1) is located in Agulhas plain in Western-Cape province on the most southern tip of South Africa and African Continent. It lies between 34^0 20" and 34^0 50" S latitude (comparable with most southern part of Europe, i.e. Cyprus Island at the northern hemisphere 34°35'N) and 19^0 30" and 20^0 30" E longitude. It is part of Eastern Overberg Tertiary catchment covering an area of 1401 km^2. This study focused on the upper Nuwejaar River sub-catchment (Figure1) covering an area of ~498km^2.

2.2. Climate

The climate of the region is of Mediterranean type, i.e. with windy, wet, cold winters and dry, warm summers. The average temperatures range between 7^0 at night and rise to 18^0 by day during winter (June to August) and can rise to 25^0 to 30^0 on hot summer (December to March) days.

The average precipitation is 400-600 mm with 80% occurring during winter months with a monthly mean of 40-100 mm on the coastal plains and up to 200 mm in the mountains, while the monthly mean for the summer months is between 10 and 50 mm. Figure 2 shows long-term rainfall, minimum and maximum temperature monthly means in the region.

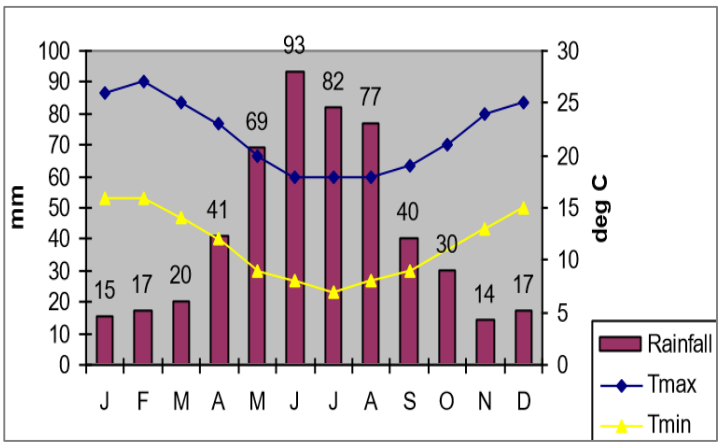

Figure 2: Climate of Western Cape (Adapted from Tadross and Johnston (2012))

2.3. Topography

The area is characterised by a low-lying landscape with elevations ranging between -14 to 833 m above sea level (Figure 1). The high elevation areas include Bredasdorpberge, Koueberge which form the source of tributaries contributing to Nuwejaars River and recharge areas for groundwater.

2.4. Landcover

Land cover is mainly natural and includes shrubland fynbos (limestone and sandplain), grassland, bushland and wetlands. Wheat, vines, orchards and livestock farming are the main activities in this region (Russell and Impson 2006). Elim town is the only urban development in the study area. Other urban areas in the Heuningnes catchment include Napier, Bredasdorp, Arnistorn, L'Agulhas and Struisbaai. Figure 3 shows land cover map acquired from UWC and percentage areal coverage for each class.

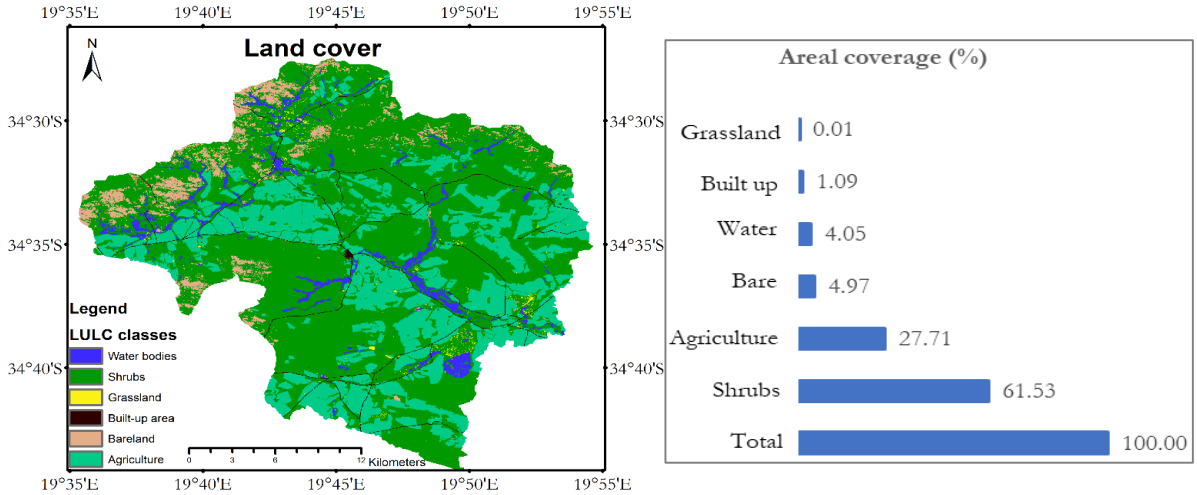

Figure 3: Land cover and percentage coverage of each class

2.5. Hydrology

The main tributaries (Figure 1) of Nuwejaars River include the Koue which rises from the Koueberge and Jan Swatskraal which rises from Bredasdorpberg. The river flows in the NW - SE direction and runs ~55 km from its primary source and drains into Soetendalsvlei. When Soetendalsvlei overflows, the excess water flows into Heuningnes river which forms an estuary draining into Indian ocean (Russell and Impson 2006). Several wetlands and pans (both seasonal and perennial) exist in the area.

2.6. Soil and lithology

Figure 4 shows the soil types in the study area. The dominant soil types in the study area are leptosols which are very shallow formed over hard rock or unconsolidated very gravelly material. These are followed by arenosols, which are mainly sand with little clay and humus featuring very little or no development. Solonetz have little concentration of organic matter, are characterised by water deficiency and require sufficient age to exhibit weathering and adequate development. Regosols occur on very limited shallow, medium to fine-textured unconsolidated parent material while luvisols, found mainly along river channels downstream of the study area are characterised by high activity clays. The soils in the catchment are very shallow with limited or no development (FAO 1995).

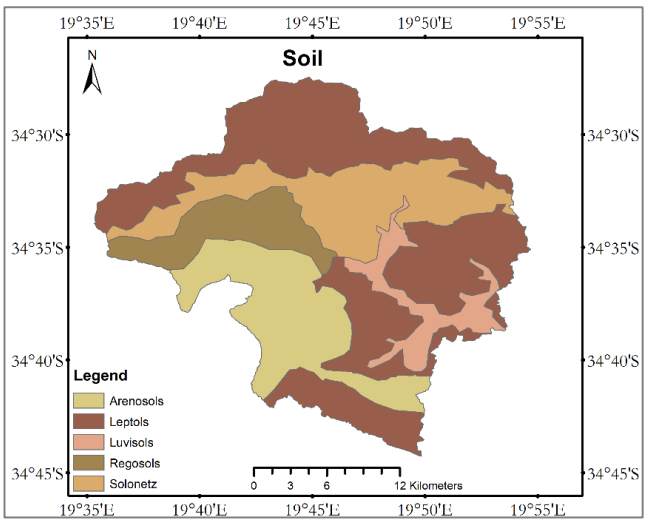

Figure 4: Dominant soil types in the study area ((FAO 1995)

2.7. Geology and Hydrogeology

The oldest rocks in the Nuwejaars catchment are the meta-sediments of Malmesbury group and Cape Granite Suite which are exposed mainly by faulting. The Malmesbury, formed during the late Precambrian period, consists of alternating layers of greywacke shale and muddy sands. An igneous rock of the Cape Granite Suite have intruded into the Malmesbury Group, and small outcrops are evident in the catchment. The Malmesbury and Cape Granite rocks are overlain by the largely arenaceous Table Mountain Group which underlies the argillaceous beds of the Bokkeveld group (DWS 2017).

The Table Mountain Group comprises the first division of the Cape Supergroup. It consists of quarzitic sandstones deposited during the Ordovician, Silurian and earliest Devonian periods and dominates the upper part of the catchment (Roets et al. 2008).

The Bokkeveld Group constitute the middle subdivision of the Cape Super Group. It consists of a succession of mudstones, siltstones and fine-grained sandstones deposited early to mid-Devonian. The Bokkeveld shale is a poor aquifer, and the little water produced from it tends to be brackish to salty (Lubke and De Moor 1998). This formation occurs in the middle section of the catchment near Elim (Delicado and Banda 2017).

In Nuwejaar catchment, the Bokkeveld formation is overlain by the Bredasdorp Group which occurs downstream around Soetandalsvlei. The Bredasdorp beds consist of Tertiary and Quaternary deposits of unconsolidated to semi-consolidated shelly, calcareous sands.

A summary of geological and lithological groups is outlined in Table 1 while Figure 5 presents the spatial variability of geology, and hydrological cross-sections for three transects across the the study area.

Era	**Period**	**Geological groups**	**Lithology**	**Hydro-stratigraphy**
Cenozoic	Quaternary & Tertiary	Bredasdorp beds	Unconsolidated to semi-consolidated shelly, calcareous sand	Low yield primary porosity aquifers
Devonian	Paleozoic	Bokkeveld	Shales and sandy shales	Low yield secondary porosity aquifers
Silurian-Ordovician	Paleozoic	Table Mountain	Quartz, sandstone, shale, siltstone and conglomerate	High yield secondary aquifers porosity, occurring at high depths
Pre-Cambrian		Cape granite suite	Basement rock	Aquiclude
		Malmesbury		

Table 1: Summary of the geological and lithological groups (Modified from Mazvimavi (2017)

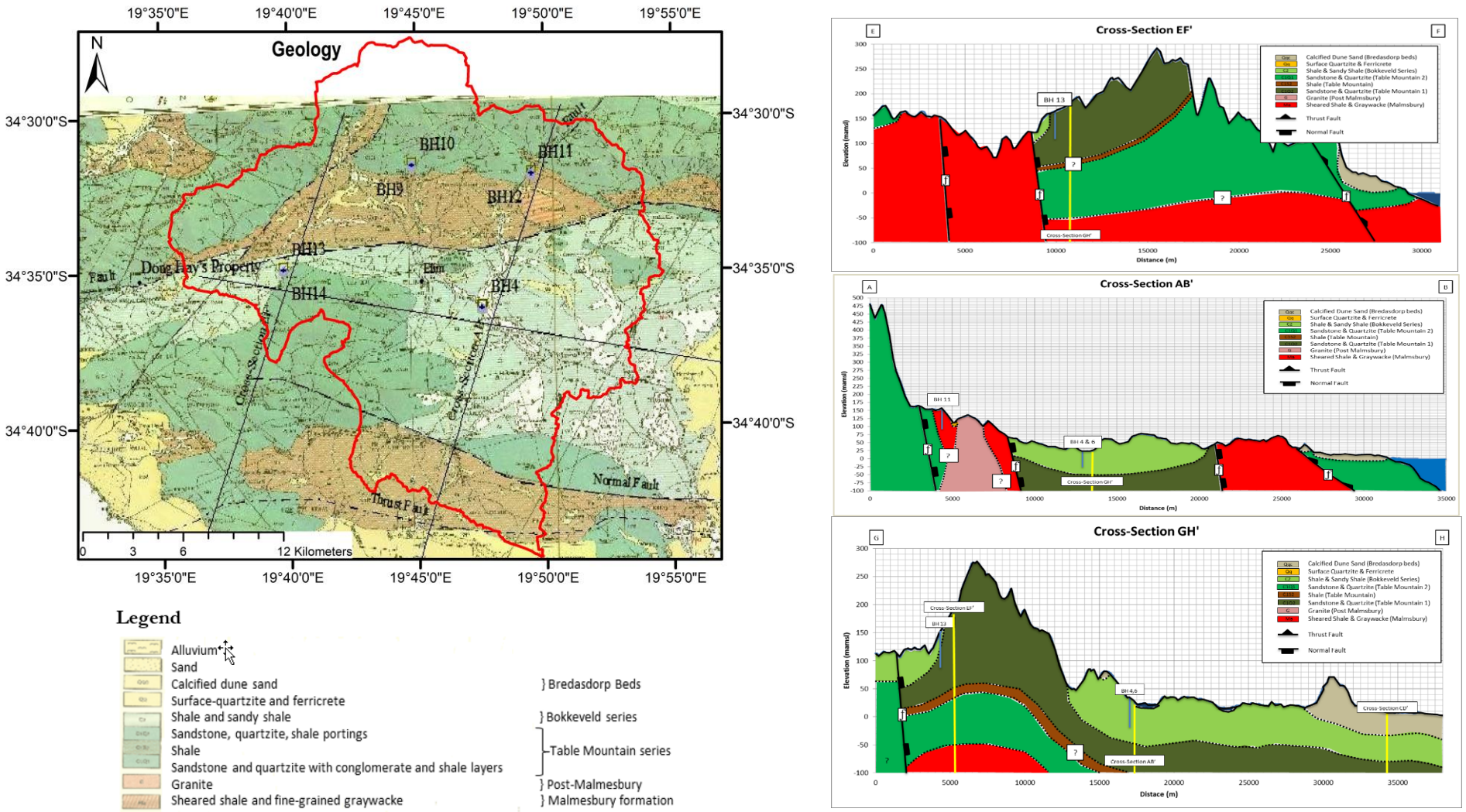

Figure 5: Geology and hydrogeological cross-sections (Delicado and Banda 2017)

2.8. Monitoring network and available data

Hydro-meteorological and hydro-geological data required (Table 2) for this study were acquired from UWC during fieldwork. The hydro-meteorological monitoring network (Figure 6) in the area comprises of 2 rain gauges, four weather stations, eight river gauges, and four groundwater level monitoring sites with 11 boreholes in total. The weather stations monitor rainfall, temperature, relative humidity, radiation and wind speed on hourly basis. The river flow and groundwater level monitoring stations are equipped with data loggers recording water levels every 15 minutes.

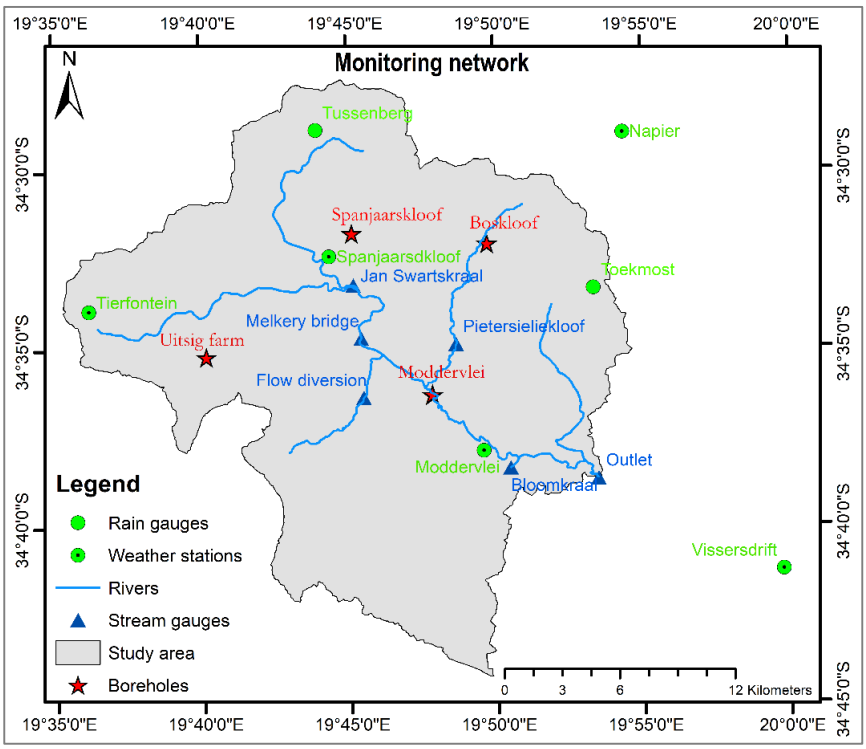

Figure 6: Monitoring network in the study area

Table 2: Available data (T_{max}- maximum temperature, T_{min} - min temperature, RH – relative humidity, K_h – saturated horizontal hydraulic conductivity, S_y – Specific yield, K_V- Vertical hydraulic conductivity of the unsaturated zone)

Required data	Available data	No. of stations	Observation period	Station symbol
Infiltration rates	Rainfall, Landcover	6	20/12/2014 – 4/9/2017	Green and dotted green circles
Potential evapotranspiration	T_{max}, T_{min}, min and max RH, Solar radiation, Air pressure	4	20/12/2014 – 4/9/2017	Green circles
Groundwater abstraction rates	-	-	-	-
Piezometric heads	Depth to groundwater	4	May 2017 – 4/9/2017	Red stars
Stream discharge	Water levels and rating curves	8	27/4/2016 – 4/9/2017	Blue triangles
Extinction depth	Land cover map	-	-	-
K_h, S_y	-	-	-	

3. METHODOLOGY

3.1. Methodology workflow

The overall methodology applied in this study is summarised in (Figure 7)

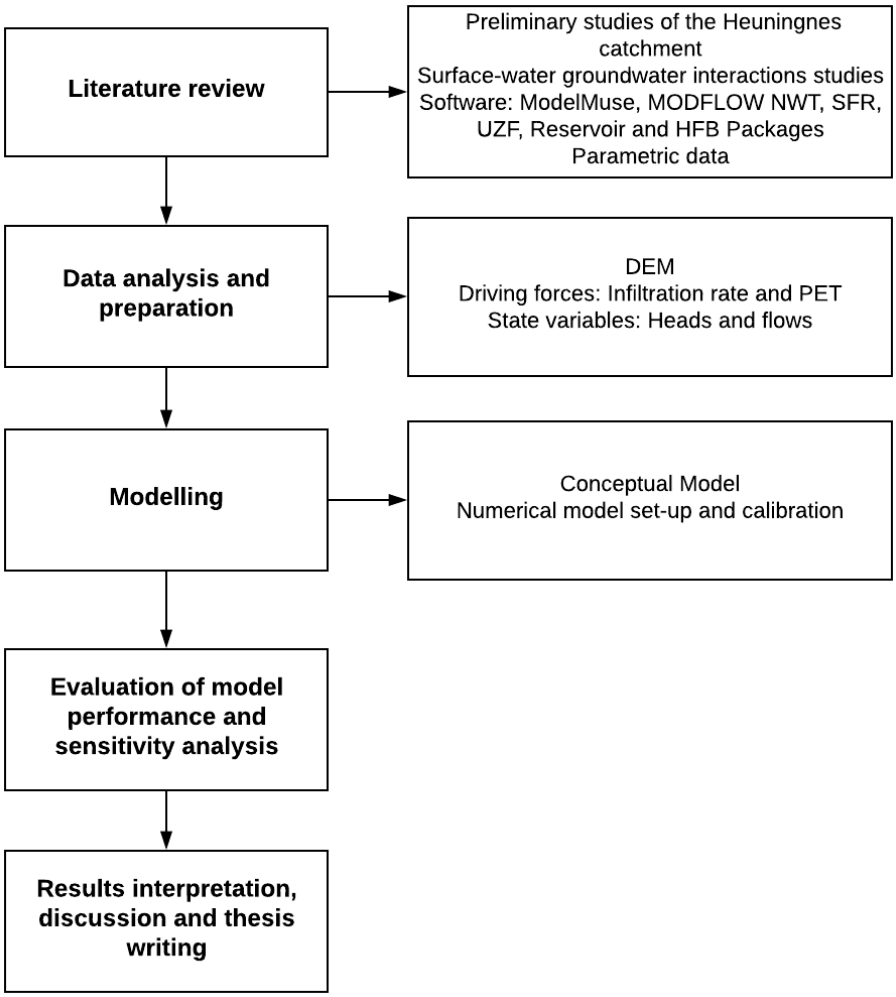

Figure 7: Schematic representation of the workflow

3.2. Review of surface-groundwater interaction studies

Several methods have been developed and used to investigate the interaction between surface water and groundwater. Three of the most used include: use of thermal data (USGS 2003), stable isotopes (Mazor 1997) and integrated hydrological models (Gupta 2010). However, each of these methods has its limitations. For instance, use of heat as a tracer violates some fundamental properties of the natural system as it assumes homogenous stream bed properties and one-dimensional groundwater flow system (Hatch 2016). On the other hand, stable isotopes assume steady-state conditions and therefore cannot provide a full picture of SW-GW interactions (Ala-Aho et al. 2015). Numerical models are data demanding and have been criticised on the basis of the validity of Darcian-based governing equations at larger scales (Sebben et al. 2013) as well as on the ability to represent small-scale hydrologic processes at a scale relevant for water resources management (Krause et al. 2014).

Anderson et al. (2015) argue that since the subsurface is hidden from view, a model is the most defensible description of groundwater system for informed and quantitative analyses as well as forecasts about the consequences of proposed actions. Process-based models are more preferred as they use processes and principles of physics to represent groundwater flow within the domain. Process-based models are solved mathematically using either analytical or numerical model. Analytical models require a high level of simplification, particularly related to spatial heterogeneity, and thus their application is limited to relatively simple systems, not appropriate for most of practical groundwater problems. Numerical models, on the other hand, allow for both steady-state and transient groundwater flow in three dimensions in heterogeneous media with complex boundaries and a complex network of sources and sinks. They are based on either the finite element or finite difference method and are most commonly used to solve groundwater and recently also surface-groundwater interaction problems.

Numerical models capable of investigating surface-groundwater interactions combine numerical solutions of surface water and groundwater flow equations. The two simultaneously simulate vertical water exchange between surface water bodies and the aquifers (Tanner and Hughes 2015) through the unsaturated zone. Some models, including Hydrogeosphere, MIKE SHE, CATHY, MODBRANCH, FHM, SWATMOD, and GSFLOW to mention a few, have been reported to have such capability of simulating both surface and subsurface water flows in a coupled manner. MIKE SHE and CATHY link ground and surface water components and were created as part of a unified model development process while MODBRANCH, FHM, SWATMOD, and GSFLOW were created by linking previously developed surface water and groundwater models (Said et al. 2005).

HydroGeosphere (Brunner and Simmons 2012) is a fully coupled numerical model that uses control finite element approach to simulate surface and sub-surface hydrological regimes and transport simultaneously. Rainfall input data is partitioned into components such as overland and streamflow, evaporation, infiltration, recharge and subsurface discharge into surface water features such as lakes and streams in a natural, physically-based manner.

MIKE SHE (Systeme Hydrologique European) is used to simulate flow and the transport of solutes and sediments in both surface water and groundwater (DHI 2007). However, it is a commercial software (Hughes and Liu 2008) and cannot handle variable grids (Said et al. 2005). The Catchment Hydrology (CATHY) model is a coupled process-based hydrological model representing 3-D saturated/unsaturated subsurface flow and 1-D overland/ channel surface flow. "The model uses a finite element solver for Richard's equation representing variably saturated porous media and a finite difference solver for the diffusion wave equation describing surface flow propagation throughout a hillslope and stream channel network identified using terrain topography and the hydraulic geometry concept" (Camporese et al. 2010). A threshold-based boundary condition switching procedure, which balances potential and actual fluxes across the land surface, is used to resolve the interactions between the surface and subsurface regimes.

SWATMOD links the SWAT model with the groundwater model, MODFLOW. A limitation of SWAT is its inability to model the unsaturated zone beyond the root zone and therefore recharge is applied directly to the groundwater table (Said et al. 2005). MODBRANCH links the one-dimensional model of unsteady flow in open channel networks (BRANCH) to MODFLOW. MODBRANCH simulates the interaction between streamflow and subsurface flow in areas with dynamic, hydraulically connected groundwater and surface water systems coupled at the stream/aquifer interface. However, the model does not include a module for simulating lake aquifer interactions. FHM links HSPF (Hydrological Simulation Program – Fortran) surface water model with MODFLOW and a GIS interface called HydroGIS which provides for the storage and analysis of all spatial data.

Ground-water and Surface-water FLOW (GSFLOW) model (Markstrom et al. 2008) is based on the integration of the U.S. Geological Survey Precipitation-Runoff Modelling System (PRMS) and the U.S. Geological Survey Modular Ground-Water Flow Model (MODFLOW). GSFLOW simulates flow within and among three regions which include: the area between the plant canopy and the lower limit of the soil zone; streams and lakes; the subsurface zone beneath the soil zone. PRMS is used to simulate hydrologic responses in the first region and MODFLOW is used to simulate hydrologic processes in the second and third regions.

Additionally, coupling standalone MODFLOW codes such as MODFLOW-2005 and MODFLOW-NWT with packages such as UZF, SFR, Lake and reservoir packages extends their capability to simulate surface-groundwater interactions.

3.3. Software and code selection

3-D transient state integrated hydrological model was required for Nuwejaar catchment to give an insight into the interactions between wetlands, streams and groundwater and their influence on water balance dynamics. MODFLOW-NWT (Niswonger et al. 2011), coupled with UZF1, SFR2 and Reservoir packages was used. MODFLOW-NWT is a Newton formulation of the finite difference MODFLOW-2005 (Harbaugh 2005). The code was selected due to (1) its ability to solve problems involving drying and rewetting nonlinearities of the unconfined groundwater flow equation as opposed to the Picard method used by MODFLOW-2005; and (2) it is an open-source software which operates under Model Muse (Winston 2009) GUI which is also available in the public domain.

ModelMuse offers the capability to define spatial inputs by drawing objects (points, lines or polygons) on top, front and side views of the model domain. These objects can be three-dimensional if they are assigned formulas that define their spatial extent. Formulas can also be used to assign spatial data both globally and for individual objects. This is advantageous since the model grids and simulation periods can be changed without altering the spatial data and boundary conditions.

MODFLOW NWT works with the Upstream-Weighting Package as a replacement to the Block-Centered Flow (BCF), Layer-Property Flow (LPF) and Hydrogeologic-Unit Flow (HUF) internal flow packages. The UPW package differs from the packages mentioned above in that it uses heads in two adjacent cells to calculate inter-cell horizontal conductance (Niswonger et al. 2011).

3.4. Conceptual model

A conceptual model is a schematization of what is known about the study area and thereby provides a basis for designing the numerical model (Kresic and Mikszewski 2013). "It consists of information on boundary conditions, hydro-stratigraphy and hydro-geological properties, flow directions, sources and sinks and preliminary water balance" (Anderson et al. 2015). Figure 8 shows the conceptualisation of groundwater flow system in the upper Nuwejaar River catchment.

3.4.1. Hydro-stratigraphic units

In this study, two hydro-stratigraphic units (Figure 8) were considered. The upper unconfined aquifer consists of Tertiary and Quaternary deposits of unconsolidated and weathered sand and shale with a thickness ranging between 10 to 25m. The second layer is a confined aquifer which extends from the top of the first layer to 100m below the mean sea level. It is composed mainly of sandstone, shale and quartzite of the Cape Supergroup (Bokkeveld and Table Mountain series). The bottom layer is underlain

by an aquiclude comprising meta-sediments of the Malmesbury group at ~100m below the mean sea level. The hydro-stratigraphic units were defined based on geological cross-sections in Figure 5 generated from borehole logs of 11 boreholes (Appendix 5) within the study area and three boreholes downstream of the study area.

3.4.2. Sources and sinks

Rainfall forms the only source of water in the catchment. Part of the incoming precipitation is intercepted by vegetation and eventually evaporated back to the atmosphere. Part of the amount that reaches the ground is infiltrated while the excess becomes overland flow which flows into the river channels and later to the lakes or sea.

The sources of groundwater in the study area include direct recharge by rainfall and seepage from rivers and wetlands. The groundwater outflows from the study area are by groundwater evaporation, groundwater contribution to the wetlands and streams, exfiltration, discharge into springs and lateral groundwater flow across the south-eastern boundary.

3.4.3. Flow direction

Nuwejaar river catchment is surrounded by Bredasdorp and Koue mountains to the north-west and north-east respectively, which form the sources of the tributaries of the Nuweejaar catchment and recharge areas for the groundwater. The conceptualisation of the groundwater flow system is therefore from the high hydraulic heads in the northern and western part to the lower heads in the south-east.

3.4.4. Boundary conditions

Boundaries conditions are defined based on either physical features such as large water bodies and impermeable rocks or stable hydraulic features such as water divides and streamlines (Anderson et al. 2015). In Nuwejaar catchment hydraulic boundaries were used as there were no physical features along the perimeter of the study area. The north-western boundary coincides with the water divide while the north-eastern and south-western boundaries are parallel to the streamlines. The south-eastern edge does not coincide with any hydraulic or physical feature, and thus the boundary conditions were defined based on the piezometric heads.

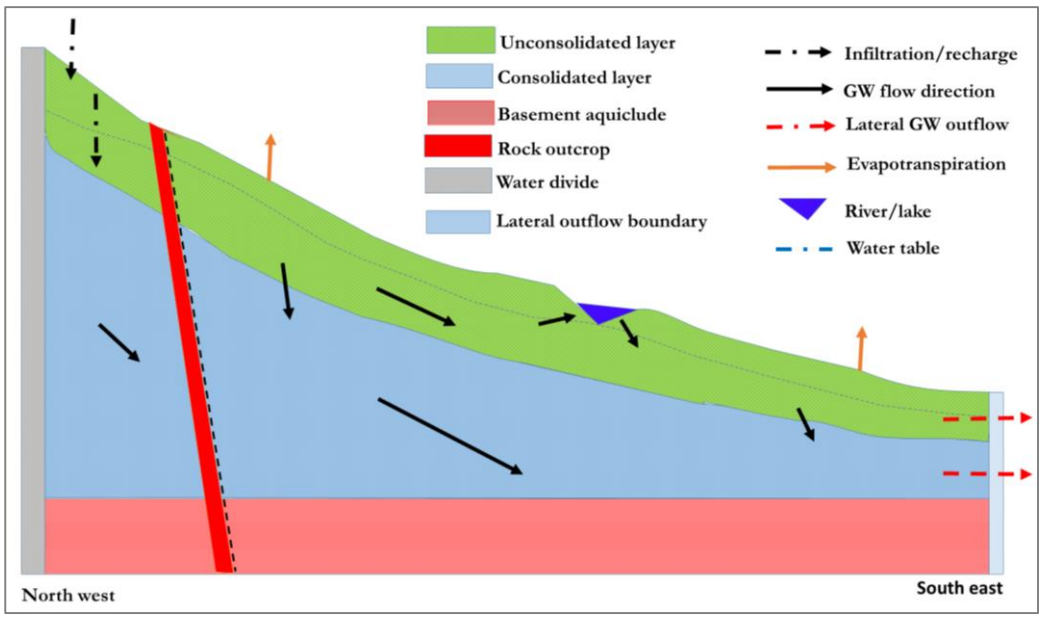

Figure 8: Conceptual model

3.5. Numerical model

3.5.1. Spatial grid design and vertical discretisation

The study area was discretised into block-centred rectangular grids of 100 m by 100 m. Such fine grid resolution was used to give a better representation of the system hence better simulation of the fluxes in the relatively flat terrain. Two layers were used to simulate vertical flow. Both layers were assigned as convertible to allow for the conversion of the bottom layer from confined to unconfined in case the water level drops below the bottom of the upper aquifer. The top layer was partly saturated, and the unsaturated zone of that layer was simulated using the UZF Package.

3.5.2. External boundary conditions

The perimeter boundary conditions defined in the conceptual model in section 3.4.4 were translated to numerical boundary conditions (Figure 99). The water divides and streamlines were simulated as specified flow (no flow) boundaries while the south-eastern boundary was simulated as a head dependent (general head) boundary. The general head boundary was used to account for lateral groundwater outflow from the study area.

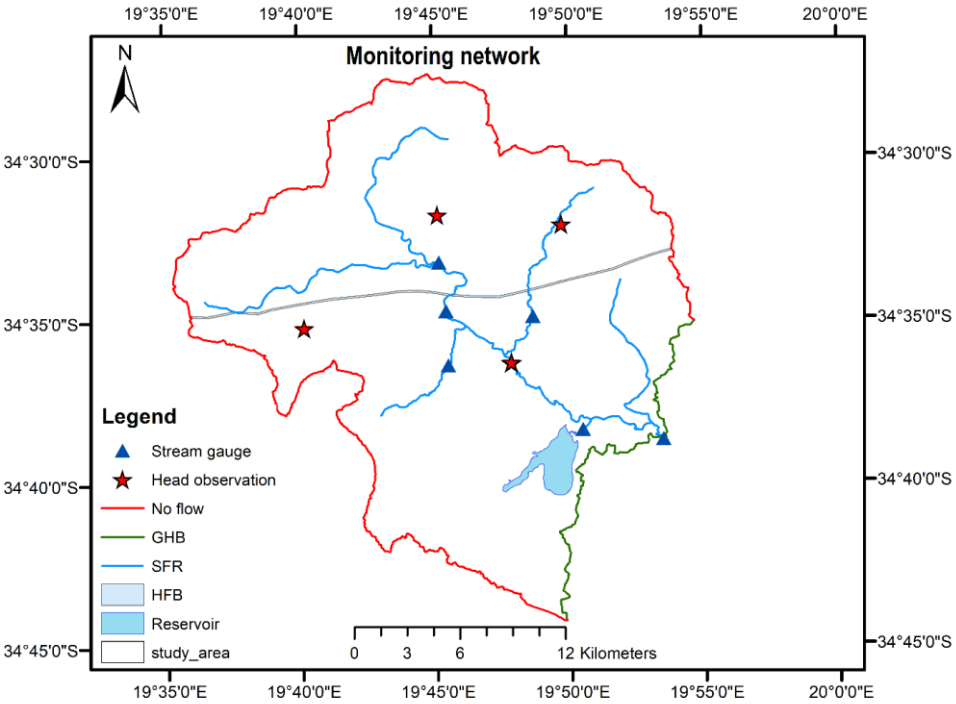

Figure 9: Numerical boundary conditions

3.5.3. Internal boundary conditions

Internal boundary conditions (Figure 9) were used to simulate sources and sinks within the study area. In this study, Reservoir (RES), Stream Flow Routing (SFR), and Unsaturated zone Flow (UZF) Packages were used to simulate vertical flow to and from the wetland, streams, recharge and groundwater evapotranspiration respectively. The Horizontal Flow Barrier (HFB) was used to simulate the fault across the study area.

Unsaturated zone

The UZF package was used to simulate flow through the unsaturated zone between the land surface and the water table. It is a substitute for both Recharge and Evapotranspiration MODFLOW packages which provides a more accurate approach for recharge estimation by taking into account the of effects of flow,

ET and storage in the unsaturated zone. The package uses a one-dimensional form of Richard's equation, to simulate flow through the unsaturated zone, and three-dimensional groundwater flow. The one-dimensional unsaturated flow is approximated by a kinetic-wave equation solved by the method of characteristic (Smith 1983) while the three-dimensional groundwater flow is solved using finite difference techniques. The one dimension simulation of unsaturated zone flow involves simplification of the Richards' equation to remove the diffusive term, assuming that the vertical flux is only driven by gravitational forces. The package calculates saturated and unsaturated zone evapotranspiration, gross groundwater recharge, groundwater exfiltration and change in unsaturated zone storage. Infiltration rate, potential evapotranspiration, evapotranspiration extinction depth, evapotranspiration extinction water content, initial unsaturated water content, saturated water content, Brooks-Corey exponent and maximum vertical hydraulic conductivity of the unsaturated zone are required as inputs.

Streams

Stream-aquifer interactions were simulated using the Stream Flow Routing (SFR2) package. Unlike River and SFR1 packages, SFR2 allows simulation of the unsaturated zone beneath the streams thanks to its compatibility with the UZF1 under MODFLOW NWT. This takes into account the time delay for water to flow from the stream to the water table especially in arid and semi-arid lands where the water table is deep.

SFR Package routes flow through a network of streams composed of segments and reaches. Each segment is assumed to have uniform rates of overland flow, precipitation, evapotranspiration and uniform or linearly changing properties. Stream-aquifer interactions are computed similarly to the River Package according to Equation (1).

$$Q = \frac{KwL}{M} * (h_s - h_a \qquad (1)$$

where Q is a volumetric flow between a given section of stream and volume of aquifer (L^3T^{-1}) , K is the hydraulic conductivity of streambed sediments (LT^{-1}), w is a representative width of stream (L), L is the length of stream corresponding to a volume of aquifer (L), M is the thickness of the streambed deposits extending from the top to the bottom of the streambed (L), h_s is the head in the stream (L), and h_a is the head in the aquifer (L).

Wetland/Lake

Hydraulic interactions between surficial aquifers and surface-water bodies, such as lakes wetlands and reservoirs can be simulated using MODFLOW Packages such as River, Reservoir (Fenske et al. 1996) and Lake Packages (Merritt and Konikow 2000) or the "high K" technique (Anderson et al. 2002). In this study, the wetland was modelled using the Reservoir Package. The package simulates leakage between lake and aquifer as the lake area expands or contracts in response to changes in lake stages. Leakages between the lake and aquifer are simulated for each active cell by multiplying the difference between lake stage and groundwater head by the conductance of the reservoir bed.

Land surface elevation of the reservoir bottom, vertical hydraulic conductivity, thickness of the reservoir bed and starting and ending stage for each stress period are required as inputs. However, the package does not allow for simulation of the unsaturated zone below the lake hence exchange between the lake and the groundwater system is assumed to be instantaneous. The package does not also account for any surface water budgets including inflow to and outflow from streams and operates independently of other stress packages (Fenske et al. 1996).

Fault

Faults can either be barriers or preferential flow channels depending on the hydraulic properties developed during deformation or can only separate units of different hydraulic conductivity (Ochoa-Gonzalez et al. 2015). The fault across the study area was simulated using Horizontal Flow Barrier (HFB) Package (Paul and Freckleton 1993) to assess whether it had any influence on groundwater flow dynamics.

3.5.4. Driving forces

Precipitation and potential evapotranspiration were required as the key inputs into the model with effective rainfall as the main driving force. The consistency and completeness of this data were thus crucial to achieve accurate spatial and temporal hydrological analysis and to ensure goodness-of-fit of the model. However, the available climatic data records were point measurements and had gaps (Figure 10). Time series reconstruction, consistency check and estimation of the spatial distribution of the data was thus required before it was input into the model.

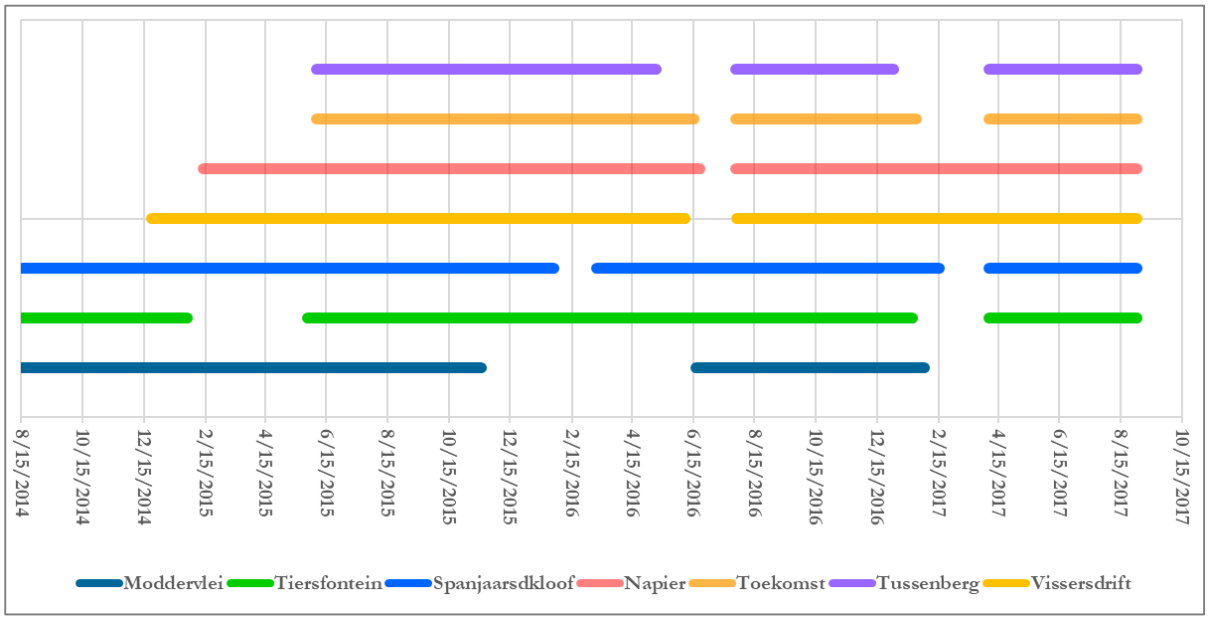

Figure 10: Record length of rainfall and weather stations

Precipitation

Processing of rainfall data involved gap filling, consistency check and spatial interpolation.

Review of available methods for time series reconstruction of rainfall data to select the most appropriate for this study negated the applicability of artificial intelligence (Kim and Pachepsky 2010) and geostatistical approaches (Ozturk and Kilic 2016) due to the high computational cost, complexity and lack of sufficient data points. Moreover, satellite rainfall estimates (CHIRPS) (Funk et al. 2015) exhibited little correlation with the in situ data and had a coarse resolution of 5 km which is not suitable for this study. Studies by (Chen and Liu 2012), (Chen and Guo 2016), showed that deterministic methods such as inverse distance weighting (IDW) method performed equally as good as geo-statistical methods. Consequently, since weather stations were reasonably well distributed in the catchment (Figure 6), exhibited high correlation in terms of data (Appendix 1) and the most distant stations were located 38 km apart (Appendix 2), IDW interpolation was applied for both time series reconstruction and spatial interpolation following Equation (2)

$$P_u = \sum_{i=1}^{n} \lambda_i P_i \qquad (2)$$

where P_u is the inverse distance estimate at the estimation location, $i = 1, \ldots n$ are the locations of the sample points, n is the number of sample points, λ_i are the weights assigned to each sample point, P_i are the conditioning data at sample points. The weights are determined as:

$$\lambda_i = \frac{\frac{1}{d_i^p}}{\sum_{i=1}^{n} \frac{1}{d_i^p}} \tag{3}$$

where d_i are the Euclidian distances between estimation location and sample points and p is the power or distance exponent value.

However, since the inverse distance weighting method is sensitive to the search distance, the number of data points and the exponent power (Babak and Deutsch 2009), it was crucial that an optimal parameter set was selected. Since the number of points were limited and were located close to each other (Figure 6), the search distance and the number of points were not defined. An exponent value of 2 was adopted following Weber and Englund (1992) who stated that "a power of 1 smooths out the interpolated surface while an increase in power reduces the weights of points located farther and thus the interpolated value tends to the value of the nearest point. Additionally, a power of 2 increases the overall influence of the known values".

After time series reconstruction, the data was checked for consistency using the double mass curve method as proposed by (Searcy et al. 1960). The Double Mass Curve is a plot of cumulative precipitation of station u against the average cumulative of neighbouring stations and is based on the principle that when each recorded data comes to same parent population, they will be consistent. A break in slope of the double mass curve plot indicates a change in precipitation pattern at station x. Precipitation at station x beyond the break point can be corrected using Equation (4).

$$P_{c(u)} = P_u \frac{M_c}{M_a} \tag{4}$$

where $P_{c(u)}$ - corrected precipitation at station x, $P_{(u)}$ - original recorded rainfall at station u , M_c - corrected slope of the double mass curve, M_a - original slope of the mass curve.

After gap filling and consistency check, the data was interpolated spatially using the inverse distance weighting method with a power of 2 in R software.

Interception

Interception loss refers to the amount of precipitation that is captured by vegetative canopy, stored temporarily as canopy storage before it is absorbed by the vegetation or it is returned to the atmosphere through evaporation (Merriam 1960). It is a function of vegetation characteristics (growth form, canopy density, plant structure and plant community structure) and climatic characteristics (precipitation amount, intensity, duration and frequency, wind speed and evaporation rates) (Chen and Li 2016). In this study, interception loss was estimated based on the land cover classes in the study area (Figure 3). The interception rates for different land cover classes were adopted from literature (Table 3) based on similarity in plant structure and climatic characteristics.

Table 3: Adopted interception rates

Land cover	Interception rate (%)	Literature
Shrubs	20	(Manning and Paterson-Jones 2007)
Agriculture (wheat and hay)	14	(Leuning et al. 1994)
Grass	7.9	(Corbett et al.)
Bare land and water bodies	0	-

Spatially variable interception loss per grid was calculated following Equation (5). Since agriculture in the study area is rain-fed, agricultural fields are cultivated only during the wet season (winter) while during the dry season (summer) they are left bare. Grass also dries out during the dry season while shrubs are evergreen. To account for this temporal variability, both grass and agricultural fields were assigned a rate of 5% (to account for interception by litter (Runyan and D'Odorico 2016)) during the dry season while a rate of 20% was applied for shrubs throughout the simulation period.

$$I = P * (I_A * A_A + I_S * A_S + I_G * A_G) \quad (5)$$

where I - canopy interception per grid cell [m day $^{-1}$], P - precipitation [mday^{-1}], I_A, I_S and I_G - interception loss rate by agriculture, shrubs and grass respectively in [%] of precipitation, and A_A, A_S and A_G – spatial coverage per grid for agriculture, shrubs and grass respectively.

Infiltration rates

Infiltration rate was required as an input in the UZF zone for simulation of unsaturated zone flow and storage, groundwater recharge and evapotranspiration. In the UZF context, infiltration rate refers to the amount of rainfall that reaches the land surface (Niswonger et al. 2006). It was estimated as rainfall minus interception loss. Since vertical flow through the unsaturated zone is limited by vertical hydraulic conductivity and the degree of saturation of the soil, infiltration excess water was routed to streams in the SFR Package.

Potential evapotranspiration

The amount of groundwater evapotranspiration depends on the availability of soil moisture, depth to water table and rooting depth among others. In MODFLOW-NWT groundwater evapotranspiration is simulated through the UZF package, and potential evapotranspiration (PET) is required as an input. In the definition of Mcmahon et al. (2013), PET refers to "the rate at which evapotranspiration would occur from a large area completely and uniformly covered with growing vegetation which has access to an unlimited supply of soil water, and without advection or heating effects".

To estimate PET, reference evapotranspiration was first calculated using the FAO Penman-Monteith equation. Reference evapotranspiration (ET_O) refers to the ET rate from an extensive surface of actively growing well-watered grass with a height of 0.12 m, fixed surface resistance of 70s m^{-1} and an albedo of 0.23 (Allen et al. 1998). The meteorological data i.e. minimum and maximum temperature, minimum and maximum relative humidity, air pressure, solar radiation and wind speed were used to calculate ET_0 following Equation (6).

$$ET_O = \frac{0.408\Delta(R_n - G) + \gamma \frac{900}{T_{mean}} u_2 (e_s - e_a)}{\Delta + \gamma(1 + 0.34u^2)} \quad (6)$$

where ET_O = reference evapotranspiration rate (mm d^{-1}), Δ = slope of the saturation vapour pressure curve (kPa^0C^{-1}), R_n = net radiation at the crop surface ($MJm^{-2}day^{-1}$), G = soil heat flux density (MJm^2day^{-1}), γ = psychometric constant (kPa^0C^{-1}), T_{mean} = mean air temperature (°C), and u^2= wind speed (ms^{-1}) at 2 m above the ground, e_s = mean saturated vapour pressure kPa), e_a= actual vapour pressure (kPa)

To reconstruct gaps in the time series data, correlation coefficients between stations were calculated for air temperature, air humidity and calculated ET_0. The correlation coefficients were quite high depicting low spatial variability of ET_0. Finally, gap filling, consistency check as well as spatial interpolation were done for the calculated ET_0 similarly as rainfall.

According to FAO-56 (Allen et al. 1998), ET_0 can be converted to PET in two ways, single and dual coefficient methods. In the single crop coefficient method, PET is calculated by multiplying the ET_0 by a single crop factor (Kc) which depends on crop type, height, albedo and its growing stage. The dual crop coefficient involves division of the crop coefficient into two factors; the first, characterises the evaporation differences and the second characterises the transpiration differences between the crop and the reference surface. The dual crop coefficient method requires more sophisticated data about crops and the soil which were not available for this study. Spatially and temporally variable single crop coefficient was thus applied following Equation (7). The K_c for summer months was assumed to be equal to the initial growing period (Table 4).

$$PET = ET_c = K_c * ET_o \quad (7)$$

Table 4: Adopted single crop coefficients (Allen et al. 1998)

Land cover	**Kc**	
	Initial and end (May to Oct)	**Mid (June to Sep)**
Shrubs	1.05	1.05
Agriculture (wheat and hay)	0.3	1.15
Grass	1	1
Bare land	0.4	0.4
water bodies	1.05	1.05

Groundwater abstractions

Due to the pretty high salinity of both surface and groundwater, agriculture in the study area is mainly rain fed. There are very few settlements within the catchment (Figure 3), and thus the water abstraction was assumed to be negligible.

3.5.5. Model parameterisation

Newton (NWT) Solver

Head tolerance [HEADTOL], flux tolerance [FLUXTOL] and 'Maximum number of outer iterations' were set as 0.0001m, 100 m^3 day^{-1} and 100 respectively and were adjusted during model calibration. Model complexity [OPTIONS] was set as complex following Niswonger et al. (2011) and Hassan et al. (2014). The portion of cell thickness used for coefficient adjustment (THICKFACT) was set as 0.00001 and the matrix solver as Chi MD(2).

UZF1

Infiltration and potential evapotranspiration rates were calculated as outlined in section 3.5.4. For the steady-state model, daily average rates, for the whole period, were used while for the transient model daily rates were used for each time step. Evapotranspiration extinction depth, which is the point below the surface where evapotranspiration ceases, was estimated based on maximum rooting depth for a given vegetation type and land cover. The rooting depths were outsourced from literature, and the adopted values are listed in Table 5. Spatially variable rooting depth per grid cells was calculated similarly to interception rates following Equation (5). Extinction water content, saturated water content, Brook's Corey exponent and vertical hydraulic conductivity of the unsaturated zone were assigned as 0.09 m^3m^{-3}, 0.5 m^3m^{-3}, 3.5 and 0.3 $m.d^{-1}$.

Additionally, recharge and discharge location was set as "Top layer", vertical hydraulic conductivity source as "specify vertical hydraulic conductivity", number of trailing waves as "15", number of wave sets as "20" and Route discharge to streams, lakes or SWR reaches, simulate evapotranspiration and calculate surface leakage options were selected. The options to specify residual water content [SPECIFYTHTR], and initial unsaturated water content {SPECIFYTHTI) were not selected. Initial and residual water content were thus calculated internally by the UZF1 Package, based on saturated water content and specific yield, to ensure continuity.

Table 5: Adopted maximum rooting depth based on land cover

Land cover	Rooting depth (m)	Literature
Shrubs	3	(Canadell et al. 1996)
Agriculture	1.8	(Allen et al. 1998)
Grass	2.3	(Shah et al.)
Bare soil	1.3	(Shah et al.)
Built-up and water bodies	0	-

SFR

For the SFR Package, options "unsaturated flow", "specify some streambed properties by reach", and "use transient streamflow routing with kinematic-wave equation" were selected. Tolerance, number of trailing wave increments, maximum number of trailing waves, maximum number of cells to define unsaturated zone, number of divisions per time step for kinematic waves, time weighting factor for the kinematic wave solution and closure criterion for the kinematic wave solution were set as 0.0001, 10, 30, 10, 1,1, 0.0001 respectively.

For each stream segment, streambed top was assigned as model top and same values as UZF were assigned to saturated volumetric water content, initial volumetric water content, Brooks-Corey exponent and maximum unsaturated vertical hydraulic conductivity. Stream slope was set as 0.025, streambed thickness as 0.8 to 2m, streambed vertical hydraulic conductivity as 0.003 to 0.3, stream width as 1 to 3m, channel roughness as 0.035 and were all adjusted during model calibration. Stream horizontal hydraulic conductivity was set as the hydraulic conductivity of the respective zone.

SFR Package allows several options for calculating stream depth which include: 'user specified stream depth [ICALC=0]', 'Manning equation for wide rectangular channels [ICALC=1]', 'Manning equation for an eight-point cross-section [ICALC=2]', 'depth-discharge and width-discharge relations ICALC=3]', or 'user-specified values of depth and width [ICALC=4]' based on observations at gauging stations (Prudic et al. 2004). However only the rectangular channel and eight-point cross-section options allow for simulation

of unsaturated zone beneath the streams (Niswonger and Prudic 2010). For simplicity, all the streams were simulated assuming rectangular channels (ICALC=1).

HFB

Barrier hydraulic conductivity for the simulation of fault was set as 1E-7 $m.d^{-1}$, barrier thickness as 100 m and was adjusted during model calibration.

Reservoir Package

Reservoir bed thickness was set as 2 m, reservoir elevation as model top and reservoir hydraulic conductivity as 0.5 m^3d^{-1} and were all adjusted during model calibration. Water levels recorded at the outlet were assigned as the starting and ending stages for each stress period.

General head boundary

The general head boundary head was assigned as 'model top', conductance per unit length as K_x, and conductance interpretation option was assigned as 'calculated'. Eventually, the GHB was changed to drain to allow for lateral groundwater outflow as the general head boundary was allowing groundwater inflow into the model domain.

Hydraulic conductivity and storage parameters

The hydraulic conductivity and storage parameters were used as model calibration parameters. Since pumping test data was not available, these parameters were estimated based on geology and lithological characteristics observed from borehole logs. The horizontal hydraulic conductivity (K_x) was estimated as 0.2 $m.d^{-1}$ for the first aquifer and 0.001 $m.d^{-1}$ based on the representative values outlined by Domenico and Schwartz (1998) and were adjusted accordingly during model calibration. Vertical hydraulic conductivity (K_z) was assigned as a tenth of K_x. Specific yield (S_y) and specific storage (S_s) are the storage coefficient for the unconfined and confined aquifers respectively. Spatially uniform values of specific yield and specific storage were assigned as 0.2 and 0.0005 respectively and were adjusted during calibration.

3.5.6. State Variables

State variables are the field observations used as calibration targets during model calibration. The field measured values are considered to be the true field conditions and thus are compared to the model simulated values during calibration to describe model fit and constrain the adjusted model parameters. In this study, groundwater heads and stream flows were used as the state variables.

Piezometric heads

There are 11 boreholes at four groundwater monitoring, (Figure 6) in the study area with time series data collected by UWC. The boreholes were drilled in May 2017 and monitoring started in mid-June 2017. Only one month of daily data was available within the simulation period (Figure 11). Boreholes 4, 6, 9, 11 and 13 monitor the bottom aquifer and the rest the top aquifer. Borehole 10, 11 and 12 had unexplainable erratic daily variations. Borehole 10 was entirely omitted during calibration while only the inconsistent values were excluded in borehole 11 and 12.

In ModelMuse, simulated heads were compared to observed heads using the Head Observation (HOB) Package. Point objects, imported as shapefiles, were used to specify the location of the head observations on model top view. The observation layer was defined by assigning the higher Z-coordinate and lower Z-coordinate of the respective layers. For each observation point, observation name, observation type time and observed head were required.

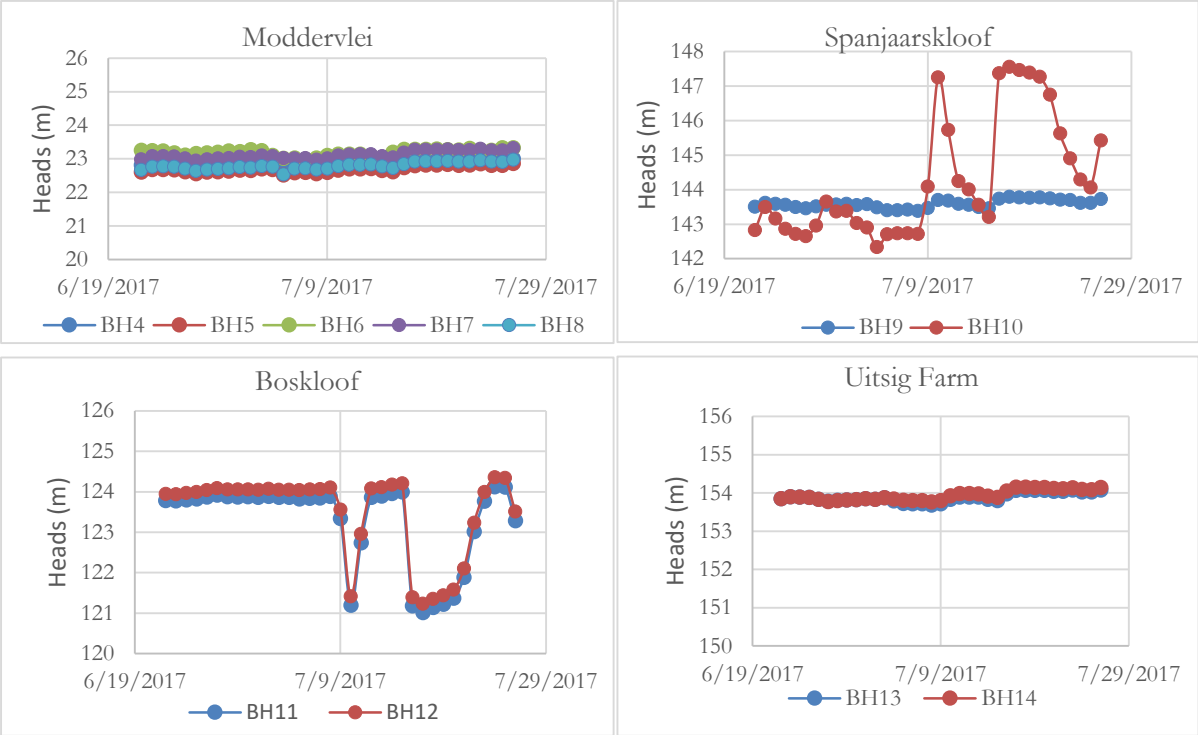

Figure 11: Observed piezometric heads

Stream flows

Nuwejaar River catchment has a total of 9 river gauging stations with 6 of them located within the study area (Figure 6). Apart from the Elandsdrift station which was installed in Dec 2014, all other nine stations were installed between April and May 2016. The stations are equipped with data loggers recording water levels every 15-minutes. The daily stages (Figure 12) were calculated by averaging the 15-minutes records and the flows estimated using the respective rating curves. In the SFR Package locations of the stream gauging stations were assigned by designating the respective stream reaches (model grids) as gauges.

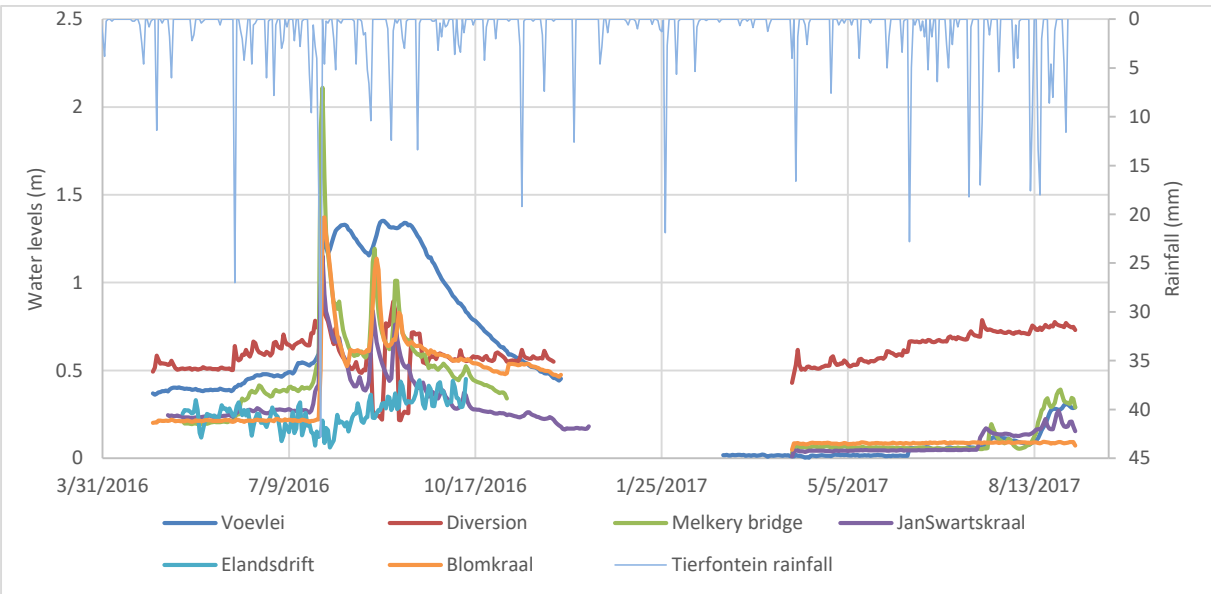

Figure 12: Observed stream levels

3.5.7. Steady and transient state simulation

The primary aim of this study was to quantify and analyse the spatial and temporal effects of surface-water and groundwater fluxes effects on water balance dynamics. To achieve this, a transient solution was required. The transient model was built for a period of 16 months (27th April 2016 to 31st Aug 2017), for which data was available. The simulation time was discretised into daily stress periods each with one time step resulting in a total of 492-time steps. The units of measurement were set to metres for length and days for time.

Model initialisation and warming up

According to Franke et al. (1987) and Anderson et al. (2015), initial time steps of transient models are strongly influenced by initial conditions. It is, therefore, a common practice to use heads generated by a steady-state model as the initial conditions for a transient model. Additionally, since steady-state models are simpler to create and execute, creation of a steady-state model before a transient simulation could give insight on system behaviour and response which could be useful in the implementation of the more complex transient solution. In this respect, a steady state model was built with interpolated heads from field observation as the starting heads. The resultant heads after calibration were used as the initial heads for the transient model.

Since large difference between initial conditions and the first time step of the transient model could lead to high water balance discrepancy (El-Zehairy et al. 2017), the transient model was warmed up for a period of 3 months to minimize the effects of the initial conditions further. However, contrary to several other studies where the warming up data was discarded (Hassan et al. (2014); Bakar (2015); Weldemichael et al. (2016), El-Zehairy et al. (2017)), three warm-up months together with the remaining twelve months of data was considered in the final transient model simulations in similar manner as Teketel et al. (2017) resulting in a total of sixteen months of valid data output.

Model calibration

Model calibration in both steady-state and transient models was done using manual trial and error method to provide an understanding of the model behaviour during the calibration process. The trial and error method involved adjustment of calibration parameters while targeting to simulate reasonable water balance and match simulated heads and flows to observed values. Calibration process was done in three steps. First, to establish the initial conditions for the transient simulation, a steady state model was calibrated based on average hydrologic conditions for the whole simulation period. This was followed in transient, by three-months warming up period to further reduce the effects of the initial conditions on the transient simulation and finally, the transient calibration was done within the whole simulation period. The steady-state model was calibrated mainly on heads.

Horizontal hydraulic conductivity (K_x), barrier hydraulic conductivity and maximum unsaturated vertical hydraulic conductivity ($K_{v(uz)}$) were used as the main calibration parameters. K_x was adjusted in zones, in the UPW Package, separately for each layer. Conductance of the drain cells and hydraulic conductivity of streambeds were adjusted as dependent on the K_x of the respective zone

Transient model, including the warming up period, was calibrated on both heads and flows. The process involved adjustment of hydraulic conductivity zones defined in the steady-state model. Additionally, stream, UZF and storage parameters as well as the hydraulic conductivity of reservoir beds were adjusted.

Evaluation of model performance

Performance of both steady-state and transient models was evaluated based on water balance closure and error in simulated heads and flows. For water balance, the model was assessed based on the discrepancy between total inflow and outflow. In most cases, an error of 0.1% is recommended though according to Anderson and Woessner (1992) an error of 1% is usually considered acceptable and was applied in this study.

Based on heads the model was evaluated using mean error (ME), mean absolute error (MAE) and root mean squared error (RMSE) following Equation (8) to (9) respectively. ME allowed for numerical check for overall bias in the calibrated model regarding over-estimation or under-estimation of heads and flows. On the other hand, MAE and RMSE were used to measure the average magnitude of errors. The RMSE was useful in checking for large errors as it gives them relatively high weights.

Additionally, a combination of calibration criterion by Anderson and Woessner (1992) and Mason and Hipke (2013), where the errors are compared to the total head loss in the model domain, was adopted. According to them, the degree of change in heads in a model domain decides the maximum satisfactory value of calibration criterion. The authors highlighted that if the maximum absolute error is less than 10% of the total head loss, MAE and RMSE are less than 2% of the total head loss and the ratio of the RMSE to the total head loss in the system is small, i.e. less than 10%, then errors are only a small part of the overall model system response.

$$\mathrm{ME} = \frac{1}{n}\sum_{i=1}^{n}(h_{obs} - h_{sim})_i \tag{8}$$

$$\mathrm{MAE} = \frac{1}{n}\sum_{i=1}^{n}|(h_{obs} - h_{sim})_i| \tag{9}$$

$$\mathrm{RMSE} = \sqrt{\left[\frac{1}{n}\sum_{i=1}^{n}(h_{obs} - h_{sim})_i{}^2\right]} \tag{10}$$

Where n, h_{obs} and h_{sim} are the number of observations, the observed head (m) and the simulated head (m) respectively.

Additionally, scatter plots of observed versus simulated values, plots of residuals were used. Scatter plots allowed for quick assessment of model fit as well as visualisation of bias in the calibration. Equal distribution of points along the central line indicated agreement between simulated and observed values hence the absence of bias.

For the transient model, visual comparison of hydrographs fit, Nash-Sutcliffe coefficient of efficiency (Nash and Sutcliffe 1970), relative volumetric error (RVE) were used to compare simulated to observed hydrographs. NS was used to assess the predictive power of the model regarding shape fitness while RVE was used to assess the mass/volumetric balance between the observed and the simulated counterparts following Equation (11) and (12) respectively.

According to Rientijes (2015), NS values of 1 indicate perfect model fit. NS values between 0.9 and 1 indicate that the model performs extremely well, values between 0.8 and 0.9 indicate that the model performs very well while values between 0.6 and 0.8 indicate that the model performs reasonably well.

Negative NS values indicate that the observed mean discharge is a better predictor than the model simulation. A relative volume error between +5% or -5% indicates that a model performs well while relative volume errors between +5% and +10% and between -5% and -10% indicate a model with reasonable performance. This criterion was used in this study.

$$\mathrm{NS} = 1 - \frac{\sum_{n-1}^{n}(Q_{obs} - Q_{sim})^2}{\sum_{n-1}^{n}(Q_{obs} - \overline{Q_{obs}})^2} \tag{11}$$

$$\mathrm{RVE} = \left[\frac{\sum_{i=1}^{n} Q_{sim(i)} - \sum_{i=1}^{n} Q_{obs(i)}}{\sum_{i=1}^{n} Q_{obs(i)}}\right] \tag{12}$$

where n is the total number of data elements, Q_{sim} and Q_{obs} are the simulated and observed runoffs at the nth time interval respectively and Q_{obs} is the mean value of the runoff over time.

Sensitivity analysis

According to Anderson and Woessner (1992) model parameters, conceptual model, observation data and boundary conditions are the four inherent sources of model uncertainties. Sources of model uncertainty can be identified through sensitivity analysis to identify parameters exerting the most influence on model results.

Sensitivity analysis of the steady-state model was based on the response of heads to the variation of selected model parameters and hydrologic stresses, and RMSE was used as the measure. Hydraulic conductivity, UZF parameters (maximum vertical hydraulic conductivity, saturated water content, extinction water content, extinction depth) and hydraulic stresses (Rainfall and PET) were tested.

Sensitivity analysis of the transient model focused on the response of groundwater fluxes (groundwater exfiltration, groundwater evapotranspiration, gross recharge and net recharge) to changes in hydraulic conductivity, storage parameters, extinction depth and maximum vertical hydraulic conductivity of the unsaturated zone.

Water balance

The water balance was analysed for the entire model domain, surface zone, unsaturated zone and saturated zone following Equation (13) to (20). The water balance of the surface zone was analysed by evaluating average precipitation and exfiltration as inputs and runoff, interception and infiltration as the outflows. The water balance of each layer in the saturated zone was evaluated using the zone budget (Harbaugh 1990). However, the water balance of the Reservoir Package was difficult to estimate as the package operates independently of other Packages and only interactions with groundwater are quantified (Fenske et al. 1996).

The entire catchment water balance can be expressed as:

$$P = ET + Q_s + Q_g \pm \Delta S \tag{13}$$

where: P - Precipitation, ET - total evapotranspiration, Q_s- stream flows at the outlet, Q_g - horizontal outflow across the south-eastern boundary of the catchment simulated through the general head boundary, ΔS - change in groundwater storage in the catchment.

The ET and ΔS terms in the above equation can be expressed as:

$$ET = ET_g + ET_{uz} + I \tag{14}$$

$$\Delta S = \Delta S_g + \Delta S_{uz} \tag{15}$$

where I is the canopy interception, ET_{uz} is the evapotranspiration from the unsaturated zone, ET_g is the groundwater evapotranspiration, ΔS_{uz} is the change in unsaturated zone storage and ΔS_g is the change in groundwater storage.

Streamflow at the catchment outlet (Q_s) can be expressed as :

$$Q_S = Q_H + Q_D + Q_B \tag{16}$$

where Q_H is Hortonian (infiltration excess) runoff, R_D is Dunnian (saturation excess) runoff and Q_B is base flow calculated as the difference between leakage from streams to groundwater ($Q_{s(in)}$) and leakage from groundwater to streams ($Q_{s(out)}$).

The land surface water balance is expressed as:

$$P + Exf_{gw} = I + Q_H + Q_D + P_{INF} \tag{17}$$

where Exf_{gw} is groundwater exfiltration

The unsaturated zone water balance is expressed as:

$$P_{INF} = R_g + ET_{uz} + \Delta S_{uz} \tag{18}$$

where R_g is the groundwater recharge and P_{INF} is the actual infiltration rate.

The saturated zone water balance of the two aquifers can be expressed as:

$$R_g + Q_{res(in)} + Q_{s(in)} = ET_g + GHB_{out} + Exf_{gw} + Q_{s(out)} + Q_{res(out)} \tag{19}$$

Following Hassan et al. (2014) and El-Zehairy et al. (2017), net recharge (R_n) is the amount of water that reaches the saturated zone less groundwater evapotranspiration and exfiltration and can be expressed as:

$$R_n = R_g - Exf_{gw} - ET_g \tag{20}$$

Figure 13 presents a schematic representation of the water balance components.

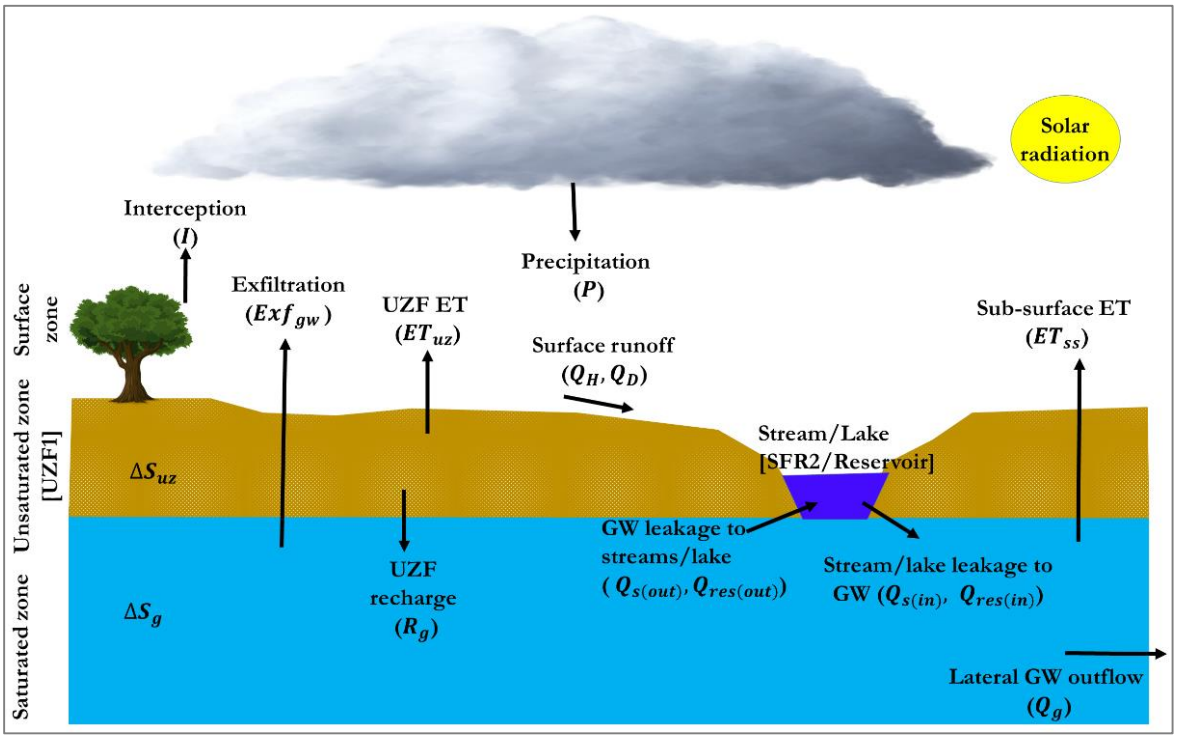

Figure 13: Schematic diagram of model set up and water balance components

4. RESULTS AND DISCUSSION

4.1. Model driving forces

4.1.1. Precipitation

Gap filling

Figure 14 shows gap filled daily time series rainfall from April 27, 2016, to August 31, 2017. The average total rainfall for the study period was 659.7 mm and a daily average of 1.4 mm. The wettest months were June, July and August with the highest rates observed in July 2016 while the driest was February to May with the lowest rates observed on March 2017. This was in agreement with the information obtained from the literature (section 2.2).

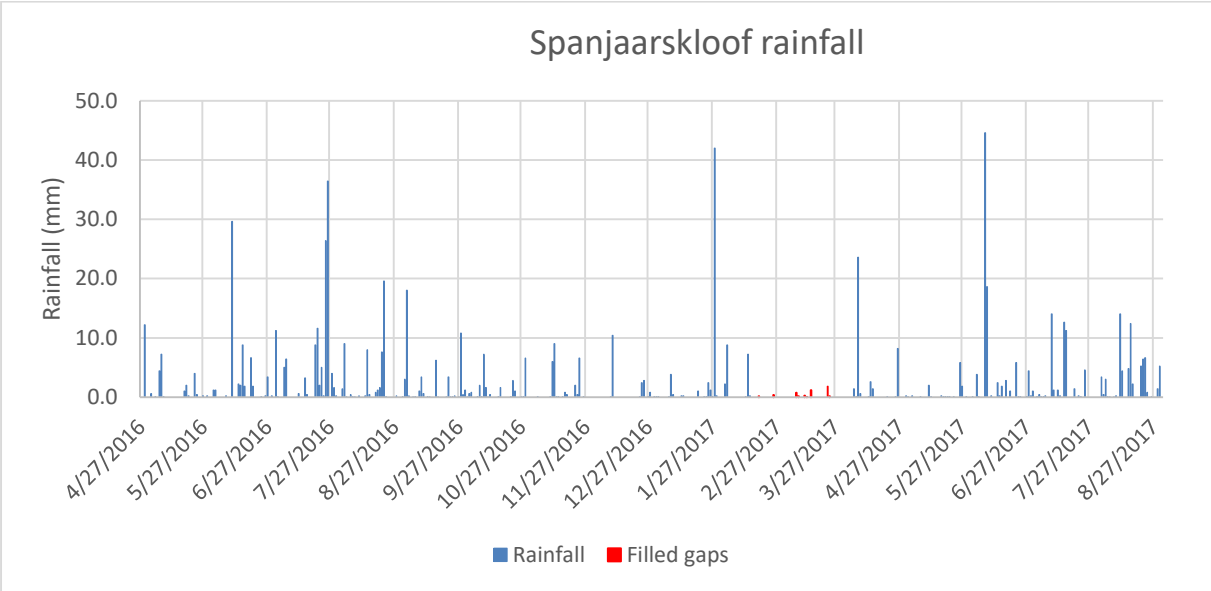

Figure 14: Gap filled time series daily rainfall at Spanjaarskloof Station

Consistency check

The double mass curve method was used to check for consistency in the gap filled time series to ensure that any trend detected in the time series data were due to meteorological causes and not to changes in the station or in observation methods. All plots (Figure 15) for the seven stations portrayed no break in slope and had regression coefficients above 0.98 which suggest a good agreement between each station and the average of a group of the remaining stations. This assured consistency of time series rainfall data hence spatial interpolation was done without applying any further correction.

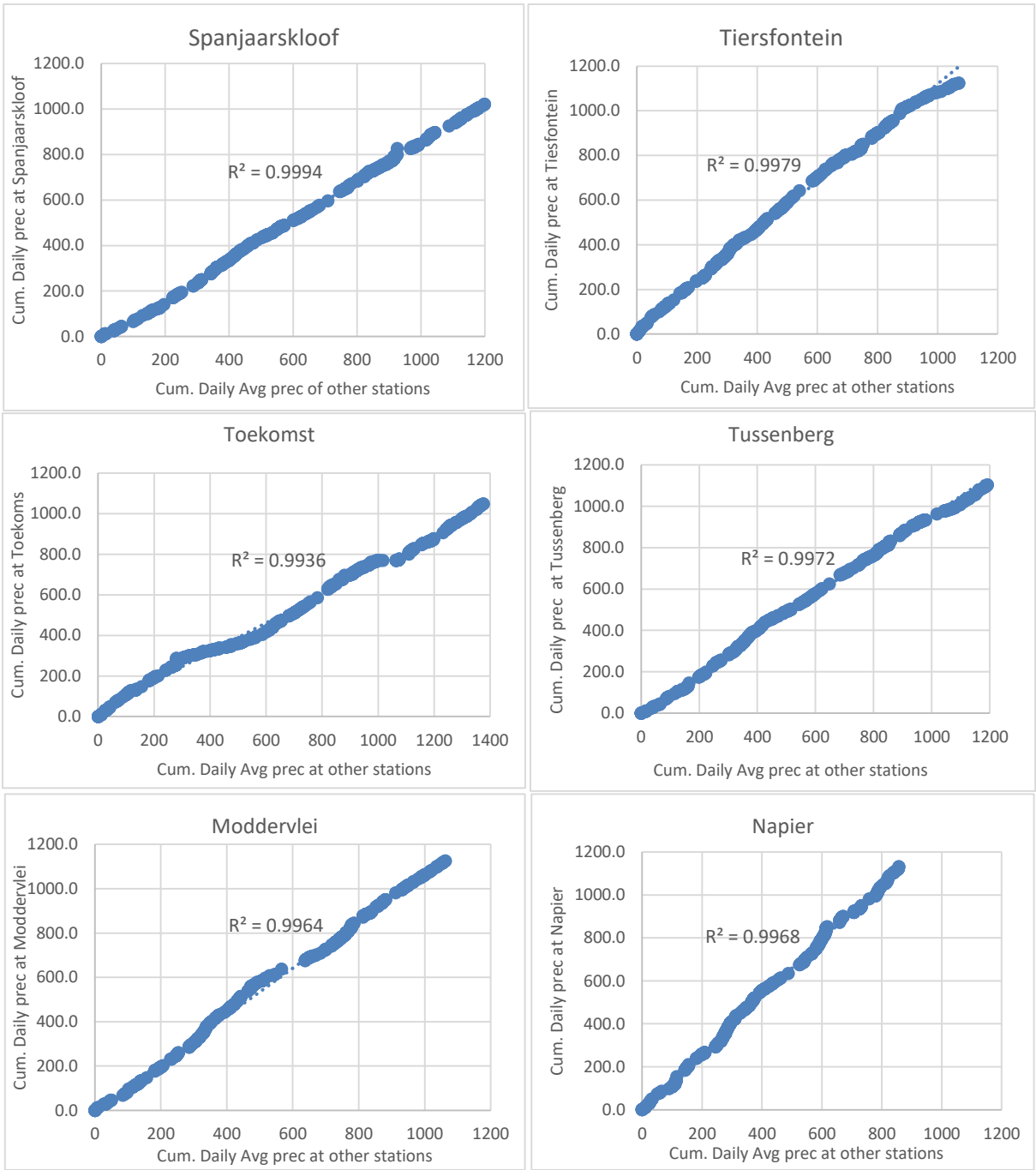

Figure 15: Cumulative daily rainfall time series for each station against cumulative daily average rainfall of the remaining stations

Spatial variability

Figure 16 shows the spatial variability of mean daily rainfall in the catchment. Rainfall portrayed a decreasing trend from upstream to downstream.

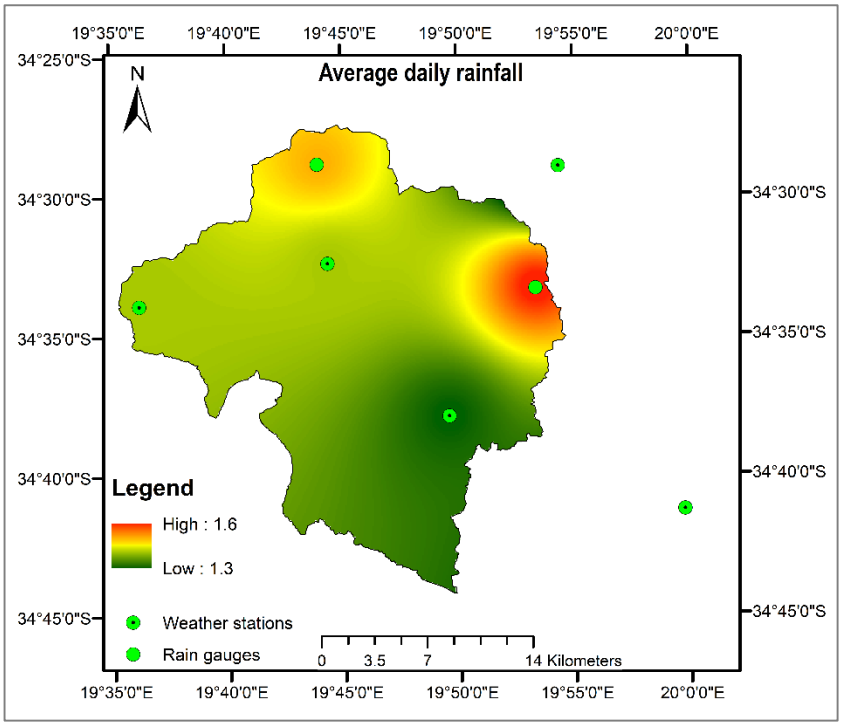

Figure 16: Spatially variability of average daily rainfall

4.1.2. Interception and infiltration rates

Figure 17 shows spatial variation of interception rates during the wet and dry season. Agricultural lands had the highest rate during the wet season and the lowest during the dry season since they are rain fed and are left bare during the dry season. Infiltration rates were calculated in the model by subtracting interception loss from rainfall.

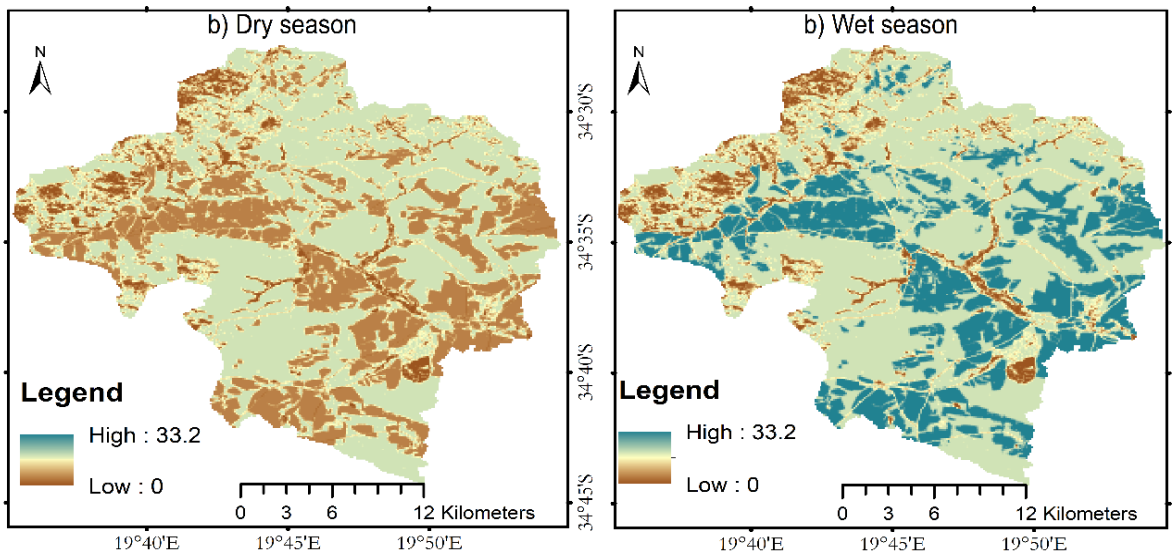

Figure 17: Interception rates during a) dry season and b) wet season, based on land cover map (Figure 3).

4.1.3. Potential evapotranspiration

Gap filling

The calculated and gap filled Penman-Monteith reference evapotranspiration at Spanjaarskloof Station is shown in Figure 18. ET_0 was highest during summer (dry season) when the net radiation was high hence high temperature, low relative humidity and eventually low high vapour pressure gradient which creates high evapotranspiration demand.

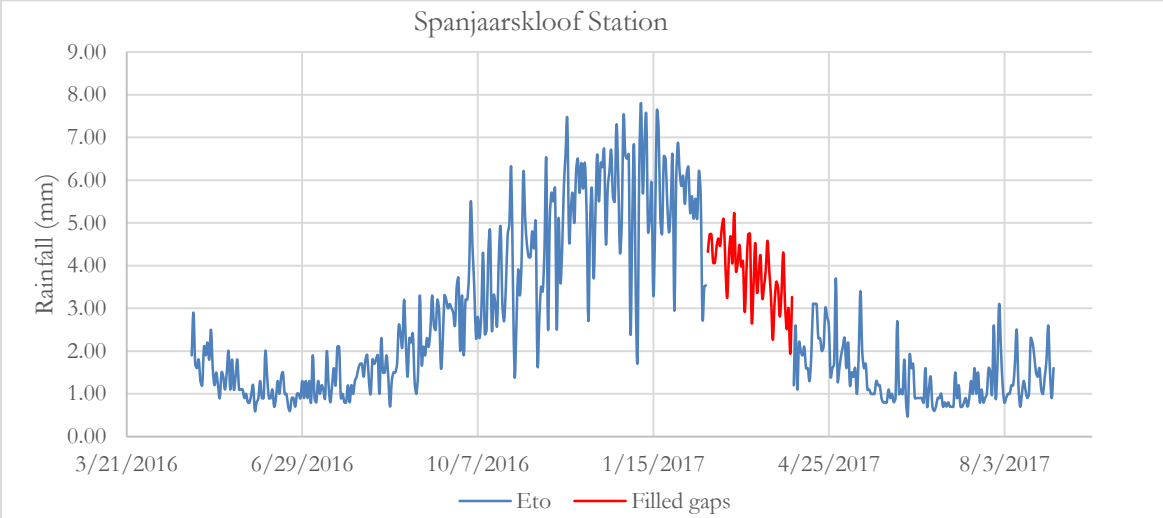

Figure 18: Gap filled reference evapotranspiration at Spanjaarskloof Station

Consistency check

The results for consistency check of gap-filled ET_0 are shown in Figure 19. No break points were observed in the reference evapotranspiration double mass curves, and the regression coefficients were more than 0.99 hence the data was interpolated without applying further corrections.

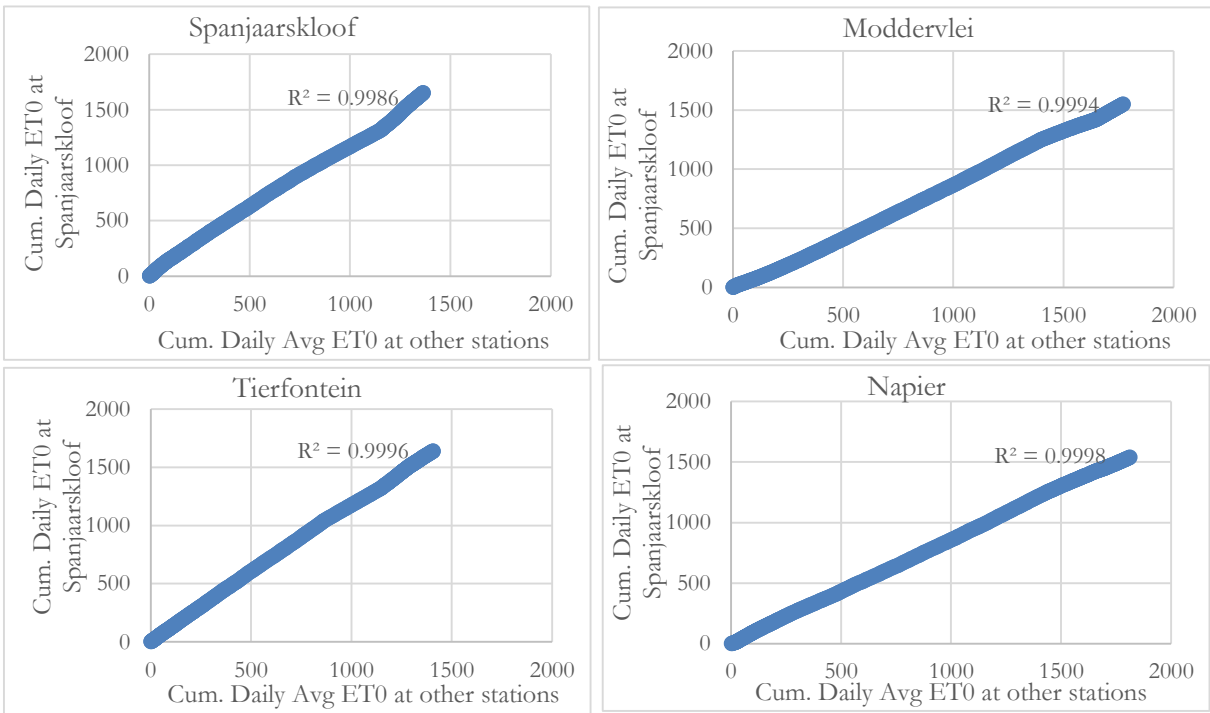

Figure 19: Plots of cumulative daily ET_0 at stations against cumulative daily averages at other stations (double mass curves)

Spatial variability

Figure 20 shows the spatial variability of reference evapotranspiration. ET_0 was found to have an inverse trend as compared to rainfall (Figure 16) with an increasing trend from upstream to downstream.

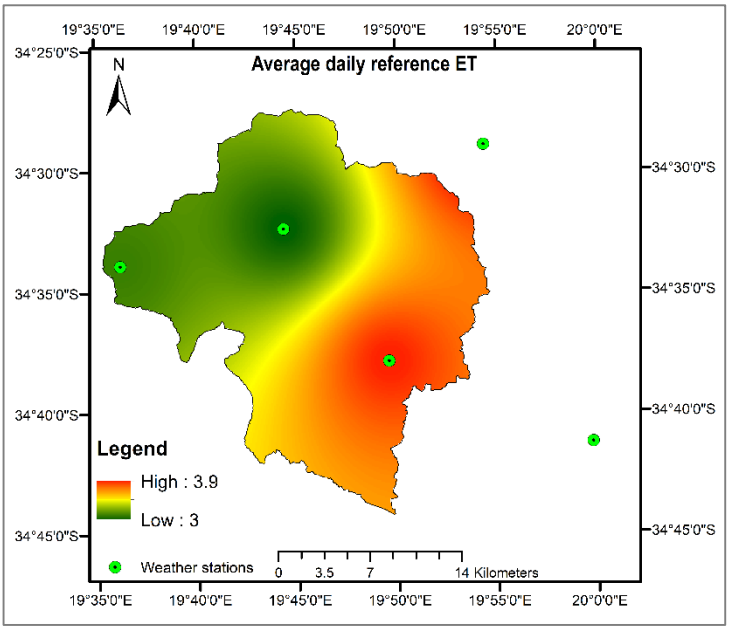

Figure 20: Spatial variability of reference evapotranspiration

Crop coefficients

Spatially and temporally variable crop coefficients used to convert ET_0 to PET are shown in Figure 21. The crop coefficients were highest for cultivated fields when the crops are actively growing and lowest for bare soil.

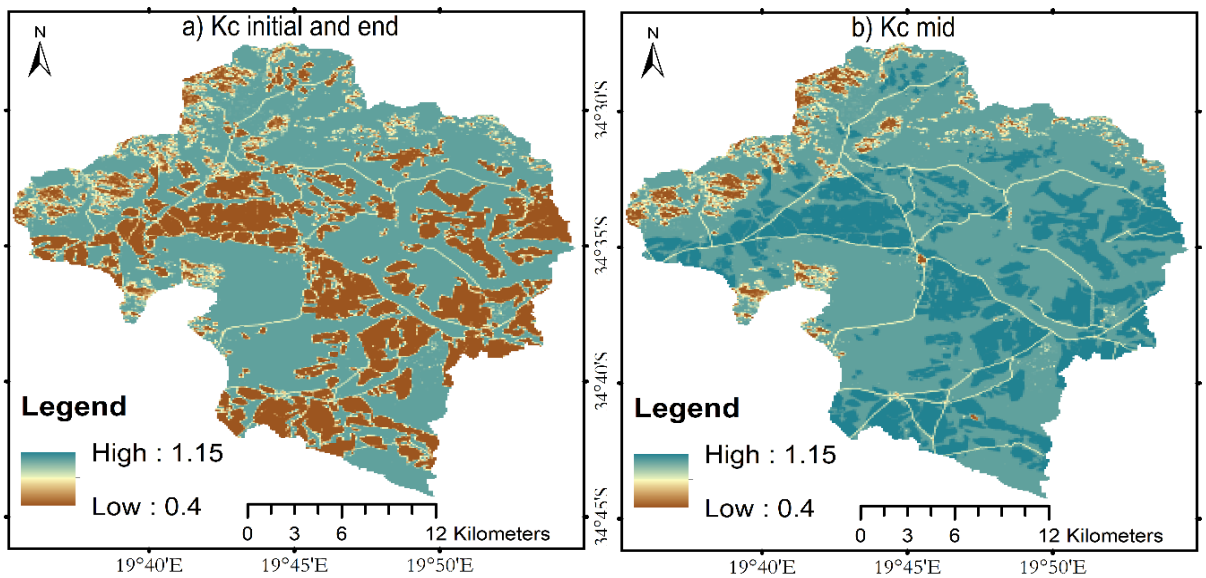

Figure 21: Kc values during a) initial and end of growing season and b) mid growing season based on land cover map (Figure 3).

4.1.4. Extinction depth

Figure 22 shows spatially variable rooting depth which was generated based on land cover map (Figure 3) and soil type (Figure 4). It varied between 0.5 to 3 m for shrubs and 0.5 for bare soil with seasonal grasses.

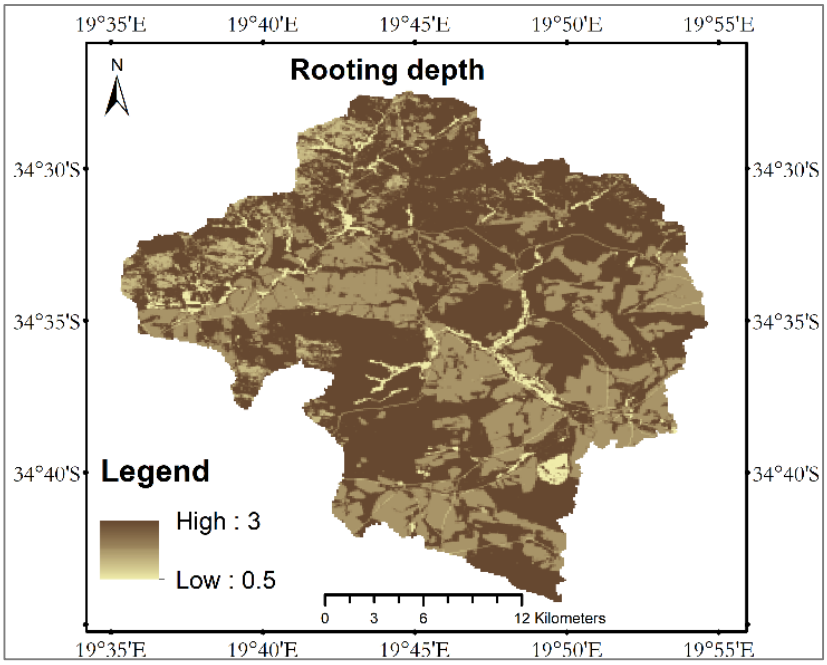

Figure 22: Extinction depth based on land cover map (Figure 3) and soil type (Figure 4)

4.2. Steady state model

4.2.1. Calibrated parameters

Calibrated horizontal hydraulic conductivity (K_h) ranged between 0.3 to 0.8 m.d^{-1} (Figure 23-a) for the first layer and was spatially uniform with a value of 0.01 m.d^{-1} for the second layer (not shown). High K_h values for the first layer were observed on one side of the Malmesbury rock outcrop and downstream where the terrain is relatively flat hence high likelihood of alluvial deposition.
Assigning low conductivity to the rock outcrop resulted in very high heads and the water table rose above the surface. This indicates that the outcrop is not a low permeability zone and probably has been subjected to faulting which is evident from the presence of two normal faults along the outcrop (Figure 5). Simulation of the fault as both, either horizontal flow barrier or preferential flow channel, had a minimal impact on the heads. The calibrated steady-state model parameters are outlined in Table 6.

Generally, groundwater flow system was found to be similar to the surface water system as seen from the contours (Figure 23-b) of the calibrated steady state model.

Table 6: Final calibrated steady-state model parameters: EXTDP - extinction depth; EXTWC - extinction water content; THT1 - initial volumetric water content; THTS – saturated volumetric water content; THTR – residual volumetric water content; K_{Vuz} –maximum vertical hydraulic conductivity of the unsaturated zone; Width- stream width; STRHC1 – streambed hydraulic conductivity; STRTOP - streambed top; STRTHICK – streambed thickness; SLOPE – stream slope; n – Manning's roughness coefficient, K – hydraulic conductivity; C_{drain} - conductance of the drain cells, HC_{res} –hydraulic conductivity of the reservoir beds – *Rbthck* - reservoir bed thickness. F indicates parameters that were assumed to be true and were not adjusted during calibration while C indicate parameters that were adjusted.

Vertical zone	Parameter	Minimum value	Maximum value	Unit	Status
Unsaturated zone	EXTDP	0.5	3	m	F
	EXTWC	0.12	0.12	m^3m^{-3}	C
	THTS	0.5	0.5	m^3m^{-3}	C
	KVuz	10	10	md^{-1}	C
Streams	Width1	0.8	3.5	m	C
	STRHC1	0.0001	0.05	md^{-1}	C
	STRTOP	0.5	2.1	m	C
	STRTHICK	0.5	1.5	m	F
	SLOPE	0.025	0.025	-	F
	n	0.035	0.035	-	F
Saturated zone	K (layer 1)	0.3	0.8	md^{-1}	C
	K (layer 2)	0.01	0.01	md^{-1}	C
Reservoir	*Rbthck*	3	3	m	F
	HC_{res}	0.008	0.008	md^{-1}	C

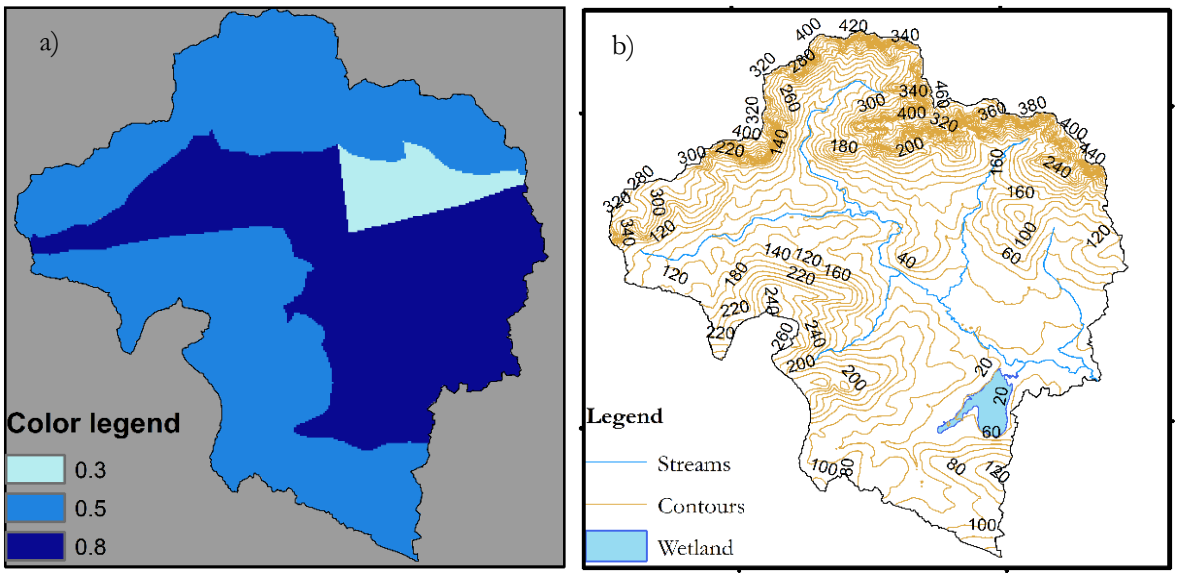

Figure 23: Steady-state model calibration results: a) Horizontal hydraulic conductivity (Kh) and b) potentiometric surface of the first layer

4.2.2. Calibrated heads and error assessment

Table 7 shows the coordinates, average observed heads, simulated heads, absolute error and squared error for each observation point. The values of ME, MAE and RMSE, were -0.12 m, 0.53 m and 0.60 m respectively. The maximum absolute error was 0.90 m. The water table (Figure 22) in the catchment ranged between 10m in the south-east and 570 m a.s.l in the north which made a head loss of 560 m.
The maximum absolute error, mean absolute error and root mean squared error were 0.06%, 0.035% and 0.04% of the total head loss respectively while the ratio of RMSE to the total head loss was 0.0004.
The mean error was -0.12 m indicating overall over-estimation of heads. This was confirmed by the plot of residuals versus heads (Figure 24) where more residuals were negative. The model was found to have fulfilled the evaluation criteria outlined in section 3.5.7 and thus was accepted as satisfactory to be used to initialise the transient model.

Table 7: Error analysis of heads after steady state calibration; H_{obs} and H_{sim} are observed and simulated heads respectively.

Station name	Observation point	Latitude	Longitude	H_{obs} (m)	H_{sim} (m)	Error (m)	Abs Error (m)	Error² (m²)
Moddervlei	BH 4	34°36'19.3"S	19°47'51.4"E	22.82	23.42	-0.60	0.60	0.36
	BH 5	34°36'19.2"S	19°47'51.2"E	22.62	23.44	-0.82	0.82	0.67
	BH 6	34°36'20.2"S	19°47'51.2"E	23.15	23.19	0.04	0.04	0.00
	BH 7	34°36'20.1"S	19°47'51.1"E	23.02	23.17	-0.15	0.15	0.02
	BH 8	34°36'19.1"S	19°47'50.8"E	22.71	23.42	-0.71	0.71	0.50
Spanjaarskloof	BH 9	34°31'46.5"S	19°45'09.2"E	143.50	143.92	-0.42	0.42	0.17
	BH 10	34°31'46.6"S	19°45'09.3"E	143.01	143.83	-0.82	0.82	0.67
Boskloof	BH 11	34°32'05.6"S	19°49'44.7"E	123.82	123.57	0.25	0.25	0.06
	BH 12	34°32'05.5"S	19°49'44.9"E	124.01	123.69	0.32	0.32	0.10
Uitsig Farm	BH 13	34°35'12.7"S	19°40'10.3"E	148.80	147.90	0.90	0.90	0.80
	BH 14	34°35'12.6"S	19°40'10.3"E	148.83	148.07	0.76	0.76	0.58
						ME	MAE	RMSE
						-0.12m	0.53m	0.60m

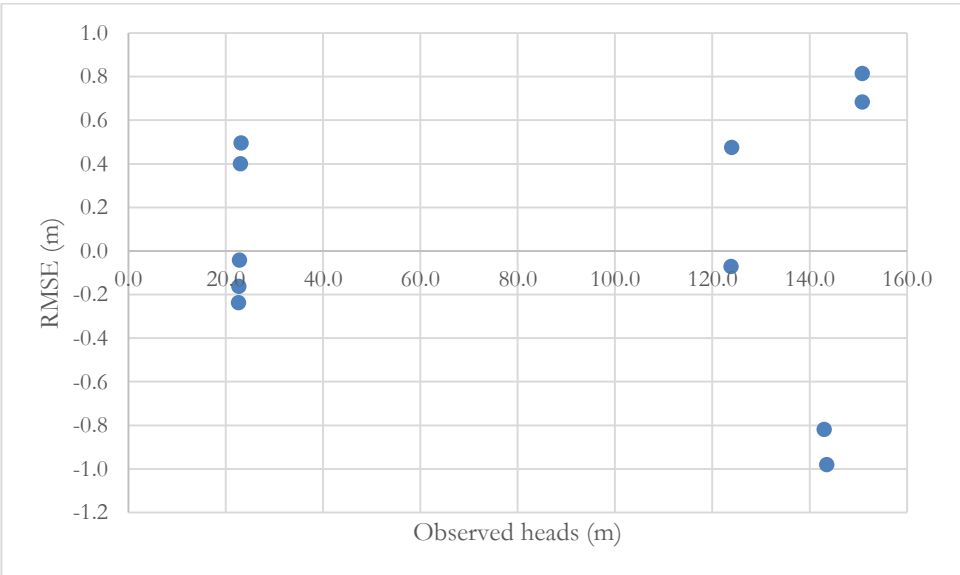

Figure 24: Plot of observed heads versus residuals

As an additional calibration control, the calibrated water table was compared to the topographic surface (DEM) to check if it was below the surface. All cells were found to have the water table below the surface (Figure 25). The water table was very shallow along the river channels and downstream of the catchment and was deepest at the mountains in the northern part of the study area.

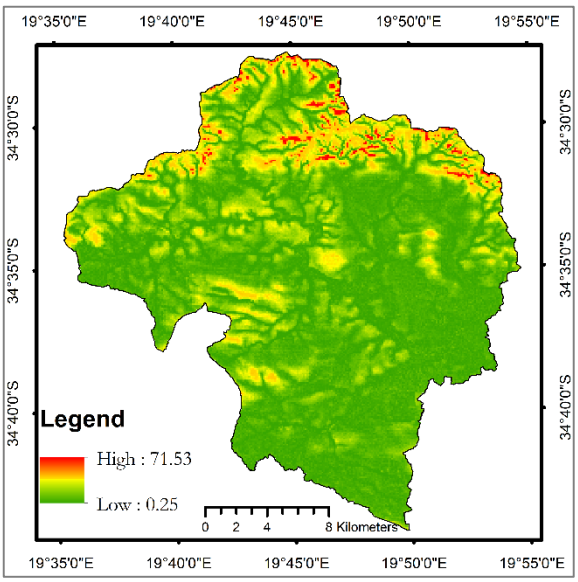

Figure 25: Depth to water table

4.2.3. Sensitivity analysis

Figure 26 shows the response of heads to changes in hydraulic conductivity. The calibrated heads were very responsive to both increase and decrease in K_h with higher sensitivity to low values.

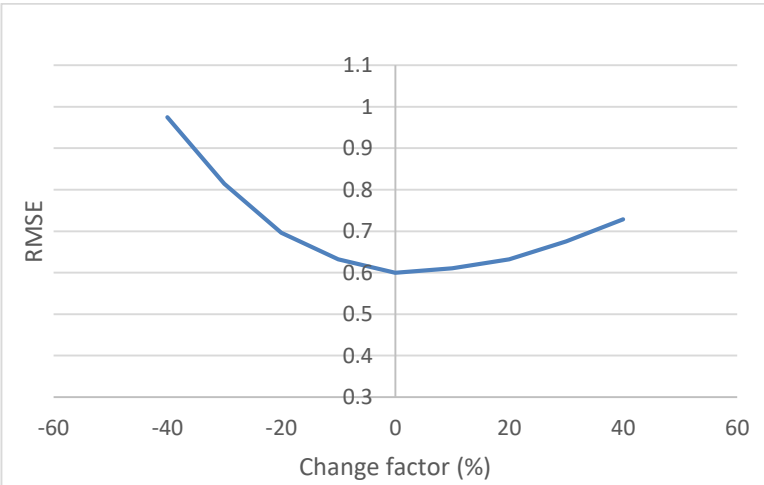

Figure 26: Sensitivity of steady state model hydraulic conductivities on heads

Head sensitivity to UZF parameters (Figure 27) was quite low with most substantial sensitivity to higher values of extinction depth (Figure 27-c) while extinction water content (Figure 27-b) and saturated water content were (Figure 27-d) were completely insensitive. Heads showed little response to changes in K_{Vuz}.

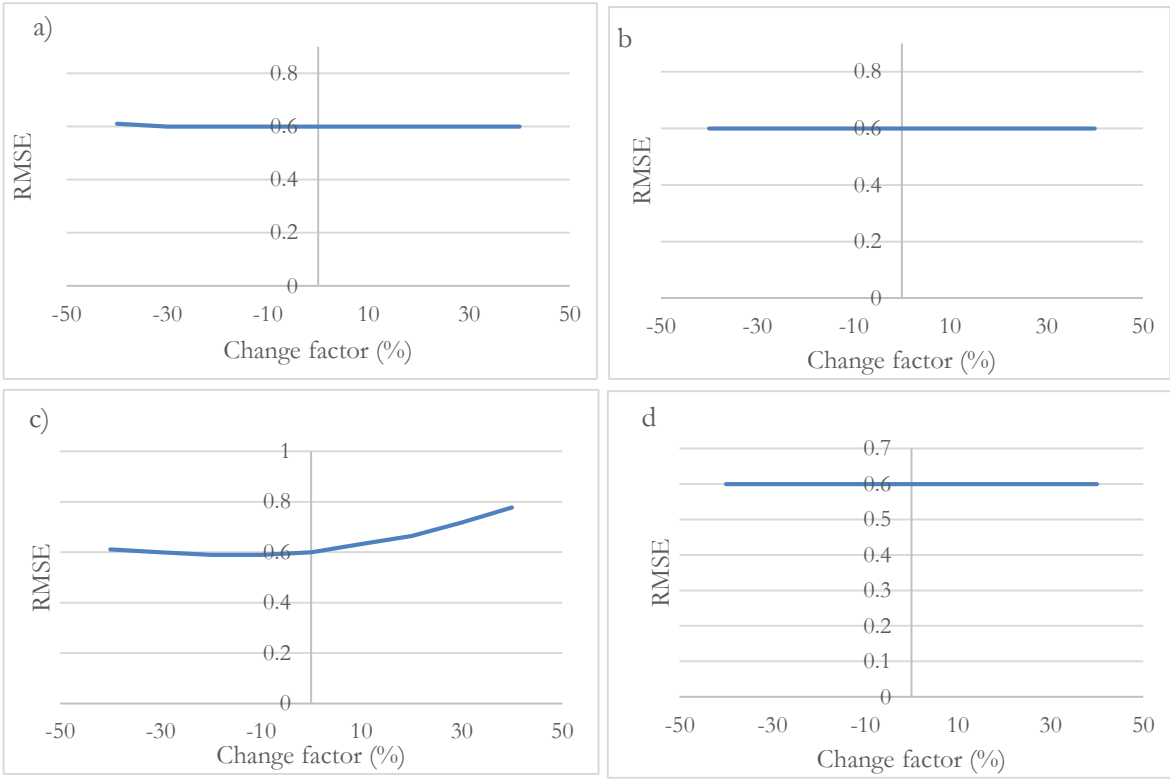

Figure 27: Sensitivity of steady state UZF parameters on heads: a) K_V of the unsaturated zone, b) saturated water content, c) extinction depth and d)extinction water content

Figure 28 shows the effect of changing hydrologic stresses (infiltration rate and PET) to calibrated groundwater heads. The model was sensitive to infiltration rates with higher sensitivity to decreasing values (Figure 28-b), and inverse response was observed with PET where the model was less sensitive with a higher response to increasing values of PET (Figure 28-a).

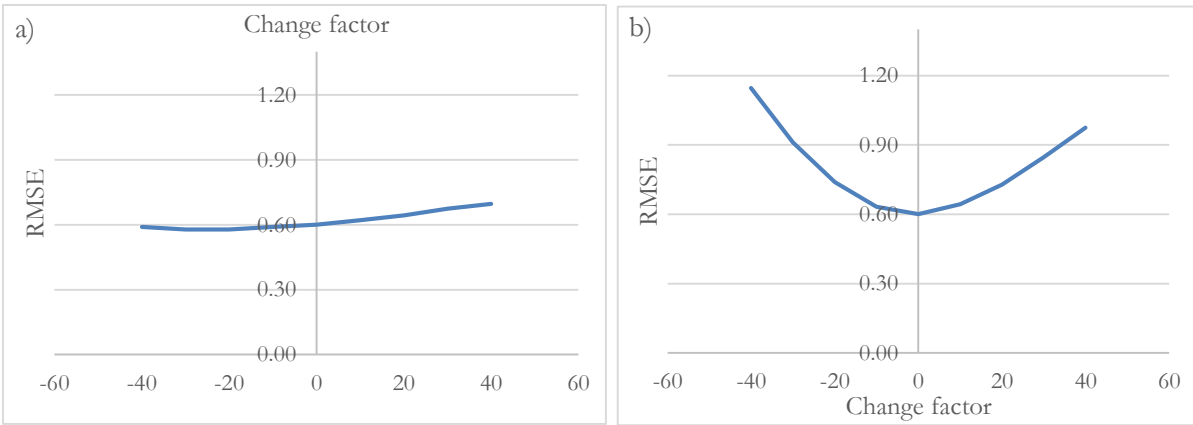

Figure 28: Sensitivity of the calibrated steady state model to hydrologic stresses: a) PET and b) Infiltration rate

4.2.4. Water balance

Water balance of the entire model domain

Table 8 presents annual average flows of the steady state model, accounting for all inflows and outflows. Precipitation was the only input into the model (P = 1.4 $mm.d^{-1}$), and outflows consisted of evapotranspiration (ET = 63.6% of P), stream discharge at the outlet (Q_s = 33.6% of P) and lateral groundwater outflow through the drain (Q_g =0.7% of P). The subsurface evapotranspiration included both unsaturated and saturated zone evapotranspiration as they are not distinguished in the steady-state model (Niswonger et al. 2006). The water balance closed with a discrepancy of 1.69%.

Table 8: Water balance of the entire model domain in steady-state condition

Budget component	In ($mm.yr^{-1}$)	Budget component	Out ($mm.yr^{-1}$)
Precipitation	511.0	Subsurface evapotranspiration	251.9
		Interception	76.5
		Lateral GW outflow	3.7
		Stream discharge at the outlet	171.6
Total in	511.0	Total out	511.0
		In - out	7.6
		Error (%)	1.5

Water balance of the surface and unsaturated zone

The water balance of the surface (Table 9) included two inflow components (P =74.9% and Exf_{gw} = 25.1%) and three outflow components, I (14.2% of P) , P_{INF} (84.2% of P), and R_0 (34.3% of P). The water balance of the surface zone closed with a discrepancy of 0.72%.

For the unsaturated zone infiltration rate was equal to the gross recharge.

Table 9: Water balance of land surface and unsaturated zone in steady-state condition

Budget component	IN ($mm.d^{-1}$)		Budget component	OUT ($mm.d^{-1}$)
Precipitation	511.0		Interception loss	76.5
Groundwater exfiltration		171.6	Infiltration	430.7
			Total Runoff	175.2
	682.6			678.9
			In - out	3.7
			Error (%)	0.5

Water balance of the saturated zone

Groundwater balance (Table 10) includes three inflow components with R_g as the main component while $Q_{s(in)}$, and $Q_{res(in)}$ were negligible; and five outflow components where ET_g = 58.5% and Exf_{gw} = 39.8% were the main components while $Q_{s(out)}$, $Q_{res(out)}$ and lateral groundwater outflow were negligible. The reservoir was found to gain from groundwater while the base flow ($Q_{s(in)}$ - $Q_{s(out)}$), was negligible.

Table 10: Water balance of the saturated zone in steady-state condition

Water budget component	IN (mm.yr^{-1})	Water budget component	OUT (mm.yr^{-1})
Stream leakage to groundwater	0.1	Subsurface evapotranspiration	252.1
UZF recharge	429.4	Groundwater exfiltration	170.0
Reservoir leakage to groundwater	1.3	Stream leakage from groundwater	0.1
		Reservoir leakage from groundwater	4.8
		Lateral groundwater outflow	3.8
Total in	430.8	Total out	430.8

Water balance of each layer (Table 11) calculated from the zone budget show similar results with that of the whole model domain where UZF recharge was the main inflow to the upper layer with ET_g and Exf_{gw} as the main outflows. The inflow into the bottom layer was only through exchange with the top layer while the outflow included exchange with the top layer (90%) and outflow through the drain (10%).

Table 11: Water balance of each aquifer layer

Water balance component	**Fluxes (mm.yr^{-1})**			
	Top layer		Bottom layer	
	IN	OUT	IN	OUT
Head dependent boundary	0.0	1.0	0.0	2.8
Reservoir Leakage	1.3	4.8		
Stream leakage	0.1	0.1		
Sub-surface ET	0.0	252.1		
UZF recharge	429.4	0.0		
Surface leakage	0.0	170.0		
Exchange between aquifers	26.5	29.3	29.3	26.5
Total	457.3	457.3	29.3	29.3

Figure 29 gives summary of fluxes between various zones and compartments in the form of a schematic diagram.

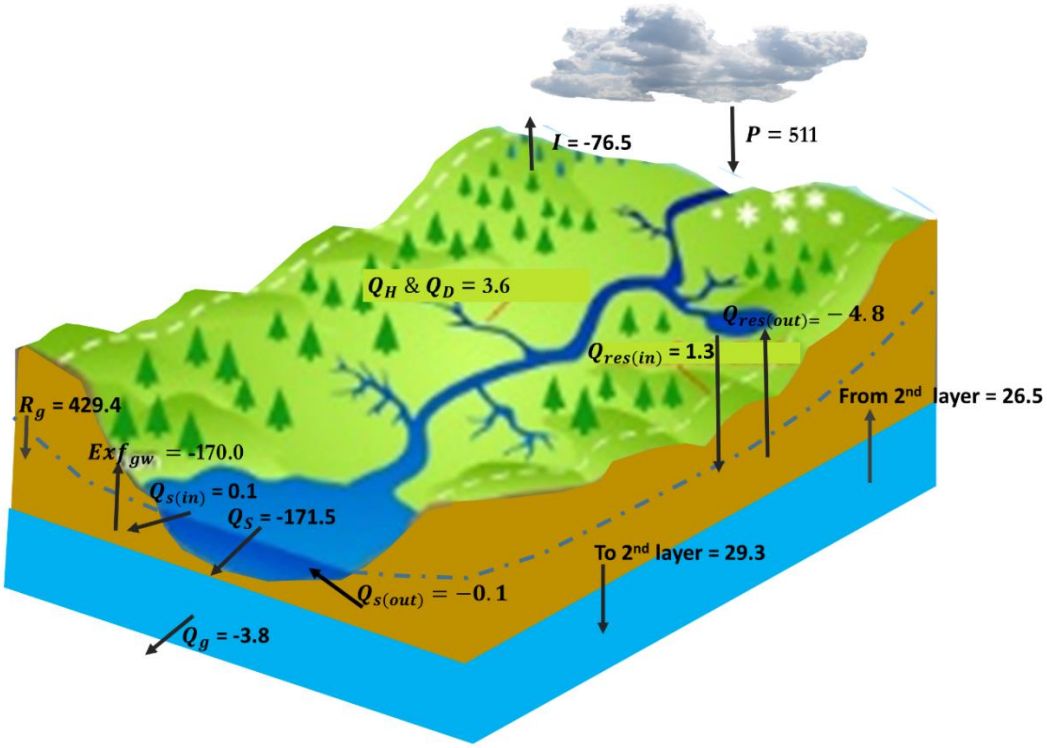

Figure 29: Simulated yearly water balance of Upper Nuweejaar River Catchment from the steady-state model

4.2.5. Spatial variability of water fluxes as per steady-state model

Figure 30 shows the spatial variability of groundwater fluxes. Spatial variability of hydrologic stresses (rainfall and PET) in the catchment was relatively low due to the Mediterranean climate (Hassan et al. 2014). Therefore spatial variation in groundwater fluxes could be due to spatially variable land cover which influences interception and runoff processes, subsurface heterogeneity of the medium, shallow but variable water table depth, geographic relief and stream network.

Subsurface evapotranspiration (ET_{ss}) varied between 0 to -4.1 mm and was highest along the stream channels and contributing tributaries owing to the shallow water table (Figure 25). Groundwater exfiltration (Exf_{gw}) ranged between 0 to -48.7 mm.d^{-1}, following a similar trend and water table dependence as ET_{ss}, with high values along the stream channels.

Gross recharge (R_g) varied between 0.8 and 1.6 mm d^{-1} and was highest on bare land and river channels followed by agriculture and was lowest on areas covered by shrubs. This could be due to the interception rate (Figure 17), which was highest for shrubs (20% of *P*) and lowest for grass (5% of P), hence lower infiltration rate. Moreover, the interception rate for areas covered by shrubs was the same in both dry and wet seasons since they are evergreen, unlike other land cover classes where a lower rate was applied during the dry season.

It was noted that most of the gross recharge was discharged back to the surface as exfiltration or lost into the atmosphere as sub-surface evapotranspiration. This occurred mainly along the stream channels where the water table was shallow resulting in negative recharge of up to -51.4 mm.d^{-1}. Overall the average net recharge in the steady-state model was of 0.02 mm.d^{-1}.

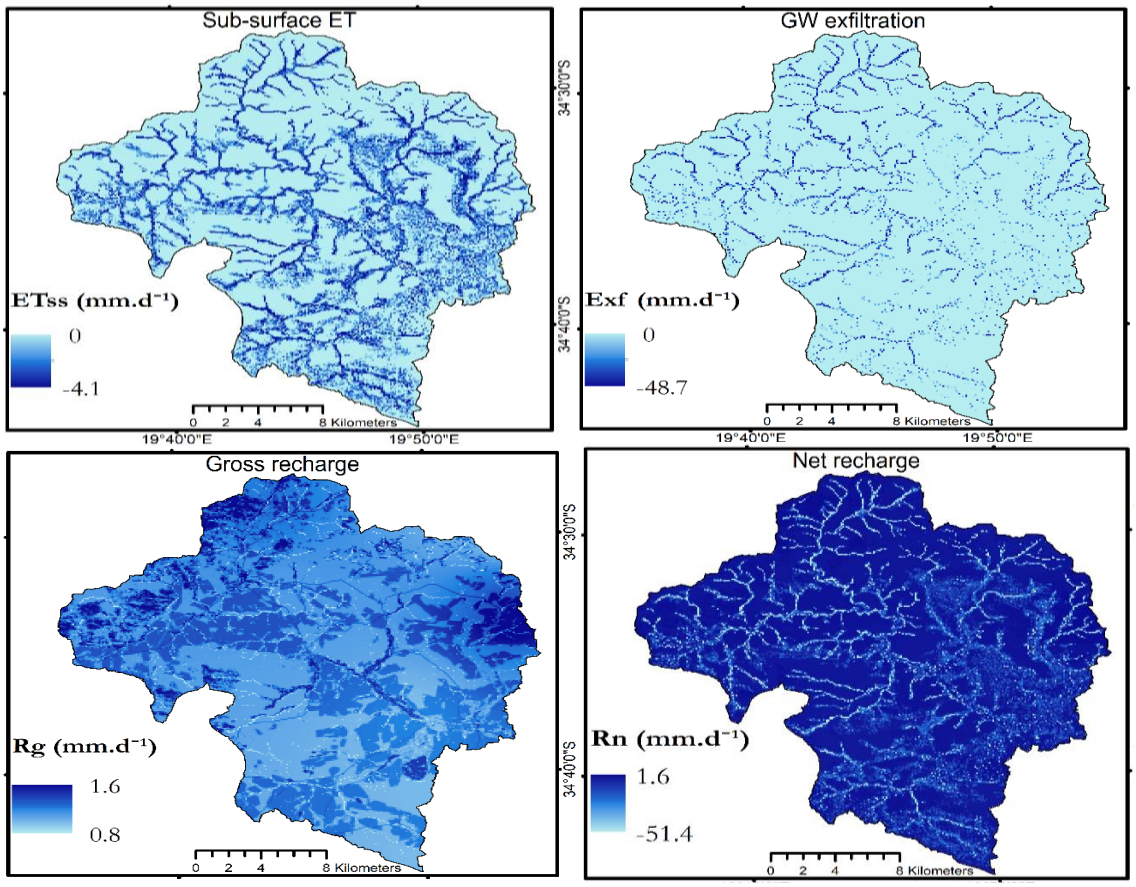

Figure 30: Spatial variability of sub-surface evapotranspiration, exfiltration, gross recharge and net recharge in mm d^{-1}

4.3. Transient state model

4.3.1. Calibrated parameters

The final calibrated model parameters are outlined in Table 12. The spatially variable hydraulic conductivities for the unconfined aquifer, calibrated in zones, varied between 0.2 to 0.8 $m.d^{-1}$ (Figure 31-a). The hydraulic conductivity of the confined aquifer (not shown) was spatially uniform with a value of 0.01 $m.d^{-1}$. The calibrated specific yield for the unconfined aquifer ranged spatially from 0.24 to 0.28 (Figure 31-b) and the spatially uniform specific storage of the second aquifer (not shown) was 0.0001.

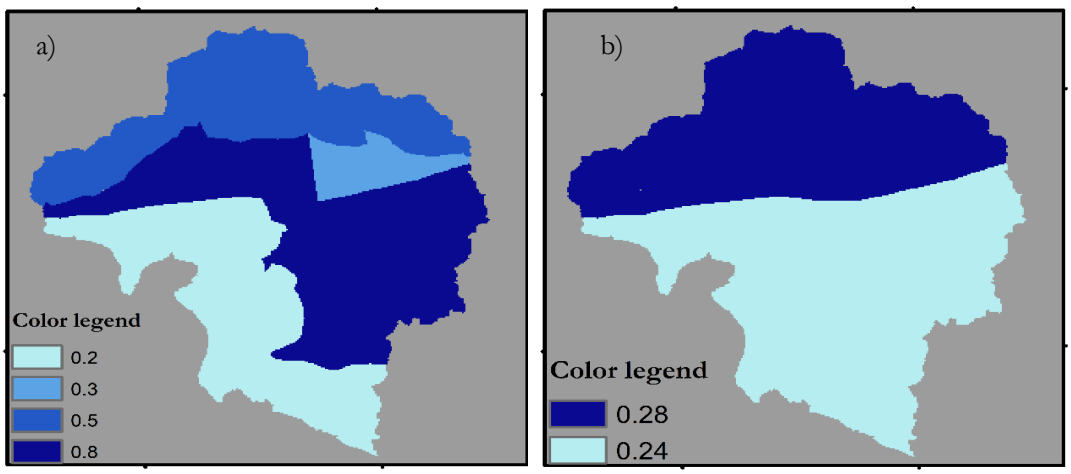

Figure 31: Calibrated a) horizontal hydraulic conductivity and b) specific yield of the first layer

Table 12: Final calibrated transient model parameters: S_y – specific yield, S_s – specific storage; other parameters are as defined in Table 6.

Vertical zone	Parameter	Minimum value	Maximum value	Unit	Status
Unsaturated zone	EXTDP	0.5	3	m	F
	EXTWC	0.1	0.1	m^3m^{-3}	C
	THTS	0.3	0.3	m^3m^{-3}	C
	K_{Vuz}	10	10	md^{-1}	C
Streams	Width	0.8	3	m	C
	STRHC1	0.008	0.05	md^{-1}	C
	STRTOP	0.5	2	m	C
	STRTHICK	0.5	1.5	m	F
	SLOPE	0.025	0.025	m^3m^{-3}	F
	Roughness coefficient	0.035	0.035		F
Saturated zone	K (layer 1)	0.2	0.8	md^{-1}	C
	K (layer 2)	0.01	0.01	md^{-1}	C
	S_y (layer 1)	0.24	0.28	-	C
	S_y (layer 2)	0.24	0.24	-	C
	S_s (layer 2)	0.0001	0.0001	m^{-1}	F
Reservoir	*Rbthck*	3	3	m	F
	HC_{res}	0.008	0.008	md^{-1}	C

4.3.2. Calibrated groundwater heads

Figure 32 to 35 show the comparison between simulated and observed groundwater heads for the transient model calibration. Observed heads were available for a very short period (22nd June to 26th July 2017), and the values were quite uncertain for some observation points (Figure 11). The outliers in borehole 11 and 12 were not used for calibration while the whole dataset from borehole was discarded. The response of the water levels in borehole 10 was thus observed from calibration with BH 9.

Generally, observed and simulated heads showed a good match. The RMSE ranged from 0.12 m to 0.56 m for individual observation points (Table 13). Likely causes of discrepancies in simulated heads include: (1)unrepresented heterogeneity; (2)errors in the system conceptualization; (3) errors in model parameterization; (4) uncertainty in the observed water levels; and (5) variability of grid-scale altitude that constrains grid-variability of simulated hydraulic heads not necessarily matching heads at the observation point (Hassan et al. 2014); for instance, the bias at BH 4, 5 and 8 was likely due the grid-scale altitude variability.

Table 13: Error analysis of heads after transient model calibration

	BH 4	BH 5	BH 6	BH 7	BH 8	BH 9	BH 10	BH 11	BH 12	BH 13	BH 14
ME	-0.33	-0.50	0.20	0.17	-0.40	-0.28		-0.23	0.44	0.27	-0.22
MAE	0.33	0.50	0.20	0.17	0.40	0.28		0.23	0.44	0.27	0.22
RMSE	0.34	0.51	0.22	0.20	0.41	0.30		0.21	0.44	0.29	0.26

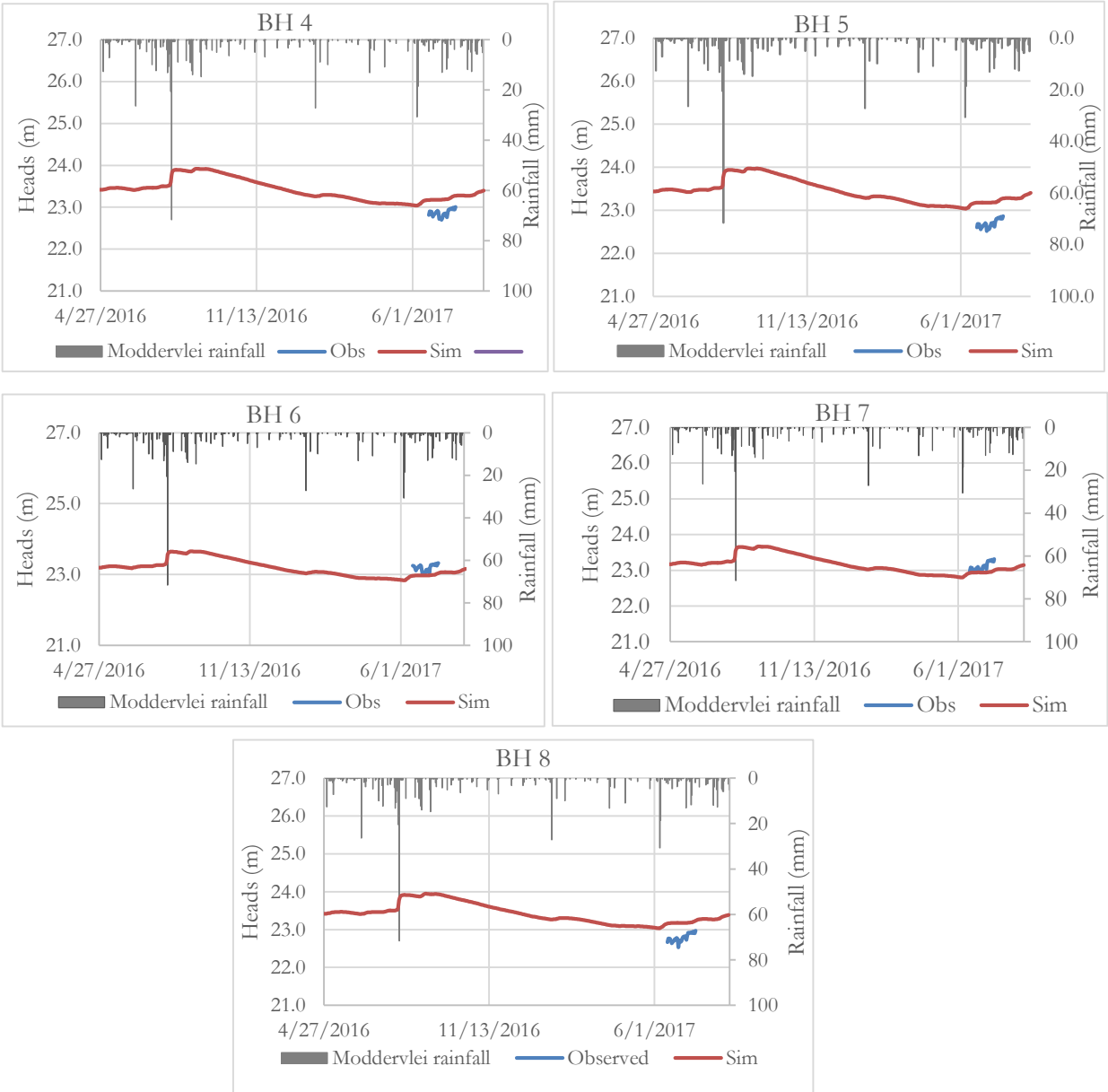

Figure 32: Observed and simulated heads at Moddervlei station

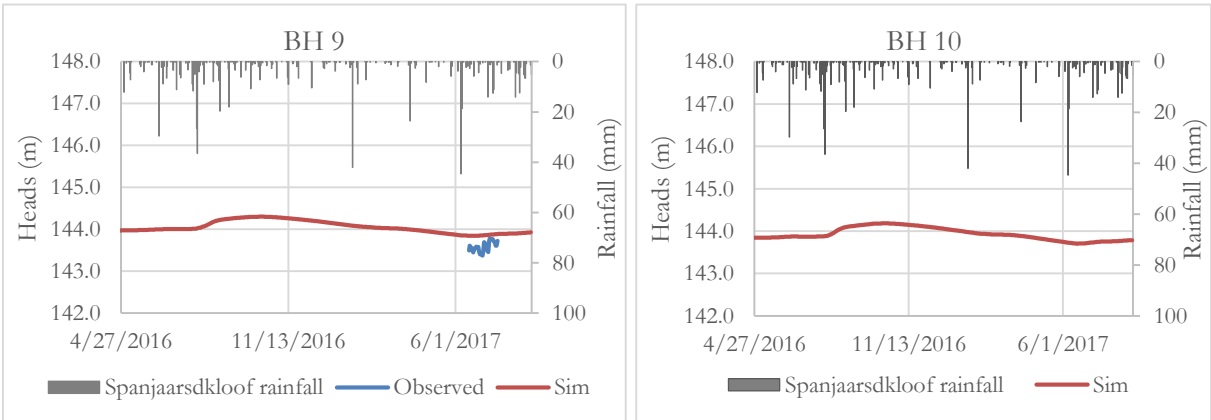

Figure 33: Observed and simulated heads at Spanjaarskloof station. Water levels in BH 10 observed from calibration with BH 9

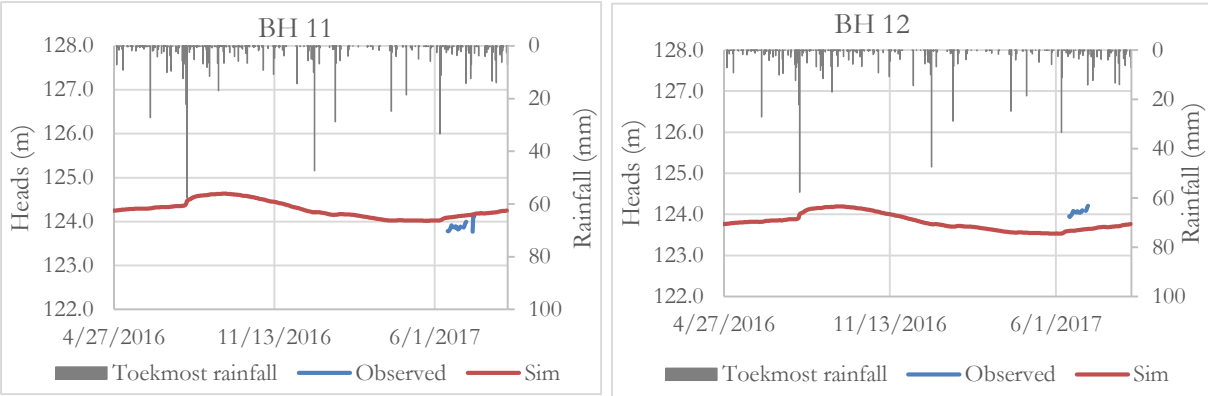

Figure 34: Observed and simulated heads at Boskloof station

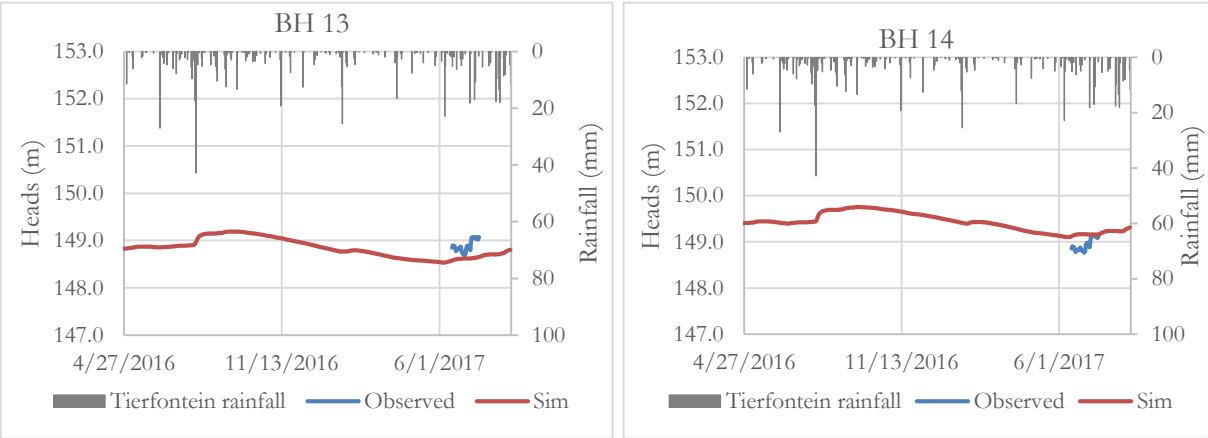

Figure 35: Observed and simulated heads at Uitsig Farm station

4.3.3. Calibrated stream flows

Figure 36 shows hydrographs of simulated and observed stream flows and Table 14 shows the error analysis. The model performed reasonably well based on the Nash Sutcliffe efficiency criteria. This means that the model was able to reproduce the shape of the observed hydrographs. However, the model performed poorly in terms of volumetric error. This was due to the inability of the model to simulate peak flows in some gauges, uncertainty in the observed water levels as well as the uncertainty in the rating curves used to calculate stream flows from the observed water levels.

Table 14: Error analysis of observed and simulated streamflows

Station Name	NS	RVE
Jan Swatskraal	0.60	0.4
Mekery Bridge	0.59	-47.95
Pietersiekloof	0.51	14.92
Blomkraal	0.58	-33.18
Outlet	0.95	-9.82

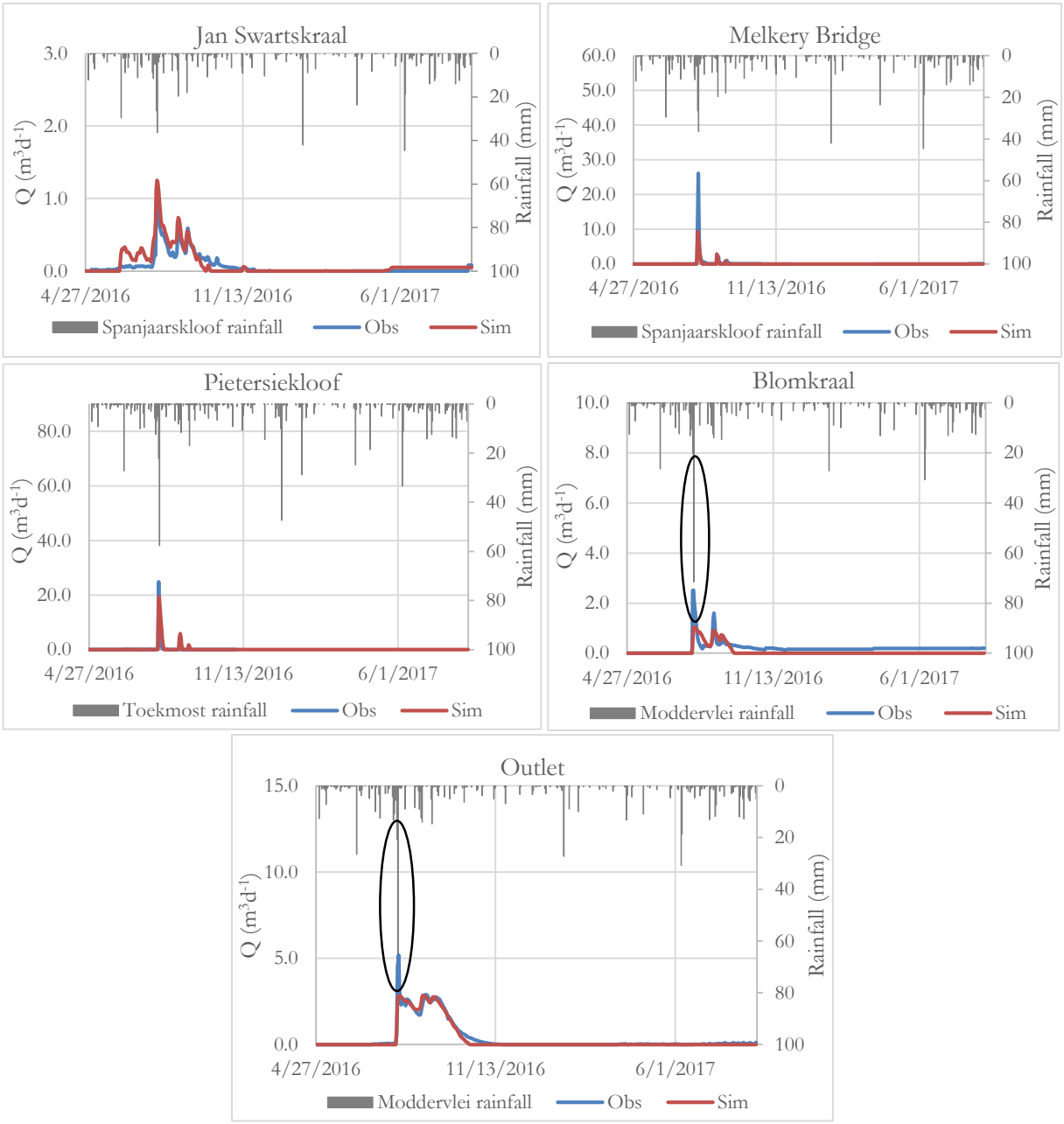

Figure 36: Relationship between observed and simulated flows in Upper Nuweejaar Catchment after transient model calibration

The model performed quite well in simulating the flows in Jan Swartskraal producing a reasonable match with observed flows in terms of shape (NS = 0.6) and volumetric error RVE = 0.4%. For the other four stations (Melkery Bridge, Pietersiekloof, Blomkraal and the outlet), the fit between the observed and simulated flows was also reasonable. However, the peaks of observed flows were much higher than the simulated. Efforts to match these peaks resulted in over-estimation of flows hence high volumetric error.

4.3.4. Sensitivity analysis

Sensitivity analysis of the transient model focused on groundwater fluxes (R_g, ET_g, Exf_{gw} and R_n). Four model parameters including hydraulic conductivity of the saturated zone (K), maximum unsaturated vertical hydraulic conductivity ($K_{V(uz)}$), specific yield (Sy) and extinction depth (EXTDP) were tested. Groundwater fluxes were found to be sensitive to hydraulic conductivity (Figure 37) where an increase in the parameter by a factor of 1.5 resulted in a decline in gross recharge and groundwater evapotranspiration and a rise in groundwater exfiltration and consequently a decline in net recharge. The sensitivity of K was more pronounced in ET_g and Exf_{gw} where a clear shift was observed for both low and high values of K. R_g, and R_n were most sensitive during peak recharge and less responsive during low recharge periods.

Sensitivity analysis of maximum vertical hydraulic conductivity of the unsaturated zone (Figure 38) shows minimal sensitivity of the fluxes to the parameter. This could be because $K_{V(uz)}$ only determines the amount of infiltration but has less impact on the processes of the saturated zone.

Sensitivity analysis of specific yield (Figure 39) show a similar response to that of hydraulic conductivity where an increase of the parameter by a factor 1.2 resulted in a decline in the fluxes. The fluxes were, however, more responsive to changes in specific yield during high flow periods and less responsive during low flow periods.

Sensitivity analysis of extinction depth (Figure 40) indicates that groundwater fluxes were sensitive to the parameter. Extinction depth had an inverse relationship with R_g, Exf_{gw} and R_n and a direct relationship with ET_g. This is because an increase in extinction depth avails more water for evapotranspiration resulting in decline in water table and subsequently decline in recharge and exfiltration

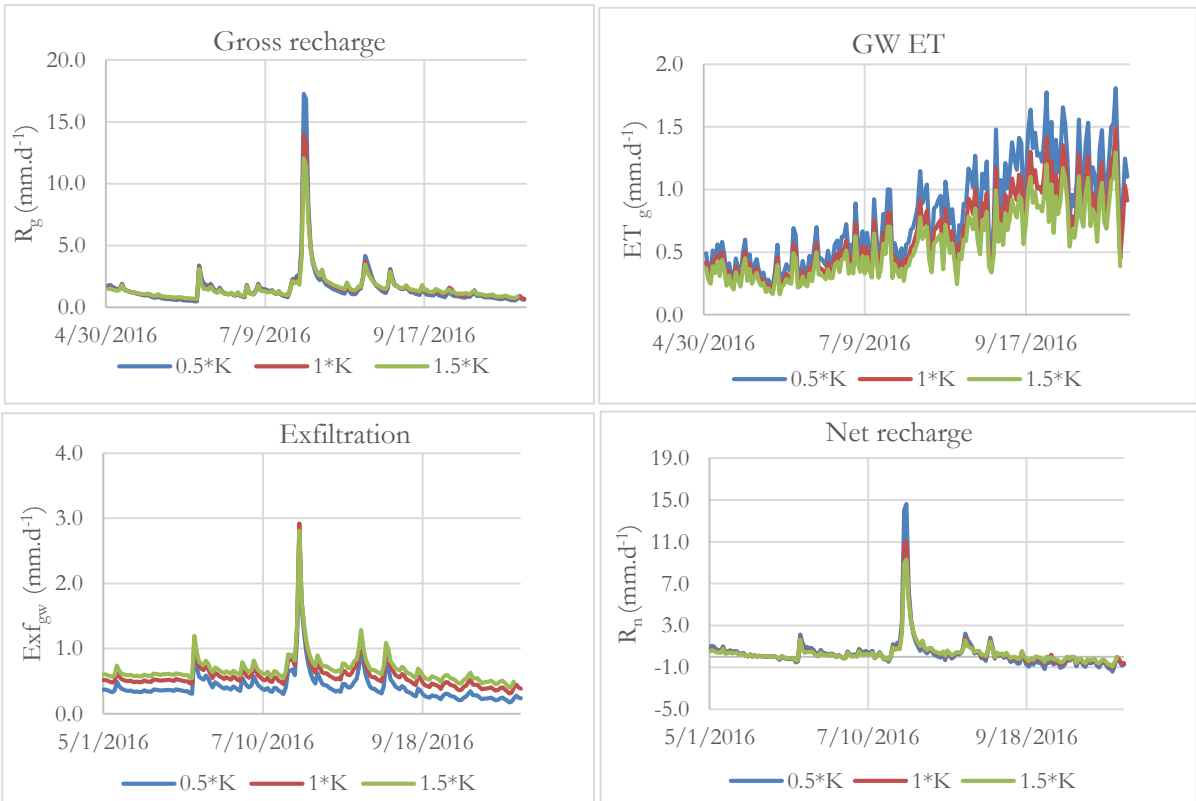

Figure 37: Sensitivity analysis of hydraulic conductivity of the first layer

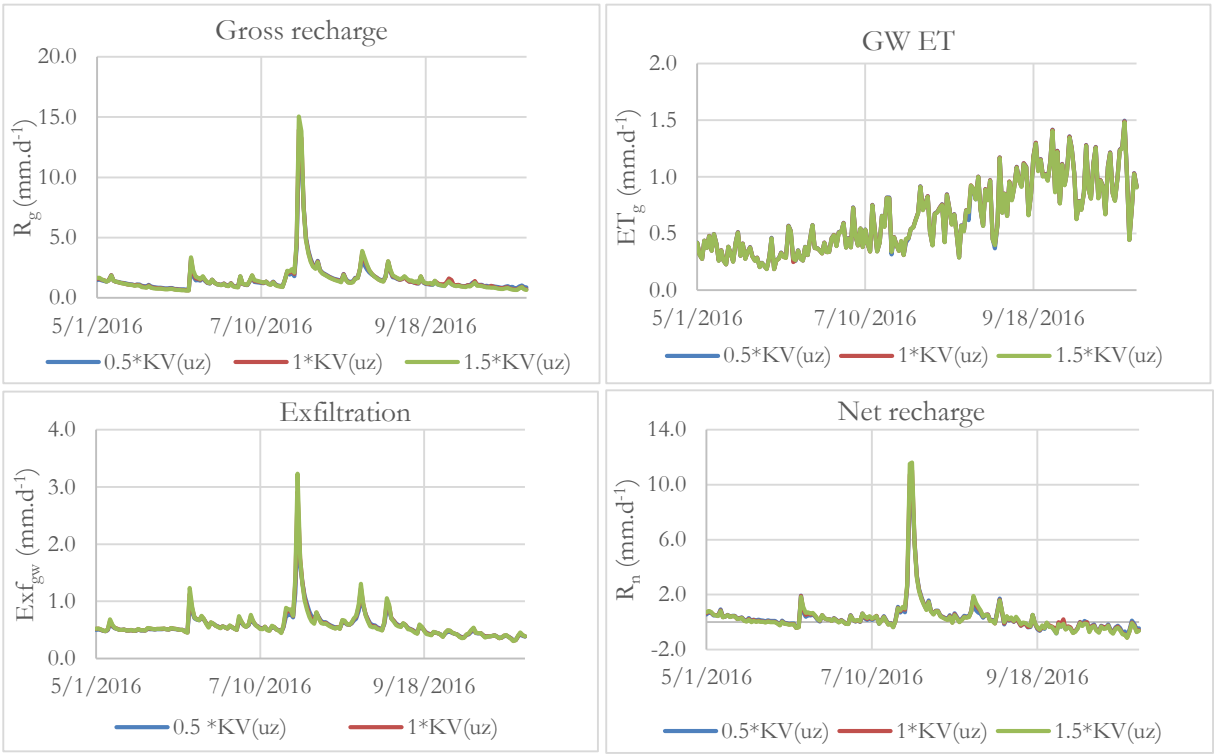

Figure 38: Sensitivity analysis of maximum unsaturated vertical hydraulic conductivity on groundwater fluxes

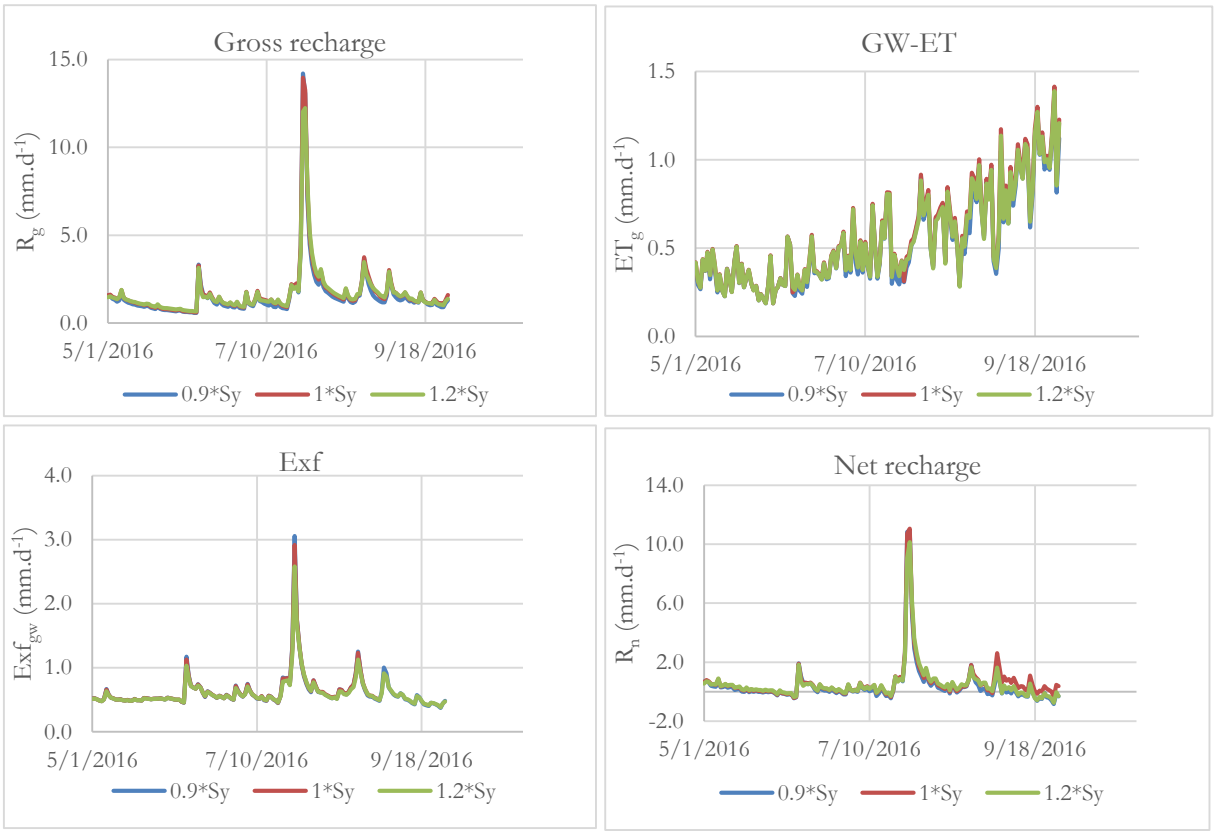

Figure 39: Sensitivity analysis of specific yield of the first layer on groundwater fluxes

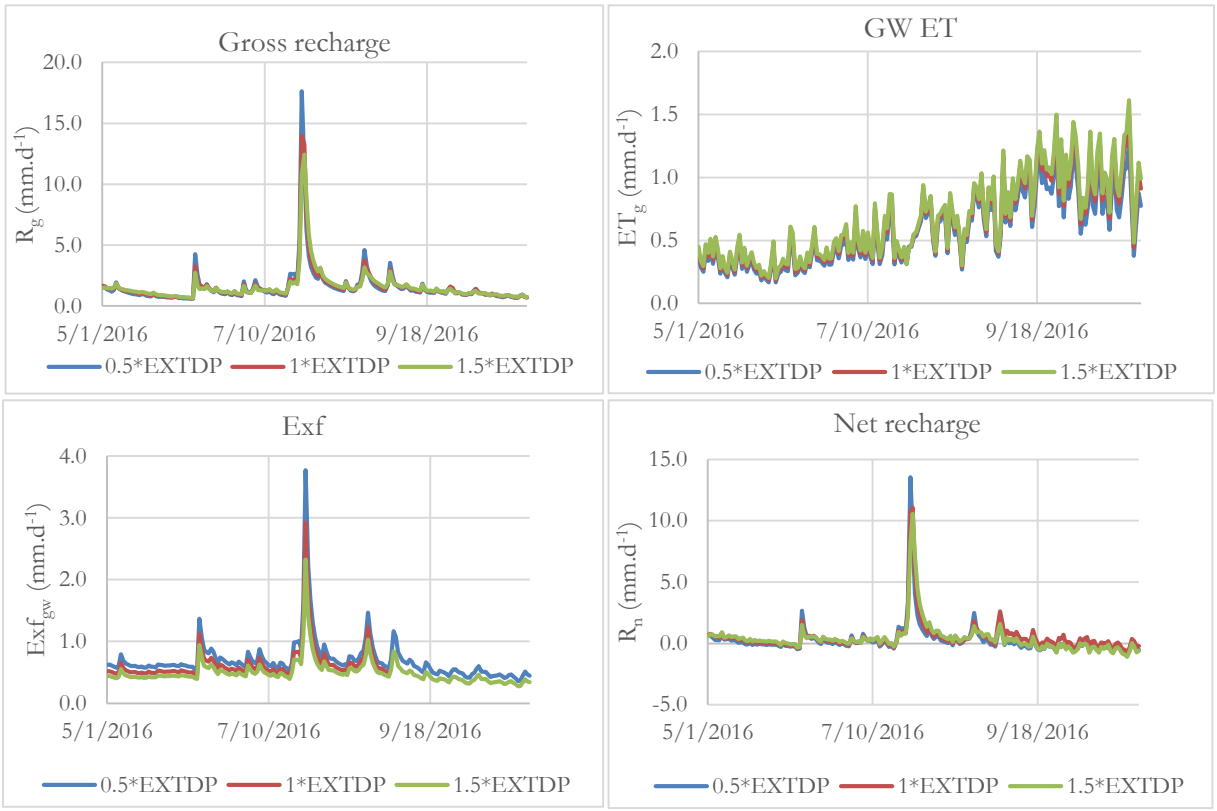

Figure 40: Sensitivity analysis of extinction depth on groundwater fluxes

4.3.5. Water balance

The average monthly water balance schema of the model after transient calibration is presented in Figure 41 while Table 15 gives monthly water balance for the whole simulation period. The average monthly water balance accounting for all inflows (P) into and outflows (ET, Q_s and Q_g) from the model domain, represented by Equation 14, consist of P = 42.2 mm.mth^{-1}, ET = 65.6% of P, Q_s =33.4% of P while Q_g was negligible.

Inflow into the saturated zone was dominated by gross recharge which accounted for 99.5% of total groundwater inflow while leakages from the streams and reservoir were negligible. ET_g was the main discharge of groundwater, accounting for 66.1 % of the total groundwater outflow followed by Exf_{gw} which accounted for 32.9% while groundwater leakage to streams and reservoir were negligible. Base flow, which is the difference between leakage into and from streams at the outlet, was zero as $Q_{s(in)}$ and $Q_{s(out)}$ were equal. Overall, the reservoir was gaining from groundwater throughout the simulation period.

A negative change in groundwater storage was observed despite the positive net recharge of 0.3 mm.mth^{-1}.

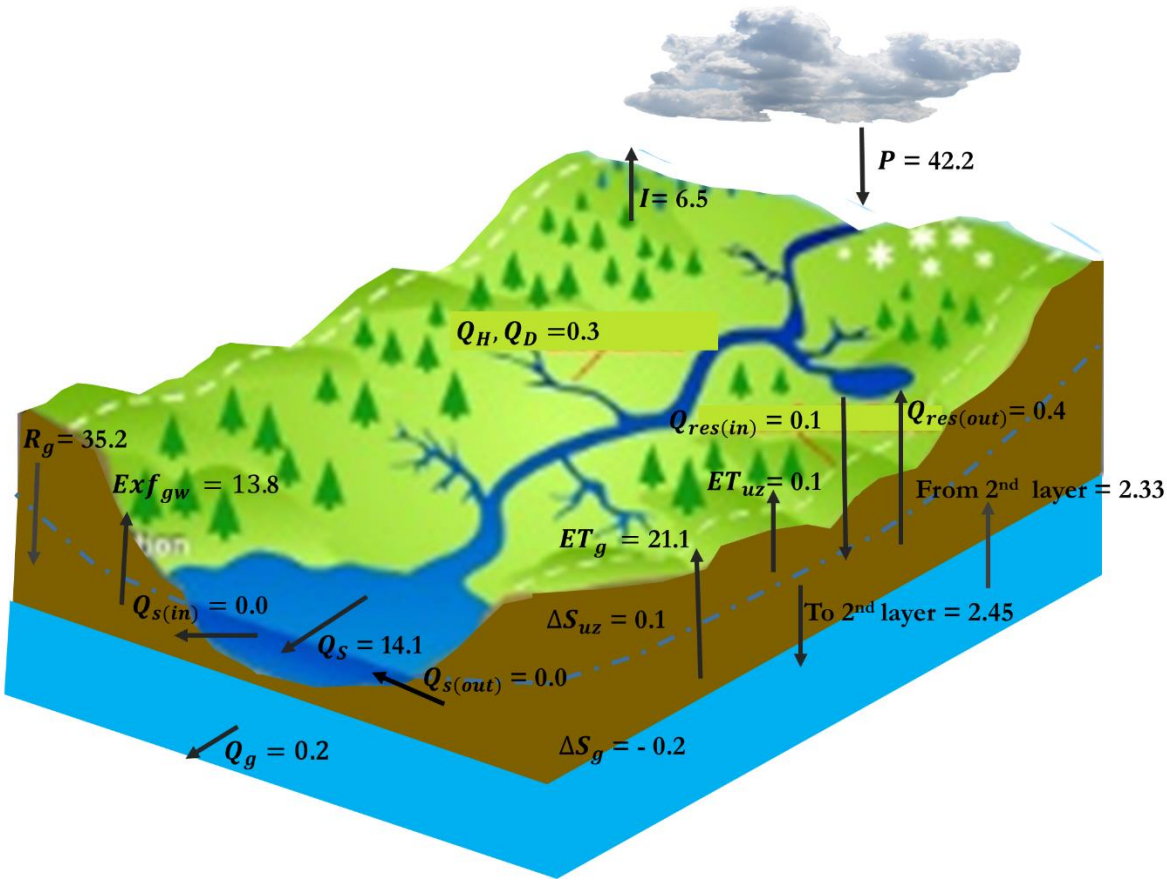

Figure 41: Average compartmental water fluxes (mm.mth^{-1}) of the whole model domain under transient conditions for the period starting from 1st May, 2016 to 31 August, 2017

Table 15: Monthly water balance means for Upper Nuwejaar River Catchment for the hydrological year starting Sep 2016 to Aug 2017 as a result of transient simulation in MODFLOW-NWT calculated according to Equation 14 to 21 in section 3.5.7. All values are in mm.month^{-1}.

Month	P	I	P_{inf}	Q_{H+D}	Q_s	Q_g	$Q_{s(in}$	$Q_{s(out)}$	Q_B	$Q_{res(in)}$	$Q_{res(out)}$	R_g	ET_g	ET_{uz}	Exf_{gw}	R_n	ΔS_g	ΔS_{uz}
May, 2016	18.9	3.0	15.6	0.1	16.0	0.2	0.0	0.0	0.0	0.1	0.4	35.0	10.2	0.0	15.9	8.8	8.4	-19.3
June, 2016	49.5	7.9	41.0	0.4	18.2	0.2	0.0	0.0	0.0	0.1	0.4	34.9	11.2	0.2	17.8	5.9	5.5	6.0
July, 2016	135.4	21.7	111.9	1.7	26.2	0.2	0.0	0.0	0.0	0.2	0.4	84.7	15.4	0.7	24.6	44.7	44.3	26.6
Aug, 2016	50.4	8.1	41.8	0.5	20.8	0.2	0.0	0.0	0.0	0.2	0.4	59.8	21.8	0.0	20.3	17.8	17.3	-18.1
Sep, 2016	44.8	7.2	37.0	0.3	16.4	0.2	0.0	0.0	0.0	0.2	0.4	43.9	28.4	0.0	16.1	-0.6	-1.1	-7.0
Oct, 2016	20.3	3.2	17.1	0.1	12.5	0.2	0.0	0.0	0.0	0.2	0.4	28.4	30.4	0.0	12.4	-14.4	-14.9	-11.3
Nov, 2016	20.6	2.7	17.7	0.1	9.9	0.2	0.0	0.0	0.0	0.2	0.3	21.4	33.8	0.0	9.8	-22.2	-22.6	-3.7
Dec, 2016	19.0	2.5	16.4	0.1	7.7	0.2	0.0	0.0	0.0	0.1	0.4	18.0	37.7	0.0	7.6	-27.2	-27.7	-1.6
Jan, 2017	51.8	6.7	44.2	0.3	8.9	0.2	0.0	0.0	0.0	0.1	0.3	27.4	31.5	0.4	8.6	-12.7	-13.0	16.4
Feb, 2017	17.0	2.2	14.7	0.1	7.3	0.2	0.0	0.0	0.0	0.1	0.3	28.4	28.3	0.0	7.2	-7.1	-7.5	-13.6
Mar, 2017	4.4	0.6	3.8	0.0	6.8	0.2	0.0	0.0	0.0	0.2	0.2	15.0	27.6	0.0	6.8	-19.5	-19.8	-11.2
April, 2017	40.1	5.2	34.4	0.2	10.9	0.2	0.0	0.0	0.0	0.2	0.3	21.1	14.7	0.0	10.7	-4.2	-4.6	13.3
May, 2017	11.0	1.8	9.2	0.1	12.0	0.2	0.0	0.0	0.0	0.2	0.3	17.3	11.2	0.0	11.9	-5.7	-6.1	-8.1
June, 2017	74.9	12.0	62.4	0.6	16.5	0.2	0.0	0.0	0.0	0.1	0.4	42.2	10.9	0.6	15.9	15.5	15.0	19.7
July, 2017	45.7	7.3	38.1	0.3	17.2	0.2	0.0	0.0	0.0	0.1	0.4	38.4	10.9	0.0	16.9	10.6	10.1	-0.3
Aug, 2017	71.9	11.5	60.2	0.5	18.5	0.2	0.0	0.0	0.0	0.1	0.5	46.7	14.3	0.0	18.0	14.4	13.9	13.5
Total	675.7	103.6	565.6	5.4	225.8	3.3	0.0	0.0	0.0	2.4	5.7	562.6	338.3	1.9	220.5	4.1	-2.9	1.3
Mean	42.2	6.5	35.3	0.3	14.1	0.2	0.0	0.0	0.0	0.1	0.4	35.2	21.1	0.1	13.8	0.3	-0.2	0.1
STD	31.6	5.1	26.1	0.4	5.3	0.0	0.0	0.0	0.0	0.0	0.1	17.5	9.4	0.2	5.0	17.8	17.8	13.8
Max	135.4	21.7	111.9	1.7	26.2	0.2	0.0	0.0	0.0	0.2	0.5	84.7	37.7	0.7	24.6	44.7	44.3	26.6
Min	4.4	0.6	3.8	0.0	6.8	0.2	0.0	0.0	0.0	0.1	0.2	15.0	10.2	0.0	6.8	-27.2	-27.7	-19.3

4.3.6. Temporal variability of water fluxes

Temporal variability of groundwater fluxes was analysed both daily (Figure 42), monthly (Figure 43)for the simulation period. Significant variability of the fluxes was observed which could be attributed to large daily and seasonal variability of rainfall and presence of shallow water table. For instance, the dry season which occurs between October and May is characterised by low recharge and exfiltration, with the lowest being 15.0 and 6.8 mm.mth^{-1} respectively in March 2017, and high evapotranspiration rates with the highest in December 2016 with a value of 37.7 mm.mth^{-1}. Conversely, wet season was characterised by high recharge and exfiltration rates, with the highest observed in July 2016 with 84.7 and 24.6 mm.mth^{-1} respectively, and low evapotranspiration with the lowest in June and July 2017 (10.9 mm.mth^{-1}).

It was also noted that groundwater recharge was responsive to rainfall events occurring during the dry season. This could be due to low storage of the unsaturated zone and shallow water table. The net recharge was highest in July 2016 and was mostly negative in September 2016 to May 2017 owing to low rainfall and high groundwater evapotranspiration.

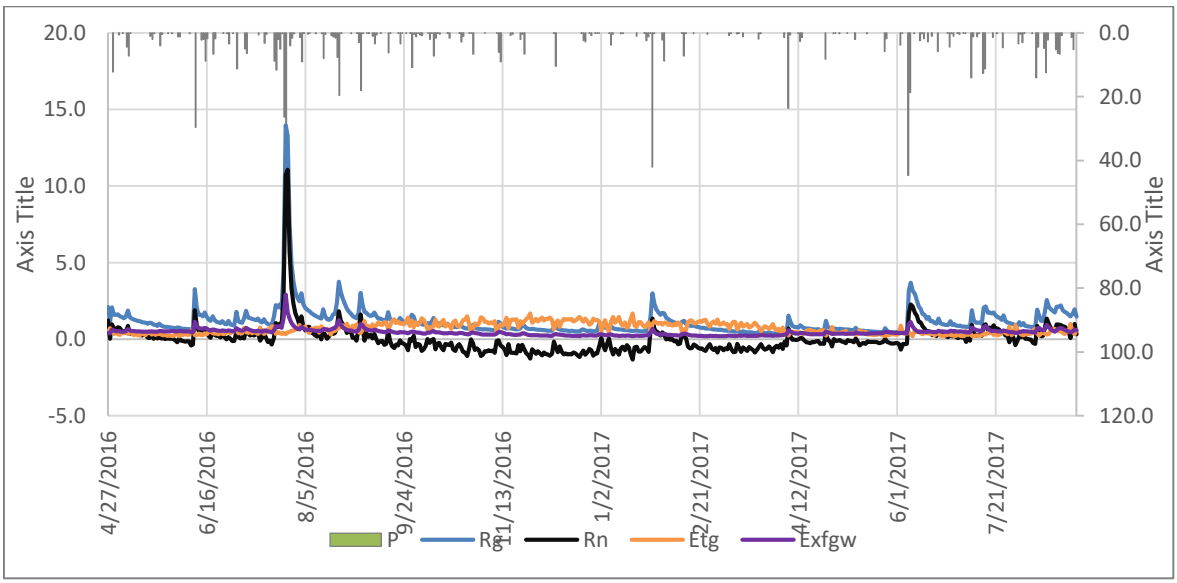

Figure 42: Daily variability of groundwater fluxes for the whole simulation period starting 27th April 2016 to 31st August 2017.

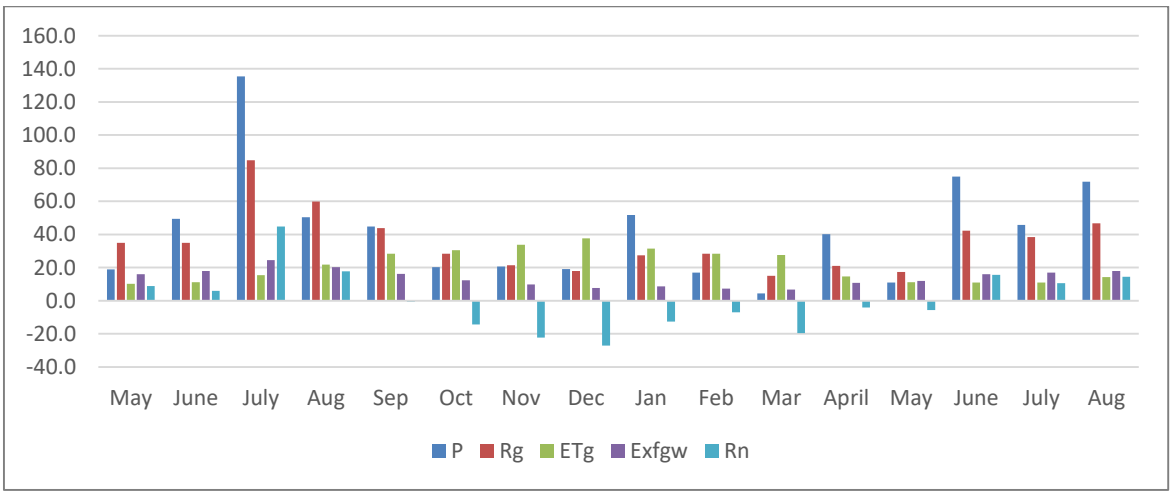

Figure 43: Monthly variability of groundwater fluxes from May 2016 to August 2017

4.4. Comparison of steady-state and transient simulations

Figure 44 presents a graphical comparison of fluxes in steady-state and transient models. In steady state, a daily average of hydrologic stresses and state variables for the whole simulation period were used. Since some of the fluxes were very little, the units were converted to $mm.y^{-1}$ rather than $mm.d^{-1}$ for better analysis. To enable for comparison with the transient model, a yearly average was estimated from the 17 months of data. Additionally, since UZF1 Package does not distinguish between groundwater and unsaturated zone evapotranspiration, in steady state, ET_g and ET_{uz} from the transient simulation were summed up to obtain subsurface evapotranspiration.

The fluxes of the steady-state model were more or less similar to the average of the transient model with slightly higher values in the steady-state model. This shows that the solutions of both steady-state and transient models are very close and thus both can be used in prediction of fluxes in the catchment.

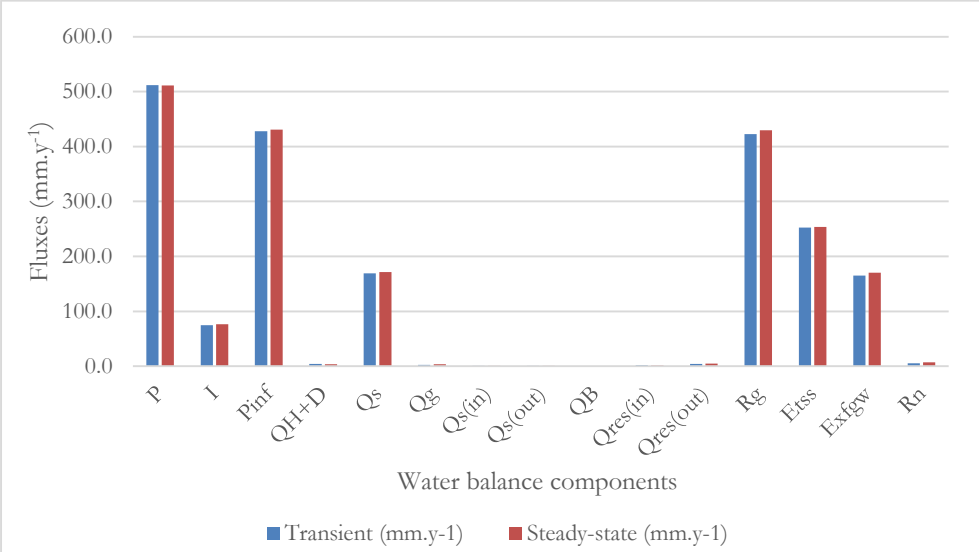

Figure 44: Comparison of water balance components in steady-state and transient models

4.5. Effects of water fluxes on water balance dynamics

The impact of surface-groundwater fluxes on water balance dynamics was quantified from the daily water balance analysis. For instance, change in groundwater storage as a result of the variable fluxes between surface and groundwater was observed. During the wet season, groundwater inflows were higher than groundwater outflows resulting to an increase in storage while the inverse was observed during the dry season. In some instances, (e.g. March, August 2016), gross recharge was higher than infiltration which could be due to release of water from the unsaturated zone which resulted in a decline in unsaturated zone storage.

It was further observed that groundwater exfiltration and surface water infiltration often had a simultaneous impact on water balance. For instance, high rainfall caused an abrupt rise in the water table in response to recharge (infiltration) which triggered discharge of groundwater to shallow soils (exfiltration) where it flowed preferentially to streams.

Additionally, perennial wetlands are maintained by lateral interaction with the adjacent aquifers during the dry season. This was observed from both steady-state and transient simulations where the wetland was found to gain groundwater.

5. CONCLUSION AND RECOMMENDATIONS

5.1. Conclusion

The objective of this research was to assess the impact of surface-groundwater interactions on water balance dynamics in Heuningnes Catchment. The interactions were modelled in both steady-state and transient simulations for 16 months, from 27th April 2016 to 31st August 2017. An integrated hydrological solution realised by coupling MODFLW-NWT, UZF1, SFR2 and Reservoir Packages was used. The model domain was discretised into two layers vertically with spatial grids of 100 m by 100 m. Time discretisation in the transient model consisted of daily time steps each representing one stress period. Both steady-state and transient models were calibrated using manual trial and error methods.

From analyses of water balance results from both steady-state and transient models, it was found that:

1. Recharge formed the main inflow into the groundwater system while groundwater evapotranspiration and exfiltration were the main outflows.
2. The reservoir was gaining from groundwater throughout the simulation while base flow was negligible.
3. Groundwater evapotranspiration was highest during the dry season and occurred mainly on areas with shallow water table and along stream channels
4. A decline, of 0.2 $mm.mth^{-1}$, in the groundwater storage was observed despite a positive net recharge of 0.3 $mm.mth^{-1}$.
5. Groundwater exfiltration, surface water infiltration and gross recharge had a simultaneous effect on water balance dynamics in the catchment and had its maximum in the wet season.
6. High rainfall resulted to an abrupt rise in water table in response to recharge triggering groundwater exfiltration hence low groundwater residence time.

5.2. Recommendations

Groundwater monitoring points were not well distributed in the catchment, and the piezometric data was available for a very short period (1 month). Additionally, the available data had uncertainties related to observation portrayed by erroneous variations in the head within a very short period. Therefore densification of the monitoring network should be considered and better observation methods adopted to ensure consistency and reliability of recorded data.

Climatic and hydrological (streamflow) network was fairly well distributed in the catchment. However, there were large gaps in both climatic and hydrological data, and gap filling was required which could lead to uncertainties.

Despite having a dense network of river gauges, the rating curves were not reliable for some gauges, as they were generated using insufficient data. Moreover, the rating curves not available for some gauges hence they were not used for calibration. Therefore development of better rating curves with altitude survey or alternative methods of discharge estimation needs attention to increase utility and reliability of recorded data.

Alternative modelling solutions, such as the use of Lake Package instead of the used Reservoir Package for simulation of water bodies is recommended provided their bathymetry as well as the time series of there inflows and outflows are available.

This work can also be extended to include effects of salinity and invasive species on groundwater flow and fluxes.

Moreover, calibration of the transient model was done for only 16 months due to data limitations. A follow-up study with sufficiently long model simulation period of the at least 3-year period would provide more reliable, quantitative representation of the system dynamics.

LIST OF REFERENCES

Ala-Aho P, Rossi PM, Isokangas E, Kløve B (2015) Fully integrated surfaceâ€"subsurface flow modelling of groundwaterâ€"lake interaction in an esker aquifer: Model verification with stable isotopes and airborne thermal imaging. doi: 10.1016/j.jhydrol.2014.12.054

Allen, Luis S. Pereira, Dirk Raes, Smith M (1998) FAO Irrigation and Drainage Paper No. 56.

Anderson M, Woessner WW, Hunt R (2015) Applied Groundwater Modeling, Second Edition: Simulation of Flow and Advective Transport.

Anderson MP, Hunt RJ, Krohelski JT, Chung K (2002) Using high hydraulic conductivity nodes to simulate seepage lakes. Ground Water 40:117–122.

Anderson PM, Woessner WW (1992) Applied groundwater modeling: Simulation to flow and advective transport.

Babak O, Deutsch C V (2009) Statistical Approach to Inverse Distance Interpolation. doi: https://doi.org/10.1007/s00477-008-

Bakar OM (2015) Integrated Hydrologic Model for the Assessment of Surface-Groundwater Interactions: The case of Ziębice Basin. University of Twente, Faculty of Geoinformation Science and Earth Observation

Braune E, Adams S, Fourie F (2014) 20 Years of Groundwater Research, Development and Implementation in South Africa 1994-2014.

Brunner P, Simmons CT (2012) HydroGeoSphere: A Fully Integrated, Physically Based Hydrological Model. Ground Water 50:170–176. doi: 10.1111/j.1745-6584.2011.00882.x

Bugan RD, Nebo ZJ, Willem PDC (2012) The water balance of a seasonal stream in the semi-arid Western Cape (South Africa)." Water SA 38.2 (2012). Water SA 382 38:12.

Camporese M, Paniconi C, Putti M, Orlandini S (2010) Surface-subsurface flow modeling with path-based runoff routing, boundary condition-based coupling, and assimilation of multisource observation data. Water Resour Res. doi: 10.1029/2008WR007536

Chen FW, Liu CW (2012) Estimation of the spatial rainfall distribution using inverse distance weighting (IDW) in the middle of Taiwan. Paddy Water Environ 10:209–222. doi: 10.1007/s10333-012-0319-1

Chen S, Guo J (2016) Spatial interpolation techniques: their applications in regionalizing climate-change series and associated accuracy evaluation in Northeast China. doi: 10.1080/19475705.2016.1255669

Chen YY, Li MH (2016) Quantifying rainfall interception loss of a subtropical broadleaved forest in central Taiwan. Water (Switzerland) 8:1–19. doi: 10.3390/w8010014

Clark D, Smithers J, Hughes D, et al (2009) DESIGN AND DEVELOPMENT OF A HYDROLOGICAL DECISION SUPPORT FRAMEWORK Water Research Commission.

Corbett ES, Crouse, Robert P Rainfall interception by annual grass and chaparral . . . losses compared.

Delicado V, Banda V (2017) Geological summary and Cross-Sections.

DHI (2007) MIKE SHE USER MANUAL VOLUME 1: USER GUIDE.

Domenico PA (Patrick A., Schwartz FW (Franklin W. (1998) Physical and chemical hydrogeology. Wiley

DWA (2010) Groundwater Strategy 2010.

DWS (2017) Western Cape IWRM Action Plan: Status Quo Report Final Draft.

DWS (2015) Groundwater Resource Assessment II. http://www.dwa.gov.za/groundwater/GRAII.aspx. Accessed 20 Aug 2017

El-Zehairy AA, Lubczynski MW, Gurwin J (2017) Interactions of artificial lakes with groundwater applying an integrated MODFLOW solution. Hydrogeol J. doi: 10.1007/s10040-017-1641-x

FAO (1995) GLOBAL AND NATIONAL SOILS AND TERRAIN DIGITAL DATABASES (SOTER) Procedures Manual.

Fenske JP, Leake SA, Prudic DE (1996) Documentation of a Computer Program (RES1) to Simulate Leakage from Reservoirs Using the Modular Finite-Difference Ground-Water Flow Model (MODFLOW).

Franke L, Reilly TE, Bennett Book GD (1987) DEFINITION OF BOUNDARY AND INITIAL

CONDITIONS IN THE ANALYSIS OF SATURATED GROUND-WATER FLOW SYSTEMS-AN INTRODUCTION.
Funk C, Peterson P, Landsfeld M, et al (2015) The climate hazards infrared precipitation with stations—a new environmental record for monitoring extremes Background & Summary. doi: 10.1038/sdata.2015.66
Gupta SK (2010) Modern Hydrology and Sustainable Water Development. John Wiley & Sons, Ltd, Chichester, UK
Harbaugh AW (2005) MODFLOW-2005, The U.S. Geological Survey Modular Ground-Water Model—the Ground-Water Flow Process.
Harbaugh AW (1990) A Computer Program for Calculating Subregional Finite-difference Ground-water Flow Model.
Hassan SMT, Lubczynski MW, Niswonger RG, Su Z (2014) Surfaceâ€"groundwater interactions in hard rocks in Sardon Catchment of western Spain: An integrated modeling approach. doi: 10.1016/j.jhydrol.2014.05.026
Hatch RJC (2016) Impacts of three-dimensional nonuniformflow on quantification of groundwater-surface water interactions using heat as a tracer. Water Resour Res 6851–6866. doi: 10.1002/2016WR018841.Received
Hughes JD, Liu J (2008) MIKE SHE: Software for integrated surface water/ground water modeling. Ground Water 46:797–802. doi: 10.1111/j.1745-6584.2008.00500.x
Hunt RJ, Feinstein DT (2012) MODFLOW-NWT: Robust Handling of Dry Cells Using a Newton Formulation of MODFLOW-2005. Ground Water 50:659–663. doi: 10.1111/j.1745-6584.2012.00976.x
Kim J-W, Pachepsky YA (2010) Reconstructing missing daily precipitation data using regression trees and artificial neural networks for SWAT streamflow simulation. doi: 10.1016/j.jhydrol.2010.09.005
Krause S, Boano F, Cuthbert MO, et al (2014) Understanding process dynamics at aquifer-surface water interfaces: An introduction to the special section on new modeling approaches and novel experimental technologies. Water Resour Res 50:1847–1855. doi: 10.1002/2013WR014755
Kresic N, Mikszewski A (2013) Hydrogeological Conceptual Site Models - Data Analysis and Visualization. Taylor & Francis Group, LLC
Leuning R, Condon AG, Dunin FX, et al (1994) Rainfall interception and evaporation from soil below a wheat canopy. Agric For Meteorol 67:221–238. doi: 10.1016/0168-1923(94)90004-3
Levy J, Xu Y (2012) Review: Groundwater management and groundwater/surface-water interaction in the context of South African water policy. Hydrogeol J 20:205–226. doi: 10.1007/s10040-011-0776-4
Lubke R, De Moor IJ (Irene J. (1998) Field guide to the Eastern & Southern Cape coasts. University of Cape Town Press
Manning J (John C., Paterson-Jones C (2007) Field guide to fynbos. Struik
Markstrom SL, Niswonger RG, Regan RS, et al (2008) GSFLOW—Coupled Ground-Water and Surface-Water Flow Model Based on the Integration of the Precipitation-Runoff Modeling System (PRMS) and the Modular Ground-Water Flow Model (MODFLOW-2005). US Geol Surv 240. doi: 10.13140/2.1.2741.9202
Mason D, Hipke W (2013) REGIONAL GROUNDWATER FLOW MODEL OF THE TUCSON ACTIVE MANAGEMENT AREA.
Mazor E (1997) Chemical and isotopic groundwater hydrology.
Mazvimavi D (2017) Finding " new " water in an " old " catchment : the case of the Heuningnes Catchment , Breede-Overberg Water Management Report to the Water Research Commission by D . Mazvimavi Institute for Water Studies University of the Western Cape March 2017.
Mcmahon TA, Peel MC, Lowe L, et al (2013) Estimating actual, potential, reference crop and pan evaporation using standard meteorological data: a pragmatic synthesis. Hydrol Earth Syst Sci 17:1331–1363. doi: 10.5194/hess-17-1331-2013
Merriam RA (1960) A note on the interception loss equation. J Geophys Res 65:3850–3851. doi: 10.1029/JZ065i011p03850
Merritt ML, Konikow LF (2000) Documentation of a computer program to simulate lake-aquifer interation using the MODFLOW Ground-Water Flow Model and the MOC3D Solute-Transport Model.
Nash JE, Sutcliffe JV (1970) River flow forecasting through conceptual models part I — A discussion of

principles. J Hydrol 10:282–290. doi: 10.1016/0022-1694(70)90255-6
Niswonger RG, Panday S, Motomu I (2011) MODFLOW-NWT , A Newton Formulation for MODFLOW-2005.
Niswonger RG, Prudic DE (2010) Documentation of the Streamflow-Routing (SFR2) Package to Include Unsaturated Flow Beneath Streams—A Modification to SFR1: U.S. Geological Survey Techniques and Methods 6-A13.
Niswonger RG, Prudic DE, Regan SR (2006) Documentation of the Unsaturated-Zone Flow (UZF1) Package for Modeling Unsaturated Flow Between the Land Surface and the Water Table with MODFLOW-2005.
Ochoa-Gonzalez GH, Carreon-Freyre D, Cerca M, Lopez-Martinez M (2015) Assessment of groundwAter flow in volcanic faulted areas. A study case in Queretaro, Mexico. GEOFÍSICA Int 3:199–220. doi: DOI: 10.1016/j.gi.2015.04.016
Ozturk D, Kilic F (2016) Geostatistical Approach for Spatial Interpolation of Meteorological Data. An Acad Bras CiencAnnals Brazilian Acad Sci 88:2121–2136. doi: 10.1590/0001-3765201620150103
Paul BA, Freckleton JR (1993) DOCUMENTATION OF A COMPUTER PROGRAM TO SIMULATE HORIZONTAL-FLOW BARRIERS USING THE U.S. GEOLOGICAL SURVEY'S MODULAR THREE-DIMENSIONAL FINITE-DIFFERENCE GROUND-WATER FLOW MODEL.
Pitman W (1973) A mathematical model for generating monthly river flows from meteorological data in South Africa. University of the Witwatersrand Department of Civil Engineering Hydrological Research Unit, Johannesburg
Prudic DE, Konikow LF, Banta ER (2004) A NEW STREAMFLOW-ROUTING (SFR1) PACKAGE TO SIMULATE STREAM-AQUIFER INTERACTION WITH MODFLOW-2000.
RHP (2011) River Health Programme state of rivers report: rivers of the Breede Water Management Area.
Rientijes T (2015) Hydrologic modelling for Intergated Water Resource.
Roets W, Xu Y, Raitt L, et al (2008) Determining discharges from the Table Mountain Group (TMG) aquifer to wetlands in the Southern Cape, South Africa. Hydrobiologia 607:175–186. doi: 10.1007/s10750-008-9389-x
Runyan C, D'Odorico P (2016) Global Deforestation. Google books
Russell IA, Impson ND (2006) Aquatic systems in and adjacent to Agulhas National Park with particular reference to the fish fauna. Koedoe 49:45–57. doi: 10.4102/koedoe.v49i2.120
Said A, Stevens DK, Sehlke G (2005) Estimating Water Budget in a Regional Aquifer Using Hspf-Modflow Integrated Model. J Am Water Resour Assoc 41:55–66. doi: 10.1111/j.1752-1688.2005.tb03717.x
Searcy JK, Hardison CH, Langbein WB (1960) Double-Mass Curves With a section Fitting Curves to Cyclic Data Manual of Hydrology: Part 1. General Surface-Water Techniques.
Sebben ML, Werner AD, Liggett JE, et al (2013) On the testing of fully integrated surface-subsurface hydrological models. Hydrol Process 27:1276–1285. doi: 10.1002/hyp.9630
Seward P, Xu Y, Brendonck L (2006) Sustainable groundwater use, the capture principle, and adaptive management.
Smith RE (1983) Approximate Soil Water Movement by Kinematic Characteristics1. Soil Sci Soc Am J 47:3–8. doi: 10.2136/sssaj1983.03615995004700010001x
Tadross M, Johnston P (2012) Southern Africa Climate Systems Regional Report.
Tanner J, Hughes D (2015) Understanding and modelling surface water-groundwater interactions.
Teketel AT, Lubczynski MW, Vekerdy Z (2017) Integrated hydrological modeling of surface-groundwater interactions,The case of Denpasar-Tabanan Basin in the Southern Bali Island. University of Twente, Faculty of Geoinformation Science and Earth Observation
Unland NP, Cartwright I, Andersen MS, et al (2013) Investigating the spatio-temporal variability in groundwater and surface water interactions: a multi-technique approach. Hydrol Earth Syst Sci 17:3437–3453. doi: 10.5194/hess-17-3437-2013
USGS (2003) Heat as a tool for studying the movement of ground water near streams.
van Wyk E, van Tonder G, Vermeulen D (2012) Characteristics of local groundwater recharge cycles in South African semi-arid hard rock terrains: Rainfall-groundwater interaction. Water SA 38:747–754. doi: 10.4314/wsa.v38i5.14
Vegter J (1995) Groundwater resources of South Africa. An explanation of a set of National Groundwater maps. WRC Report No. TT 74/95.

Weber D, Englund E (1992) Evaluation and comparison of spatial interpolators. Math Geol 24:381–391. doi: 10.1007/BF00891270
Weldemichael MY, Lubczynski MW, Becht R (2016) INTEGRATED NUMERICAL MODELING APPLYING STRATIFORM HYDROGEOLOGICAL CONCEPTUAL MODEL, SARDON CATCHMENT STUDY CASE, SPAIN.
Winston RB (2009) ModelMuse: A Graphical User Interface for MODFLOW-2005 and PHAST.
Woodford A, Rosewarne P, Girman J (2005) How much groundwater does South Africa have?

APPENDICES

Appendix 1: Pearson correlation coefficient between rainfall stations based on data from June to November 2015

	Moddervlei	Tiersfontein	Spanjaarsdkloof	Vissersdrift	Napier	Toekomst	Tussenberg
Moddervlei	1.00						
Tiersfontein	0.86	1.00					
Spanjaarsdkloof	0.95	0.90	1.00				
Vissersdrift	0.90	0.85	0.85	1.00			
Napier	0.85	0.89	0.88	0.83	1.00		
Toekomst	0.73	0.83	0.82	0.72	0.67	1.00	
Tussenberg	0.88	0.89	0.92	0.85	0.93	0.75	1.00

Appendix 2: Euclidian distance (km) between weather stations

	Moddervlei	Tiersfontein	Spanjaarsdkloof	Vissersdrift	Napier	Toekomst	Tussenberg
Moddervlei	0.00						
Tiersfontein	18.33	0.00					
Spanjaarsdkloof	9.05	12.80	0.00				
Vissersdrift	20.69	38.49	28.65	0.00			
Napier	16.93	29.27	16.58	24.14	0.00		
Toekomst	10.12	26.26	13.84	17.58	8.23	0.00	
Tussenberg	15.04	15.10	6.60	33.26	15.95	16.59	0.00

Appendix 3: Person correlation coefficient of reference evapotranspiration between weather stations

	Tiersfontein	Spanjaarsdkloof	Vissersdrift	Napier	Moddervlei
Tiersfontein	1.00				
Spanjaarsdkloof	0.79	1.00			
Vissersdrift	1.00	0.80	1.00		
Napier	0.96	0.80	0.96	1.00	
Moddervlei	0.97	0.80	0.97	0.97	1.00

Appendix 4: NDVI images

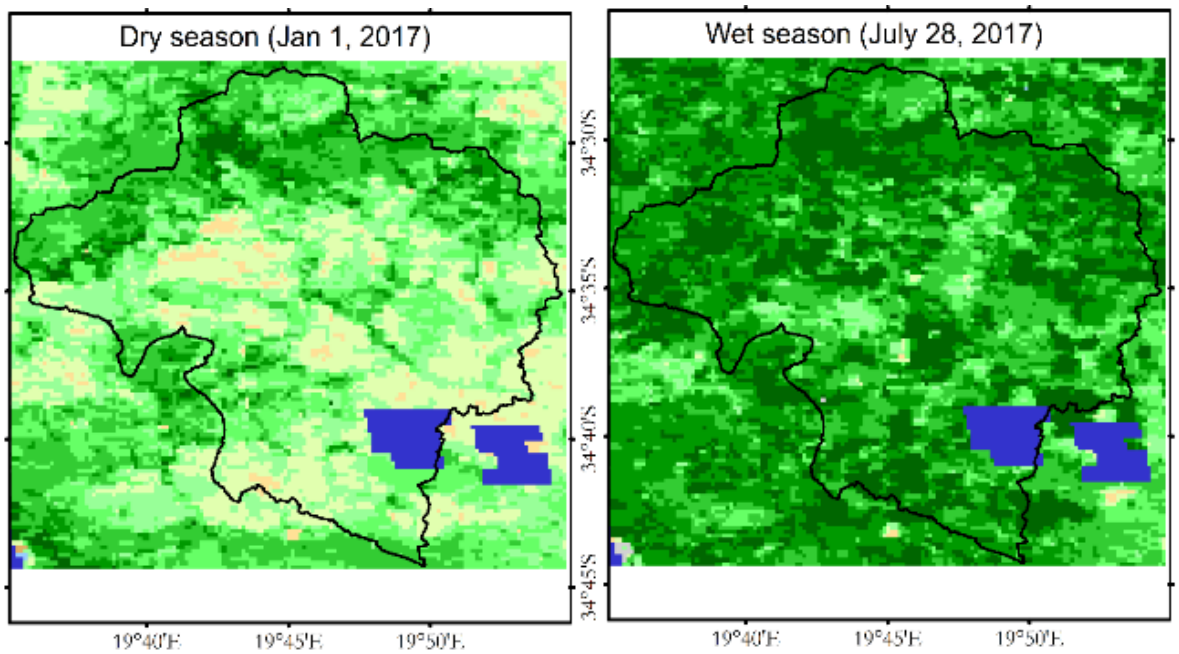

Appendix 5: Borehole logs

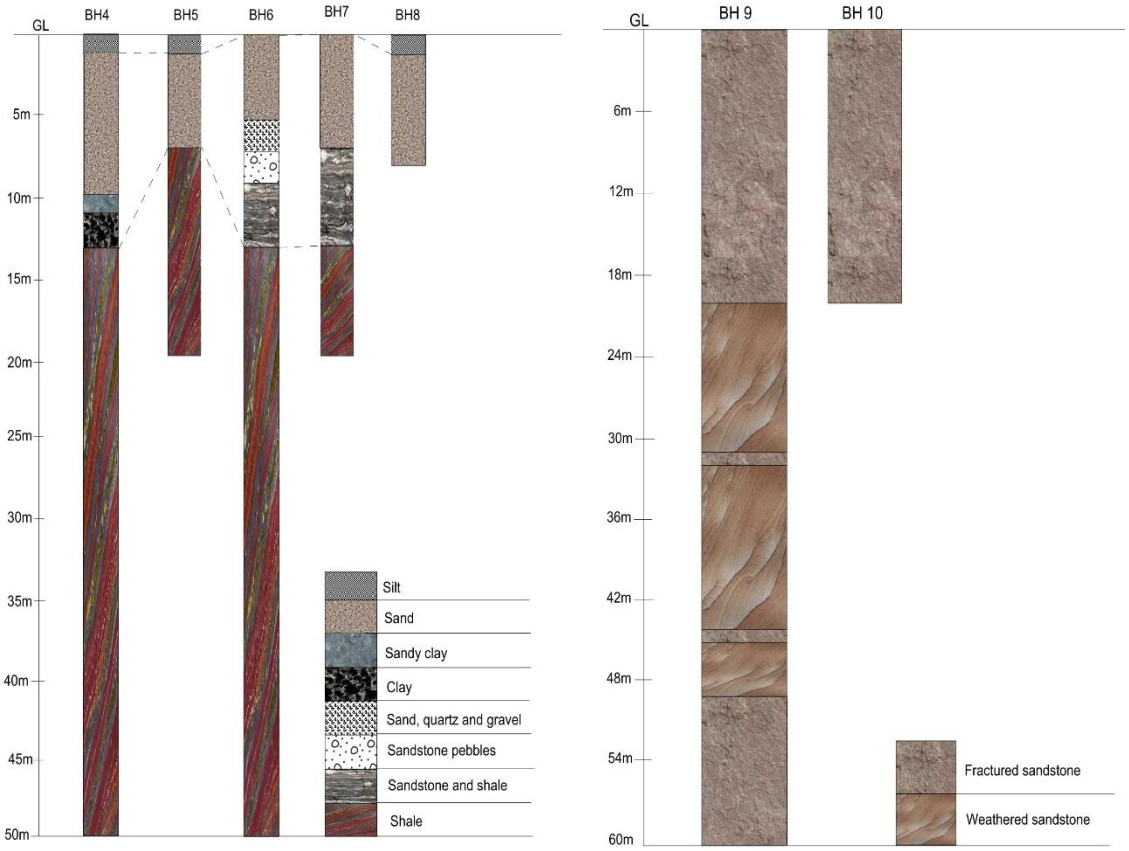


GL
BH 11
BH 12
6m
12m
18m
24m
30m
36m
42m
48m
54m
60m
Conglomerate and sandstone
Weathered sandstone
Weathered and fractured sandstone


GL
BH 13
BH 14
5m
10m
15m
20m
25m
30m
35m
40m
45m
50m
55m
Fractured sandstone
Weathered sandstone
Weathered and fractured sandstone